Spring 5-15-2022

Regulation and Function of Integrin β3 in Bone-Metastatic Breast Cancer Cells in the Therapeutic Setting

Gregory Chandler Fox
Washington University in St. Louis

WASHINGTON UNIVERSITY IN ST. LOUIS

Division of Biology and Biomedical Sciences
Molecular Cell Biology

Dissertation Examination Committee:
Katherine N. Weilbaecher, Chair
Abdel Kareem Azab
Jason C. Mills
David M. Ornitz
Sheila A. Stewart
Deborah J. Veis

Regulation and Function of Integrin β3 in Bone-Metastatic Breast Cancer Cells in the Therapeutic Setting

by

Gregory Chandler Fox

A dissertation presented to
The Graduate School
of Washington University in
partial fulfillment of the
requirements for the degree
of Doctor of Philosophy

May 2022
St. Louis, Missouri

Table of Contents

List of Figures

Acknowledgments

To all my family, friends, co-workers, and classmates, I could never have arrived at this moment without you. Thanks to Dr. Adair, for your endless patience and grace as I stepped fresh into the world of research for the first time. In Saint Louis, thanks go especially to my spectacular lab mates, particularly Michael, the consummate senior graduate student, and Xinming, who never doesn't want to talk science with me. To Kathy, words cannot express how thankful I am to have had you as my mentor for the past 5½ years. I liked science before, but you helped make me a scientist, all while exuding an awe-inspiring compassion for your patients and enthusiasm for their care that I'll be trying to emulate for the rest of my career. Thank you for everything.

To my Journey family, you have been a balm in dry seasons and a light in darkness. I am blessed to call you brothers and sisters in the One we serve.

To my MSTP cohort, thank you for laughter and learning, for good food, better wine, and the best of company. It'll be nice to see a lot of you more regularly again now that this is written.

To my wife, my Lindsey, there is the time before I met you, and there is after; I'm really lucky I get to live in the after, and can't wait to face all the things the Lord is calling us toward with you by my side. Also, you provisioned me with coffee while I was writing this, which practically makes you second author.

Finally, to my wonderful parents, I dedicate this dissertation to you. Let it be an emblem for, testament to, and hopefully reflection of the even more endless hours of love, care, and wisdom you have so generously and freely given me.

Gregory C. Fox

Washington University in St. Louis, May 2022

ABSTRACT OF THE DISSERTATION

Regulation and Function of Integrin β3 in Bone-Metastatic Breast Cancer Cells in the Therapeutic Setting

by

Gregory Chandler Fox

Doctor of Philosophy in Biology and Biomedical Sciences

Molecular Cell Biology

Washington University in St. Louis, 2022

Professor Katherine N. Weilbaecher, Chair

Breast cancer is the most common non-cutaneous malignancy in women, with over 250,000 patients diagnosed each year in the United States alone. The bone is the most common site of recurrence in breast cancer, affecting over two-thirds of patients with metastatic disease and presenting as the only evidence of distant spread in up to 30%. Clinically, breast cancer bone metastases manifest most often as profoundly osteolytic lesions that negatively impact survival and patient quality of life. Bone-targeted therapies such as bisphosphonates and the anti-RANKL monoclonal antibody denosumab have revolutionized the treatment of bone metastases through inhibition of osteoclast-mediated bone destruction; however, these agents have failed to improve survival in the majority of patients. While other therapeutic options such as systemic chemotherapy exist, response to treatment is difficult to quantify, and bone metastases frequently exhibit resistance to anti-tumor interventions. Better, more specific therapies for these patients are urgently needed.

Compared to common sites of visceral metastasis in breast cancer such as the lung and liver, the bone microenvironment represents a highly unique tumor niche, with distinct

biophysical parameters, cellular and extracellular matrix (ECM) composition, and nutrient and chemical milieu. It is increasingly clear that interaction with this singular microenvironment promotes bone-specific tumor phenotypes that can be therapeutically exploited. In another study focused on delivering the common breast cancer chemotherapeutic docetaxel (DTX) to the bone metastatic microenvironment, we found that micelle nanoparticles targeted against the αvβ3 integrin heterodimer preferentially homed to bone metastases. To our surprise, this organ-specific targeting was driven not by microenvironmental αvβ3, but rather by upregulation of the integrin β3 (β3) subunit on bone-resident breast cancer cells not observed in visceral metastatic sites.

Integrin heterodimers recognize ligand moieties present in the ECM and can initiate downstream signaling events with a wide array of consequences for cellular function. Tumoral αvβ3 integrin expression can promote bone metastasis and initiation of osteolysis, but its functional role in established metastases was largely unknown, particularly in the setting of chemotherapy. To investigate this aspect of bone metastatic biology, we generated *Itgb3* knockout derivates of two bone-tropic murine breast cancer cell lines. While we found minimal differences in resistance to DTX *in vitro*, β3KO cells were significantly more sensitive to DTX attenuation in the bone microenvironment, and rescue of β3 expression in a β3KO clone restored resistance in the bone in a signaling-dependent manner. Ultrastructural, transcriptomic, and functional analyses revealed a β3-mediated alternative metabolic response to DTX characterized by increased protein production, oxygen consumption, and reactive oxygen species (ROS) generation. mTORC1 inhibitors, either free or loaded into αvβ3-targeted nanoparticles, could be combined with DTX to counteract this response and synergistically attenuate bone metastases.

Our findings highlight the importance of the bone microenvironment as a driver of therapy resistance and provide proof of principle for a new, bone-specific combination therapy.

We were also interested in elucidating the molecular mechanism responsible for upregulation of β3 on tumor cells in the bone microenvironment. A bone factor screen uncovered TGF-β as a candidate, and *in vitro* and *in vivo* inhibitor experiments confirmed the necessity of canonical TGF-β signaling through SMAD2/3 for tumoral β3 upregulation in bone metastases. Although TGF-β is known to be present at its highest concentration in the bone ECM, it is ubiquitous in most tumor microenvironments, prompting us to consider differences in active TGF-β bioavailability as the most important factor for β3 upregulation in metastatic cells. To explore this, we developed a TGF-β-responsive dual-luciferase reporter breast cancer cell line to use in the direct detection of TGF-β activity. Importantly, in a mouse model of Marfan syndrome with elevated active TGF-β in certain tissues, lung metastases exhibited elevated tumoral β3 expression and were resistant to DTX compared to similar tumors in wild type mice. These results establish bioavailable TGF-β as the causal microenvironmental factor in tumoral β3 upregulation and cement the importance of tumoral β3 for resistance to chemotherapy in breast cancer metastases.

Together, our work demonstrates the profound influence of the microenvironment on tumor phenotype, even among different metastases present in the same animal. Future work focusing on direct targeting of both the β3-mediated alternative metabolic response to DTX and TGF-β signaling, as well as more basic questions surrounding the biology of tumor adaptations to treatment in the bone microenvironment, will be crucial for development of more effective therapeutic interventions for patients with bone metastases.

He put another parable before them, saying, "The kingdom of heaven is like a grain of mustard seed that a man took and sowed in his field. It is the smallest of all seeds, but when it has grown it is larger than all the garden plants and becomes a tree, so that the birds of the air come and make nests in its branches."
Matthew 13:31-32

Chapter 1

Introduction

1.1 Breast Cancer Bone Metastases

1.1.1 Overview

Distant recurrence in the bone is one of the most frequent manifestations of metastatic spread in breast cancer patients. Clinical management of these lesions can be challenging, marked by difficulties in initial detection, tracing of therapeutic response, and palliation of opioid-refractory pain. In their most dramatic presentations, these tumors can precipitate deleterious sequelae (skeletal-related events, SREs) such as pathological fracture, severely impacting patient quality of life and survival. Though less immediately threatening, more indolent bone lesions, and even individual disseminated tumor cells (DTCs) in the bone marrow, remain notably resistant to standard therapies and contribute to diminished recurrence-free survival (RFS). These features emerge from the unique relationship between bone-resident breast cancer cells and the bone microenvironment, which harbors unique cell types and biophysical properties that evoke phenotypes not observed in the primary tumor or at visceral metastatic sites. Despite our evolving understanding of these interactions and their contribution to therapy resistance and poor patient outcomes, more research is still needed to aid identification of clinically actionable targets.

1.1.2 Incidence and Clinical Presentation

Breast cancer is the most common malignancy in the United States, with an age-adjusted incidence of 125.1 new cases per 100,000 women[1]. The past 50 years have seen an encouraging decline in mortality in these patients, likely due to widespread adoption of standards of care that incorporate chemotherapy alongside surgical resection[2]. which has proven to be particularly beneficial in patients with regionally invasive disease[3]. Unfortunately, while modifications to screening and detection protocols have shifted the overall burden of breast cancer diagnoses

towards patients with smaller, localized tumors (contributing somewhat to the observed mortality decline[4]), the absolute incidence of regional and distant disease remains unchanged[3]. This indicates that increased screening is largely failing to identify high-risk patients who will go on to develop the aggressive recurrences that account for the majority of breast cancer-related deaths[5].

Indeed, despite advances in screening, detection, and treatment, roughly 30% of patients with breast cancer will eventually experience distant recurrence[5]. In the late 19th century, the English surgeon Stephen Paget, describing the predilection of sojourning cancer "seeds" for specific metastatic "soils," noted that "in cancer of the breast, the bones suffer in a special way"[6]. The robustness of this observation has only intensified with further analysis. It is now understood that even in patients with localized breast cancer, 30-50% will exhibit detectable DTCs in bone marrow aspirates, an indicator of early, occult micrometastasis associated with diminished survival likelihood and elevated risk of overt recurrence[7, 8]. In patients with clinically appreciable macrometastasis, 30-40% will present with bone as the first and only site of distant spread[9, 10], and cumulatively, 50-70% of patients with metastatic disease go on to exhibit bone involvement[11, 12]. While clinical data have repeatedly highlighted a discrepancy in bone tropism between estrogen receptor (ER) positive and ER- breast cancer subtypes[13, 14], a recent integrative analysis of distant relapse found that ER status did not have an effect on cumulative incidence of bone metastasis, suggesting that slower-growing bone lesions might simply lack sufficient time to develop in ER- patients who experience high mortality resulting from aggressive early recurrence[15].

Irrespective of subtype, these data point to bone relapse as an unmistakable reality faced by patients with metastatic breast cancer. Clinically, bone metastases manifest as predominantly

osteolytic lesions of the axial skeleton and large long bones marked by substantial osteoclast recruitment and resulting resorptive activity[16, 17]. This bone destructive phenotype is accompanied by a high risk of adverse skeletal-related events (SREs), including pathological fracture, hypercalcemia of malignancy, spinal cord compression, and neuropathic bone pain, with devastating consequences for patient mobility, quality of life, and survival[12]. Patients presenting with a solitary bone recurrence have generally superior overall survival compared to those whose first relapse occurs in a visceral site such as the lung, liver, or brain, consistent with a more indolent, manageable course[9, 10]. However, even in this subset of cases, resistance to systemic therapies is common[18–20], and the majority of patients eventually succumb to their disease as bone tumor burden accumulates over time[12, 21].

1.1.3 Treatment

Therapeutic options for the treatment of breast cancer bone metastases have been of historically limited effectiveness, tending to focus more on symptomatic relief than on cure [21]. Until relatively recently, standard of care for these patients entailed radiation for pain relief, surgery for patients at risk for imminent fracture, and systemic hormonal and chemotherapy, none of which was associated with a significant benefit in overall survival[18, 19, 21, 22].

This paradigm has fundamentally shifted with the advent of bone-targeted agents (BTAs), specifically nitrogen-containing bisphosphonates such as zoledronic acid (ZA) and the anti-RANKL monoclonal antibody denosumab[23, 24]. ZA functions by binding directly to the hydroxyapatite bone matrix, where it can remain at therapeutic concentrations for years[25] and is taken up by osteoclasts, inhibiting their maturation and survival through direct inhibition of the key mevalonate pathway enzyme farnesyl diphosphonate (FPP) synthase[26, 27]. Denosumab, meanwhile, inhibits bone destruction through neutralization of the receptor activator of NF-κB

ligand (RANKL), a master inducer of osteoclastogenesis[28–30].

Together, both classes of BTA have dramatically altered the therapeutic landscape, enabling relatively bone-specific therapy for the first time. By focusing on the interruption of osteoclast activity, both of these agents are able to dramatically reduce the frequency of SREs in bone metastatic breast cancer patients, improving quality of life and simplifying clinical management [31, 32]. Early data pointed toward survival benefit and recurrence reduction in patients receiving ZA[33], and clinical trials have suggested that the combination of ZA with chemotherapy can sensitize resistant DTCs to treatment[34]. Despite its even more robust prevention of SREs[32], however, denosumab did not demonstrate an effect on bone metastasis-free survival in a large clinical trial[35]. A series of more expansive studies in ZA have likewise indicated that its benefits for survival and recurrence reduction are largely restricted to postmenopausal women[36, 37]. While the exact reasons for this lack of unqualified benefit are not fully understood, it is clear that osteoclast targeting alone is not sufficient to reduce bone metastatic outgrowth, further highlighting the urgent need for bone-targeted therapies specifically focused on the tumor cells themselves[24].

1.1.4 The Bone Metastatic Cascade

Metastasis, the process by which cancer cells invade beyond the confines of their tissue of origin and successfully colonize distant sites, has been recognized as a hallmark of malignant behavior responsible for significant morbidity and mortality[38]. This is of particular relevance for breast cancer, one of the few cancer types in which the cumulative risk of recurrence only increases over time[39]. Like the proverbial elephant in the dark, much about this process remains shrouded in mystery; however, careful experimental dissection of the invasion-metastasis cascade has gleaned some insights.

A seminal study in breast cancer cell lines with differing intrinsic metastatic capacities was instructive for defining the broad contours of the metastatic cascade: invasion beyond the primary site, intravasation into either the lymphatic or hematogenous vasculature, survival in circulation, extravasation into secondary organ parenchyma, and successful proliferation in the foreign "soil"[40–42]. Over time, some of the cellular and molecular specifics of this process have come into sharper focus, as well. Epithelial-mesenchymal transition (EMT), a developmental program active during embryonic migration, has been causally linked to invasive capacity, passage into and out of the circulation, and survival in metastasizing cancer cells[43]. Meanwhile, mesenchymal-epithelial transition, its opposing program, has been found to be crucial for proliferation by cells that successfully arrive in a conducive secondary site[44–46]. Cross-talk with a number of host cell types, including macrophages[47], platelets[48], bone-marrow derived hematopoietic progenitors[49, 50], and cancer-associated fibroblasts[51, 52] has likewise been demonstrated to coordinate invasive phenotypes, promote survival in the circulation, and even prepare distant metastatic sites for arrival and growth of tumor cells.

Within this stereotyped process, it has become clear that a broader division can be made between properties that facilitate primary escape and those that contribute to establishment of successfully proliferating tumors at the secondary site[41, 42]. The difficulty inherent in bridging the gap between these two phases was first noted as early as 50 years ago, when Fidler found that fewer than 0.01% of intravenously injected B16 melanoma cells survived to give rise to detectable lesions in a murine model of experimental lung metastasis[53]. This so-called “metastatic inefficiency”[54] of circulating malignant cells is evident in patients[55] and has been confirmed in other preclinical models, with one early study in particular noting millions of tumor cells shed into the efferent circulation by a primary tumor that nevertheless exhibited little propensity for

metastasis[56]. Clearly, dissemination and metastasis are distinct processes requiring distinct cellular adaptations, without either of which distant outgrowth is impossible.

The necessity of profound, coordinated adaptation for successful metastasis was given a new wrinkle in a run of watershed studies published by Massagué and colleagues during the first decade of the 21st century. Through *in vivo* enrichment of breast cancer cell lines for bone[57], lung[58], or brain[59] metastatic tropism, they were able to identify discrete sets of genes which, when expressed concomitantly in breast cancer cells, dramatically increased rates of metastasis to their respective organs. Importantly, these gene sets were entirely different from one another, underscoring the fundamental role of the metastatic microenvironment as an arbiter of cancer cell fate.

It is at this point that more specific discussion of breast cancer bone metastasis, and particularly the transition from isolated disseminated tumor cell to proliferative metastatic lesion, becomes especially salient. Breast cancer cells rely on a number of mechanisms to home to and anchor themselves within the bone microenvironment, including integrin αvβ3[60] and various integrin β1 heterodimers[61], as well as the hematopoietic stem cell CXCL12-CXCR4 axis [62,63,64]. Once established on the bone surface, these DTCs experience an indeterminate period of quiescence marked by infrequent or absent proliferation and profound resistance to therapy[34, 65]. Cells capable of outgrowing after this stage must at some point be "reactivated"[65], potentially as a stochastic consequence of local bone remodeling[66]. Despite recent advances, the molecular mechanisms that underlie malignant dormancy and subsequent reactivation in the bone remain poorly characterized[65].

The transition from lone disseminated tumor cell to actively proliferating lesion is driven by

osteoclastic bone resorption, which liberates latent growth factors embedded in the osteoid bone matrix such as TGF-β[67, 68], IGFs, and Ca^{2+}[69] that enhance tumor proliferation and invasion[70]. Crucially, this osteoclastic bone resorption is itself precipitated and sustained by tumor cell-expressed pro-osteoclastic factors, including parathyroid hormone-related peptide (PTHRP)[71], Jagged-1 and IL-6[72], and IL-11[57], all of which, remarkably, are themselves further upregulated in response to osteoclast-mediated increases in bioavailable TGF-β[57, 72, 73]. This relentless paracrine loop, sometimes referred to as the "vicious cycle" of bone metastasis[16], conspires to produce constant, osteoclast-mediated bone turnover that fuels tumor cell growth in an environment dominated by TGF-β signaling[70,74, 75]. While studies have demonstrated that pharmacological blockade of TGF-β signaling can attenuate bone tumor burden[76], the full range of functional changes induced in tumor cells exposed to this milieu is unknown.

1.1.5 Unique Properties of the Bone Tumor Microenvironment

The bone tumor microenvironment is characteristically distinct from the primary tumor and visceral metastatic sites, differing in a number of ways that directly contribute to tumor cell phenotype. It has been demonstrated that differences in substrate compliance and tension can elicit profound effects on cellular function[77], and that malignant cells in particular exhibit altered mechanotransductive responses[78]. Compared to essentially all other microenvironments, the bone surface itself is extremely rigid[79]. Tumor cell adaptation to this rigidity is dependent on the Rho-associated protein kinase (ROCK)[80], which translates mechanical tension experienced by tumor cells on the bone surface into an array of functional cellular responses, including enhancement of osteolysis through increased production of PTHRP[79, 81].

While rapidly proliferating solid tumors develop regions of hypoxia as their growth outstrips local blood supply[82], the entirety of the bone marrow cavity has been found to exhibit profoundly

low oxygen tension, likely a result of the high cellular density it maintains as the seat of hematopoiesis[83]. As such, the behavior and phenotype of bone metastatic cells is shaped by the need for adaptation to hypoxia from their first entry into the bone marrow. The reality of this adaptation is manifested in the observed enrichment of bone metastases for hypoxia-inducible factor 1α (HIF1α) [84], which could contribute to tumor cell persistence through treatment[85] and further drive the osteolytic phenotype[86].

The bone is the primary repository for calcium in the body, and physiological bone resorption and formation function to carefully titrate systemic calcium concentrations in homeostatic conditions[87]. Accordingly, during pathological bone destruction driven by osteolytic breast cancer bone metastases, local Ca^{2+} concentrations are much higher than is typically the case[88]. In breast cancer[69], as well as in other tumors that metastasize to bone[89, 90], this increased calcium availability has been found to promote survival and proliferation in the bone microenvironment.

Bone degradation by osteoclasts depends on the creation of a highly acidic resorptive space to dissolve the mineral component of the osteoid matrix[91]. In osteolytic bone metastases with abundant osteoclast recruitment, this activity results in an acidic tumor microenvironment[92]. Modulation of environmental pH can have profound effects on both tumor and host cells, driving macrophages toward an immunosuppressive phenotype[93], altering signaling through critical transduction pathways such as mTOR[94], and precipitating metabolic adaptations that amplify cancer proliferation[95]. pH reduction has also been shown to promote activation of integrin αvβ3[96], which might further drive its role in breast cancer bone colonization through enhancement of ligand binding capacity.

Beyond these biophysical parameters and the abundance of matrix-embedded growth factors

already mentioned, the bone microenvironment is host to several unique cell types that interact with breast cancer cells in a way that promotes tumor growth and survival. Bone-resorbing osteoclasts, as already discussed extensively, serve to directly shape the bone metastatic microenvironment, altering a wide range of physical and chemical properties with significant consequences for tumor cell signaling and function. In addition to their role in synthesizing osteoid bone matrix and promoting osteoclastogenesis though expression of RANKL and macrophage colony-stimulating factor (M-CSF)[70], bone-forming osteoblasts are of great interest for the direct cell-cell interactions they can establish with tumor cells. Evidence from prostate cancer[63] and multiple myeloma[66] suggests that osteoblasts can function as a "safe harbor" for cancer cells, guiding them into the bone niche and inducing a quiescent state that shields them from therapeutic attenuation. In bone-resident breast cancer cells, direct engagement with osteoblasts has been demonstrated to elicit calcium signaling that promotes tumor progression[69] and to drive therapy resistance through a Jagged-1-mediated pro-survival program[97]. While the bone contains many other unique cell types, including matrix-embedded osteocytes[70], cartilage-producing chondrocytes, mesenchymal stem cells[98], megakaryocytes[99], and whole lineages of immune cells[100], the details of their interactions with and influence on breast cancer cells have yet to be fully elucidated.

1.1.6 Experimental Modeling of Bone Metastasis

Unfortunately, there are no genetically modified mouse models (GEMMs) that spontaneously and consistently recapitulate all aspects of the breast cancer bone metastatic cascade from primary mammary fat pad tumor to active bone lesion[101]. This has necessitated the use of bone-tropic breast cancer cell lines such as human MDA-MB-231[102] in immunocompromised mice or murine 4T1[103] in immunocompetent mice, inoculated by various routes depending on

experimental question. Though this limitation has undoubtedly hampered clinical translation from data obtained in mice to successful treatments in human patients, several reliable techniques using breast cancer cell lines have nevertheless been developed.

In the most artificial method, tumor cells are injected directly into the mouse tibia. While this ensures robust tumor establishment, it elides numerous steps in the bone metastatic cascade, and is only truly representative of phenotypes observed in end-stage osteolytic lesions[104].

On the other end of the spectrum is the orthotopic resection model, in which tumor cells are inoculated into the murine mammary fat pad and allowed to grow initially as a primary tumor, followed by surgical resection and monitoring for metastases in the lungs and bones. Though this method once again skips tumorigenesis seen in GEMMs, the rest of the metastatic process is largely conserved, allowing for modeling of treatment and the impact of genetic manipulations in a fashion that roughly models a number of the stages observed in human patients[105]. Unfortunately, as is also observed in human patients, the development of bone metastases in this model is much more stochastic, complicating the design of therapeutic studies with numerous treatment groups and increasing the number of mice needed for robust evaluation of the effects of therapeutic interventions.

Bridging the gap between these two techniques are models that achieve systemic dissemination of tumors cells by inoculation into the circulation[105]. Though these methods sacrifice evaluation of the early steps of the metastatic cascade, tumor establishment in the bone is much more predictable. Of the several routes that have been demonstrated to yield proliferating bone lesions, the most reliable is intracardiac (i.c.) injection into the left ventricle. This method results in broad dissemination of tumor cells via the arterial circulation, yielding robust tumors in the lung, liver,

kidneys, and bone with consistent tumor burden from experiment to experiment. As a major focus of this work centers around overcoming chemoresistance through combination therapy, the majority of its *in vivo* experiments were performed using mice with bone metastases established utilizing this technique.

In all models, tumor cell lines genetically modified to express a fluorescence marker (e.g. GFP) and firefly luciferase[106] can be used to enable *in vivo* monitoring of tumor burden and *ex vivo* quantitation and downstream analysis. Modalities such as X-ray or micro-computed tomography (μCT) analysis of osteolytic lesion area, histomorphometric quantitation of tumor burden and osteoclast number, and serum chemistry analysis can all be useful for further characterization and phenotypic evaluation.

1.2 The β3 Integrin Subunit

1.2.1 Overview

As the principle receptors for ligand moieties in the ECM, integrin heterodimers serve as essential hubs for cellular interaction with and adaptation to the local microenvironment in both homeostatic conditions and disease. Integrin structure uniquely informs integrin function, determining ligand specificity and enabling precise, tunable activity based on environmentally-responsive activation status. Signaling through integrins is notably context and cell-type specific, with downstream ramifications for cellular functions ranging from proliferation to survival. Integrin dysregulation is common in the malignant setting, where it contributes to loss of tissue integrity, invasion, and therapeutic resistance. The integrin β3 subunit (β3) is of particular interest in breast cancer bone metastases, where its expression on host and tumor cells contributes to the malignant phenotype. Integrin β3 has previously been associated with altered

therapeutic responses, prompting questions surrounding its functional role in bone-resident breast cancer cells in the therapeutic setting.

1.2.2 General Principles of the Integrin Receptor Family

Integrins are a family of transmembrane receptors, comprised of 8 α and 18 β subunits, that associate to form 24 unique heterodimers[107]. First appreciated as an interrelated family in the late 1980s after sequencing revealed substantial homology[108], integrins are unique to metazoans[109], where they likely evolved as a way for different cell layers to parse and respond appropriately to extracellular substrates, thereby enabling more complex organization and specialization of tissues[107].

Although a small subset of integrins facilitates cell-cell interactions (e.g. binding of the VLA-4 integrin heterodimer to VCAM1[110]), the majority recognize short, repeated peptide motifs present in extracellular matrix constituents such as fibronectin[111], laminin, or collagen[112], among many others[113]. Integrin binding of ligand moieties takes place via a ligand binding pocket, located at the interface between the α and β subunits[114, 115]. Under homeostatic conditions, integrin heterodimers are "inactive," with transmembrane regions clasped together and extracellular domains folded over in a bent confirmation that precludes binding to all but the smallest soluble moieties[116, 117]. Exposure of this binding pocket for high-affinity ligand interaction requires integrin activation[107], which is itself a response to "inside-out" signaling, wherein complex networks of intracellular signals and context-dependent responses to extracellular stimuli (e.g. Mn^{2+}[107]) are integrated and translated into conformational change at the membrane surface[118]. This binary behavior allows integrins and their signaling to be switched on and off as needed, enabling dynamic functional responses that are specifically restricted to the circumstances in which they are most helpful[107].

Platelets are particularly illustrative of the utility of this paradigm[119]. As critical constituents of the thrombotic system, platelets must be poised to rapidly activate and aggregate to form fibrous clots[120]. At the same time, however, this activity must be functionally restricted to sites of endothelial injury, lest aberrant thrombus formation occlude downstream vasculature and precipitate ischemic tissue damage. This fine balance is achieved by linking platelet activation to integrin signaling through the αIIbβ3 heterodimer, which recognizes motifs in fibrinogen and von Willebrand factor (VWF). Under normal circumstances, platelet αIIbβ3 is inactive; however, exposure of platelets to endothelial damage signals such as thrombin initiates a rapid inside-out signaling cascade that activates αIIbβ3, enabling subsequent ligand binding, platelet activation, and thrombus formation in an exquisitely site-specific manner[119].

In contrast with inside-out signaling, which aggregates a number of molecular inputs to potentiate integrin activation, "outside-in" signaling occurs when activated integrins bind their cognate ligands in the ECM, freeing the cytoplasmic tail of the β subunit for full interaction with downstream binding partners[107, 121]. The talin adaptor protein, in addition to serving as the "final common step" for integrin activation[122], anchors ligand-bound integrins to the actin cytoskeleton[123], permitting transmission of mechanical force across the cell membrane[124] and providing a stable scaffold around which focal complexes comprised of molecular adaptors and phosphoproteins can form[124, 125]. When initiated by a sufficient number of clustered integrins[126], these complexes are able to activate effectors such as SRC and focal adhesion kinase (FAK), igniting signal transduction through a wide variety of downstream pathways, including MAPK, PI3K, and YAP/TAZ[127].

Integrin subunits themselves have no enzymatically active signaling domain; accordingly, the functional pathways activated downstream of integrin ligand binding tend to be particularly cell

and context-dependent, relying wholly on adaptor and effector protein partners expressed at the plasma membrane interface[128]. Because of this, integrin signaling often overlaps with and can therefore explicitly regulate signal transduction through receptor tyrosine kinase (RTK) growth factor pathways such as EGF and PDGF[107, 129, 130]. As a function of both this signaling diversity and extensive cross-talk between pathways, integrins have been reported to exert regulatory control over almost every cellular function imaginable, from proliferation[131] and migration[132] to survival[133] and apoptosis[134]. Mechanosensation and transduction across ECM-integrin-cytoskeletal bridges adds yet another layer of complexity and context dependence, precipitating transcriptional and gene regulatory changes in response to alterations in microenvironmental tension[135].

1.2.3 Integrins in Cancer

From a teleological perspective, integrins help cells to know their role in a tissue and stick to it, equipping them to respond to microenvironmental cues in the manner most beneficial to the overall health and integrity of their organ of residence. Unsurprisingly, then, integrin dysregulation is a common feature of malignant transformation. Indeed, compared to benign cells from the same tissue of origin, many cancer types exhibit dramatically altered patterns of integrin subunit expression[136], with integrins related to growth inhibition or unligated apoptosis downregulated at the same time that heterodimer expression associated with survival and migration is enhanced[137]. Expression changes often occur in concert with uncoupling phenomena, in which malignant cells either escape negative regulatory signals downstream of integrins they express[138] or somehow compensate for important survival signals from integrin subunits they have downregulated[139]. Freed of these restraints, overexpressed integrins on tumor cells can actively promote invasive, therapy resistant, and metastatic phenotypes[127], sometimes

signaling even in the absence of ligand binding through aberrant clustering[140, 141] or by heterotypic association with growth factor receptors[142].

The impact of integrin expression and signaling in cancer is not limited to the tumor cells themselves, a lack of specificity that has made integrin inhibitors and targeted therapies challenging to deploy as anti-tumor treatments in the clinical setting[143]. Tumor neoangiogenic blood vessels express and are dependent on signaling through the αvβ3 integrin heterodimer[144–146]. In cancer-associated fibroblasts, integrin signaling can lead to microenvironmental remodelling that potentiates invasive tumor phenotypes[147]. Bone marrow-derived myeloid and endothelial progenitors rely on α4β1 heterodimers for homing and adhesion to primary tumor microenvironments[148, 149], while the pro-tumor phenotype of immunosuppressive infiltrating macrophages is actually restrained by their expression of αvβ3[150]. Finally, tumor-derived exosomes that participate in the establishment of pre-metastatic niches are directed to specific organ sites in part based on their expression of various integrin heterodimers[151].

1.2.4 Integrin β3 in Breast Cancer Bone Metastases

Our lab has a long-standing interest in the bone tumor microenvironment and integrin β3, which heterodimerizes with the αIIb subunit in platelets and the αv subunit in all other cell types, including breast cancer cells[107, 108, 152]. Beyond vitronectin, the namesake for which it exhibits exquisite affinity, the αvβ3 heterodimer (originally identified as the "vitronectin receptor" [152]) recognizes RGD peptide moieties across a wide range of ligands expressed in tumor microenvironments, including osteopontin[153], fibronectin[154], vWF[155], periostin[156], tenascin C[157], Cyr61[158], and connective tissue growth factor (CTGF)[159]. In contrast with more constitutively expressed integrins, β3 expression is low in most normal adult tissues[136], though it can be upregulated as a consequence of "activated" phenotypes seen during neoangiogenesis[144],

alternative macrophage activation[150], or osteoclastic bone resorption[160]. Over almost two decades, we and other have shown that integrin β3 in the tumor microenvironment is functionally important for a variety of host cells, including platelets[161], osteoclasts[161, 162], endothelial cells[163, 164], and immunosuppressive, tumor-infiltrating macrophages[150], whose disruption can profoundly affect primary tumor growth and metastasis.

αvβ3 expression by breast cancer cells themselves has been linked with progression and metastasis, as well. As transplanted PyMT-MMTV tumors grow and disseminate, they upregulate integrin β3[165]; likewise, several groups have described populations of integrin β3+ stem-like breast cancer cells with high tumor-initiating capacity[140, 166–168]. Integrin β3 expression has also been demonstrated to amplify breast cancer cell responsiveness to TGF-β signaling[169, 170], further reinforcing malignant phenotypes through the promotion of EMT[171].

For our lab, one of the most relevant consequences of integrin β3 expression on breast cancer cells is its enhancement of their capacity to metastasize to bone. In an evaluation of clinical samples during the late 90s, integrin β3 was found to be consistently expressed in human bone metastases[172]. Two preclinical studies from the 2000s confirmed a role for tumor β3 expression in the bone metastatic cascade. In one, overexpression of β3 in a non-bone-metastatic breast cancer cell line enabled spontaneous dissemination to the vertebral spine from orthotopic MFP tumors[173]. The second study confirmed that αvβ3 overexpression enhanced bone colonizing capacity, and subsequently demonstrated that preventative pharmacologic blockade of αvβ3 integrin could dramatically reduce tumor burden in bone metastases established by tail vein inoculation[60]. Finally, a further study in 2015 showed that integrin β3 could cooperate with TGF-β receptors to enhance osteolytic activity[174]

Just as I was beginning my graduate training in the Weilbaecher lab, our senior graduate student Michael Ross found that tumoral integrin β3 expression was high in murine and human bone metastases but low in primary tumors and visceral metastases[175], suggesting that exposure to the bone microenvironment was somehow upregulating β3 expression on breast cancer cells through an unknown mechanism. Based on evidence that TGF-β can upregulate integrin β3 in breast cancer[167, 176], we hypothesized that increased TGF-β signaling in the bone microenvironment was driving tumoral integrin β3 expression in breast cancer bone metastases. My work alongside Michael on this hypothesis (published in *Cancer Research*[175]) in addition to subsequent follow-up, is featured in Chapter 3 of this dissertation.

The main question driving my thesis work, however, was this: is β3 upregulation functionally important for bone-resident breast cancer cells, particularly in established tumors? As discussed above, signaling through integrins touches almost every aspect of cellular behavior; it seemed inconceivable to consider that β3 upregulation in the osteolytic bone metastatic microenvironment was not continuing to have a profound effect on the resulting tumor biology beyond initial colonization.

In answering this question, I ended up focusing primarily on the role of tumoral β3 in resistance of bone metastases to systemic taxane chemotherapy. There was previous evidence for β3 involvement in chemoresistance in breast cancer[158, 159], but little if any *in vivo* data, a perfect opportunity for a lab like ours that focuses on understanding how the microenvironment and tumor cells interact. Through the use of techniques such as RNA-Seq, *ex vivo* transmission electron microscopy, and extracellular flux analysis of oxygen consumption rate, this strategy provided a fascinating window into both integrin and bone metastatic biology and raised several key questions surrounding how the bone microenvironment shapes the response of breast cancer

cells to therapy. The results of this work, including mechanistic characterization of a β3-mediated chemoresistant phenotype in bone metastases and the development of an effective combination therapy to reverse it, can be found in Chapter 2 and are based heavily on a manuscript now published in *Molecular Cancer Therapeutics*[177].

Taken as a whole, my work in the Weilbaecher lab has highlighted the profound and unique impact of the bone microenvironment on tumor phenotype and demonstrated some of the ways in which these changes can be leveraged in a targeted fashion for therapeutic benefit.

Chapter 2

Integrin β3 signaling links chemoresistance and metabolism in breast cancer bone metastases

This chapter contains data, figures, and text from the following paper, for which I was the primary experimentalist, data analyst, interpreter, author, and editor:

> **Fox GC**, Su X, Davis JL, Xu Y, Kwakwa KA, Ross MH et al. Targeted Therapy to β3 Integrin Reduces Chemoresistance in Breast Cancer Bone Metastases. Mol Cancer Ther. 2021;20:1183-98.

2.1 Abstract

Breast cancer bone metastases are common and incurable. Tumoral integrin β3 (β3) expression is induced through interaction with the bone microenvironment. Though β3 is known to promote bone colonization, its functional role during therapy of established bone metastases is not known. We found increased numbers of β3+ tumor cells in murine bone metastases after docetaxel chemotherapy. β3+ tumor cells were present in 97% of post-neoadjuvant chemotherapy triple negative breast cancer patient samples (n = 38). High tumoral β3 expression was associated with worse outcomes in both pre- and post-chemotherapy triple negative breast cancer groups. Genetic deletion of tumoral β3 had minimal effect *in vitro*, but significantly enhanced *in vivo* docetaxel activity, particularly in the bone. Rescue experiments confirmed that this effect required intact β3 signaling. Ultrastructural, transcriptomic, and functional analyses revealed an alternative metabolic response to chemotherapy in β3-expressing cells characterized by enhanced oxygen consumption, reactive oxygen species generation, and protein production. We identified mTORC1 as a candidate for therapeutic targeting of this β3-mediated, chemotherapy-induced metabolic response. mTORC1 inhibition in combination with docetaxel synergistically attenuated murine bone metastases. Further, micelle nanoparticle delivery of mTORC1 inhibitor to cells expressing activated αvβ3 integrins enhanced docetaxel efficacy in bone metastases. Taken together, we show that β3 integrin induction by the bone microenvironment promotes resistance to chemotherapy through an altered metabolic response that can be defused by combination with αvβ3-targeted mTORC1 inhibitor nanotherapy. Our work demonstrates the importance of the metastatic microenvironment when designing treatments and presents new, bone-specific strategies for enhancing chemotherapeutic efficacy.

2.2 Introduction

Bone metastases remain a significant, unmet challenge in the treatment of breast cancer. The majority of patients with metastatic breast cancer will develop clinically detectable bone involvement[11], with predominantly osteolytic lesions accompanied by refractory pain, increased risk for debilitating fracture, and decreased survival likelihood[12]. Bone-targeted therapies such as bisphosphonates and the anti-RANKL monoclonal antibody denosumab have substantially improved quality of life for these patients, reducing fracture incidence and impeding bone metastatic progression. Unfortunately, these agents are associated with a survival benefit in only a subset of patients[24], and resistance to more traditional treatments such as chemotherapy and radiation is common[70].

Interaction between the tumor microenvironment and cancer cells has been recognized as an important mechanism driving chemoresistance[97, 178], confounding studies that focus on *in vitro* treatment data. The bone represents a distinct metastatic niche, comprised of unique cell types, extracellular matrix (ECM) components, and soluble factors compared to visceral metastatic sites such as the lung or liver. Moreover, the progression from single, disseminated tumor cells on a quiescent bone surface to floridly outgrowing osteolytic lesions is a highly dynamic process, with the importance of individual microenvironmental factors likely varying over time[70, 179]. While some critical factors have been identified at different stages of bone metastatic progression, more targeting candidates are urgently needed to enhance the efficacy of available therapies against clinically detectable lesions.

Integrins are heterodimeric transmembrane receptors that bind ligand moieties in the ECM, initiating signaling events with broad consequences for cell survival, proliferation, and migration[180]. Integrin β3 (β3, as part of αvβ3 and αIIbβ3 heterodimers) can be a marker of tumor

aggressiveness and is expressed on cells in the bone tumor microenvironment, including activated endothelium, osteoclasts, platelets, and immune cells[150, 161, 163, 180–182]. We recently showed that β3 is upregulated on breast cancer cells as a consequence of TGF-β signaling in the bone microenvironment and can be exploited for bone-specific nanoparticle drug delivery[175]. β3 has been identified as an important factor for bone colonization by breast cancer cells[60, 161], and has also been shown to promote resistance to EGFR inhibition across multiple cancer types[140]. While studies have previously linked β3 signaling and chemotherapy resistance[158], its role *in vivo*, and particularly during therapy of established bone metastases, is poorly characterized.

In this study, we provide evidence for β3 as an important promoter of resistance to taxane chemotherapy in breast cancer bone metastases. We show that β3 expression is associated with an alternative metabolic response to taxanes *in vitro* and *in vivo*, and that β3-mediated resistance can be defused by combination therapy with mTORC1 inhibitors. Taken together, our work demonstrates the importance of the specific metastatic microenvironment when designing treatments and presents new, bone-specific strategies for enhancing chemotherapeutic efficacy.

2.3 Results

Integrin β3 is increased in breast cancer cells after chemotherapy

Dysregulated expression of integrin β3 (β3) is associated with increased aggressiveness and drug resistance in cancer[140]. We first asked if exposure to docetaxel (DTX), one of the most commonly prescribed chemotherapeutic agents in patients with breast cancer, alters the proportion of β3-expressing cells in tumor populations. To test this, the 4T1 and PyMT-BO1 murine breast cancer cell lines (modeling triple negative and luminal B disease, respectively) were administered DTX *in vitro* and cell surface β3 expression was assessed by flow cytometry.

We observed an increase in the percentage of β3+ cells in both cell lines after DTX treatment (Fig. 2.1A), with a stronger dose-dependent response in the PyMT-BO1 line. Interestingly, we found that β3 expression was also increased after *in vitro* treatment with a range of targeted agents, including the CDK4/6 inhibitor LEE001 (ribociclib, Fig. S2.1A), the MEK inhibitor U0126 (Fig. S2.1B), and the mTORC1 inhibitor RAD001 (everolimus, Fig. S2.1C).

We next evaluated integrin β3 expression after therapy in the bone metastatic environment. We had previously demonstrated increased tumoral β3 in bone metastases compared to primary breast tumors, both in human patients and in 4T1 and PyMT-BO1 preclinical models[175]. We found that DTX failed to attenuate osteolytic lesions generated by 4T1 and PyMT-BO1 (Fig. 2.1B), indicating that both cells lines were fairly chemoresistant. This prompted us to measure β3 expression in the resistant tumor cells that remained. Given their greater β3 response to DTX *in vitro*, we focused on PyMT-BO1 bone metastases, harvesting live, GFP+ tumor cells for assessment of β3 expression by *ex vivo* flow cytometry. We found a significant increase in the proportion of GFP+β3+ tumor cells in bone metastasis samples from mice receiving DTX compared to those from mice receiving vehicle (vehicle: 33% β3+; DTX: 54% β3+, $p<0.0001$) (Fig. 2.1C, Fig. S2.1D).

To gauge the translational relevance of this finding, we assessed tumoral β3 expression in a tissue microarray (TMA) of high-risk, post-chemotherapy clinical specimens taken from 38 patients with localized TNBC who did not achieve pathological complete response (pCR) after neoadjuvant chemotherapy (Fig. 2.1D). We evaluated tumor cell-specific β3 expression by immunohistochemistry (IHC), designating samples as either Low or High based on staining intensity and β3+ cell frequency (see Materials and Methods). Of the 38 usable cores with residual tumor present after chemotherapy, 97% of tumor specimens had positive tumoral β3

staining. 27 (71%) were characterized as Low tumoral β3 expression, while 11 (29%) were High (Fig. 2.1D and E). As expected, we observed a consistent vascular pattern of strong β3 expression on neoangiogenic endothelium in the tumors, which served as a positive control for β3 staining (Fig. S2.1E)[183]. Kaplan-Meier analysis of differences in recurrence-free survival (RFS) between patients with β3 Low and High post-chemotherapy residual tumors revealed a trend toward increased risk of recurrence in the High group, particularly after the first 1.5 years after diagnosis (note curve cross in Fig. 2.1F), though this was not statistically significant in our relatively small sample (HR 1.75, 0.66-4.74; p=0.254) (Fig. 2.1F). To validate this finding in a larger cohort, we used a publicly available gene microarray database to perform a separate RFS analysis in 315 TNBC patients who had received chemotherapy [184]. In this data set, patients with increased tumoral β3 expression (High, upper three quartiles) were twice as likely to experience recurrence compared to patients in the lowest quartile of expression (Low) (HR = 2.01, logrank p<0.0095) (Fig. 2.1G). Together, these data suggest that β3 expression is increased and associated with worse outcomes after chemotherapeutic challenge.

Integrin β3 promotes docetaxel resistance in bone metastases

We next considered that functional differences in β3+ tumor cells might drive poor outcomes after chemotherapy. To evaluate this, we measured proliferation changes in cells with high and low β3 expression after chemotherapy *in vitro*. PyMT-BO1 cells were exposed to DTX *in vitro* and BrdU incorporation was assessed by flow cytometry in β3hi (High) and β3lo (Low) populations. The β3lo population of DTX-treated PyMT-BO1 cells exhibited significantly reduced BrdU incorporation compared to β3lo cells receiving vehicle (48% reduction, p<0.0001). Interestingly, BrdU incorporation by β3hi cells present in the same cultures was unchanged between DTX and vehicle-treated samples (Fig. 2.2A), suggesting that β3-expressing

cells respond differently to DTX. To address this, we employed CRISPR/Cas9 technology to generate *Itgb3* knockout (β3KO) derivatives of the PyMT-BO1[185] and 4T1 (Fig. S2.2A) murine breast cancer cell lines.

Cell viability of β3KO derivatives was measured using the MTT assay. Both β3WT and β3KO 4T1 cells were sensitive to DTX administration *in vitro*, with β3WT cells showing only modestly higher viability (Fig. 2.2B). Given that integrins enhance cell adhesion[180], and that tumor cell co-culture with bone marrow stromal cells (BMSCs) increases chemoresistance[186], we also assessed the DTX viability of β3WT and β3KO 4T1 derivatives in BMSC co-culture. In these conditions, β3WT 4T1 cells exhibited enhanced resistance to DTX compared to single culture, while BMSC co-cultured β3KO 4T1 derivates remained sensitive (Fig. 2.2B). We found similar *in vitro* DTX viability trends in β3WT and β3KO PyMT-BO1 derivatives (Fig. S2.2C).

Given the contribution of the tumor microenvironment to therapeutic responses[178], we next interrogated the role of β3 in chemoresistance in murine bone metastases. Mice bearing systemically disseminated β3WT or β3KO 4T1 cells were administered either DTX or vehicle and assessed for differences in organ tumor burden by *ex vivo* BLI. Across all organs analyzed (kidneys, lung, liver, and hindlimb bones) in β3WT tumors, there was no significant difference in bioluminescence between vehicle and DTX-treated groups (Fig. 2.2C, Fig. S2.2B). By contrast, hindlimb bones from DTX-treated mice bearing β3KO cells exhibited significantly (50.6-fold) reduced tumor burden compared to vehicle, with visceral organs also exhibiting trends toward decrease (kidneys: 5.3-fold; lung: 1.2-fold; liver: 5.7-fold) (Fig. 2.2C, Fig. S2.2B). Parallel experiments using β3WT and β3KO PyMT-BO1 cells revealed similar findings, with β3KO bone metastases showing the greatest decrease after DTX (Fig. S2.2D and E). Taken together, these results suggest that tumoral β3 not only marks cells with increased proliferative capacity after

chemotherapy, but also plays a functional role in their chemoresistant phenotype.

Rescue of integrin β3 expression restores chemoresistance in a signaling-dependent manner

Having established that β3 deletion sensitizes bone metastases to DTX, we next asked if β3 rescue in β3KO breast cancer cells was sufficient to restore DTX resistance. To do this, clone #1 β3KO PyMT-BO1 cells (β3KO1-BO1) were retrovirally engineered to express either an empty vector (pMx), a functional human integrin β3 construct (hβ3), or the DiYF integrin β3 mutant (Δβ3), which can bind ligand but is incapable of downstream signaling (Fig. 2.3A)[145]. *In vitro*, hβ3-expressing cells were significantly more viable than pMx-expressing cells by MTT after DTX exposure (~3.6nM vs. ~1.6nM IC50, p<.0001). Rescue with signaling-deficient Δβ3 mutant, by contrast, had no effect on viability (~1.2nM vs. ~1.6nM IC50, p=0.3678) (Fig. 2.3B). These data were further corroborated by diminished apoptosis and enhanced proliferation in hβ3-expressing cells compared to both empty vector and Δβ3-rescue after DTX exposure (Fig. 2.3C and D). In BMSC co-culture, hβ3 rescue resulted in a highly significant increase in DTX resistance compared to wild type PyMT-BO1 cells (Fig. S2.3A), which have lower β3 expression at baseline.

To confirm this phenomenon *in vivo*, we established β3KO1-BO1 derivative metastases in mice and administered DTX or vehicle as before. As expected, empty vector β3KO metastases of the kidneys, lungs, and hindlimbs were sensitive to DTX (4.8-fold, 2.5-fold, and 6.3-fold decrease from vehicle, respectively). Organs harboring hβ3-expressing tumors, meanwhile, exhibited no significant difference in BLI between DTX and vehicle-receiving mice. Importantly, signaling-deficient Δβ3-rescued tumors were notably sensitive to DTX, with statistically similar fold decreases to empty vector groups (Fig. 2.3E).

To evaluate the role of β3 rescue for chemoresistance in the setting of early dissemination, we established orthotopic mammary fat pad (MFP) tumors using either pMx empty vector (β3KO) or hβ3-rescued β3KO1-BO1 cells and performed resection once they had reached a similar size by caliper measurement (~1100mm^3). After survival surgery, mice were assigned to receive three rounds of either vehicle or DTX based on post-resection tumor weight (Fig. S2.3B). 2.5 to 3 weeks post-surgery, mice were sacrificed for *ex vivo* evaluation of metastasis by BLI and quantification of occult tumor burden in the bone marrow by qPCR (see experimental schema, Fig. 2.3F). We did not observe any significant differences in overt metastatic burden between the treatment groups by BLI (data not shown). In marrow flushed from BLI-negative bones, however, we detected a significant decrease in *Luc2* burden after adjuvant DTX treatment of pMx-expressing disseminated tumor cells. The burden of hβ3-expressing DTCs, meanwhile, was not significantly altered by adjuvant DTX administration (Fig. 2.3F).

Taken together, these results suggest that β3 expression was sufficient to promote increased resistance to DTX *in vitro* and *in vivo*, and that this phenotype requires intact integrin signaling.

Integrin β3 mediates an alternative metabolic response to docetaxel

Our results suggested that β3-mediated chemoresistance was most evident in the bone metastatic microenvironment. To evaluate the role of β3 expression in the DTX response of individual tumor cells in this context, we performed ultrastructural analysis of DTX-treated β3WT and β3KO 4T1 murine bone metastases by transmission electron microscopy (TEM) (Fig. 2.4A). Vehicle-treated bone metastases were grossly similar, with no evident differences in organelle morphology or ECM composition. In DTX-treated β3KO tumors, many breast cancer cells exhibited membrane blebbing and fragmentation, consistent with a higher level of cell death. Individual mitochondrial area was increased compared to vehicle in β3KO (Fig. S2.4A), but the

ratios of neither total mitochondrial area nor rough endoplasmic reticulum (RER) area to cytosolic area was altered (Fig. 2.4B and C). In DTX-treated β3WT bone metastases, breast cancer cells remained largely intact, and were notably embedded in abundant fibrillar ECM not observed in vehicle-treated tumors. In contrast to β3KO, rough ER area was markedly increased from vehicle, with pronounced cisternae clearly visible (WT vehicle: 4.5% RER-to-cytosol; WT DTX: 14.9% RER-to-cytosol, $p<0.0001$) (Fig. 2.4B). Similar to DTX-treated β3KO tumors, individual mitochondrial area was increased in DTX-treated β3WT (Fig. S2.4A), while total mitochondrial area was unchanged. Together, these results suggest that DTX administration elicits tumoral β3-dependent changes in the cellular and microenvironmental ultrastructure of bone metastases.

To further identify a potential mechanistic link between β3 expression and chemoresistance, we generated RNA-Seq transcriptomic profiles of β3WT and β3KO cells after DTX or DMSO exposure *in vitro*. Gene set enrichment analysis (GSEA) of biological process and cellular compartment gene ontology (GO) terms in 4T1 profiles revealed β3-dependent enrichment of genes associated with endoplasmic reticulum, the unfolded protein response, and collagen-containing ECM after DTX administration (Fig. 2.4C, Fig. S2.4B). We further leveraged hallmark GSEA[187] to isolate functional pathways of interest, focusing on those where β3WT and β3KO DTX responses were most different. A group of metabolism-related pathways was the most enriched during the β3-mediated DTX response in PyMT-BO1 cells, many of which were also positive in the 4T1 analysis (Fig. 2.5A, see dashed line box). Interestingly, the hallmark pathway with the greatest positive difference in both 4T1 and PyMT-BO1 was OXPHOS (4T1: +3.2 net NES; BO1: +7.3 net NES) (Fig 2.5A).

To functionally validate OXPHOS enrichment during the β3WT DTX response, we performed *in*

vitro extracellular flux analysis of oxygen consumption rate (OCR) in both 4T1 and PyMT-BO1 lines. We found significantly increased maximum OCR after DTX in hβ3-expressing β3KO1-BO1 cells, while empty vector (β3KO) exhibited no or minimal increase compared to vehicle treatment (Fig. 2.5B). Likewise, in 4T1, we found significant increases in maximum OCR after DTX in β3WT not seen in β3KO cells (Figure 2.5B). Interestingly, the differences in OCR between 4T1 β3WT and β3KO were observed on plates coated with vitronectin (a ligand recognized by activated αvβ3 integrin) but not on regular tissue culture-treated plates (Fig. S2.5A and B).

These differences in bulk oxygen handling after chemotherapy prompted investigation of reactive oxygen species (ROS), another pathway identified in our hallmark analysis (Fig. 2.5A). Galuminox, a novel fluorescent metalloprobe[188], allowed us to directly image hydrogen peroxide and superoxide in live 4T1 cells by confocal microscopy. These studies revealed a nearly 5-fold increase in β3WT ROS after DTX, while ROS after DTX in β3KO cells was not significantly different (Fig. 2.5C). Taken together, our results suggest that β3 mediates an alternative metabolic response to DTX treatment in breast cancer cells.

mTORC1 inhibition reverses β3-mediated chemoresistance

We searched our hallmark GSEA for metabolically relevant signaling pathway targets that could be used in combination with DTX to overcome resistance. We found mTORC1 activity and its target E2F, both established regulators of mitochondrial metabolism and protein synthesis[189], to be among the most significantly enriched signaling pathways in hβ3-expressing cells exposed to DTX (mTORC1 NES 3.7, $q<0.0001$; E2F NES 4.1, $q<0.0001$) (Fig. 2.6A). To functionally validate the importance of mTORC1 activity in β3WT 4T1 cells without chemotherapy, we assessed viability after exposure to the mTORC1 inhibitor everolimus (mTORCi). β3WT 4T1

cells exhibited significant viability reduction compared to DMSO control, while β3KO viability was unaffected (Fig. 2.6B). Our *in vivo* TEM images revealed that β3WT cells undergo RER expansion after exposure to DTX, possibly as part of an unfolded protein stress response (Fig. 2.4). To determine the effect of combination DTX and mTORCi on this phenotype *in vitro*, we assessed *de novo* protein synthesis by incorporation of a fluorescent HPG-methionine analog in β3WT and β3KO 4T1 cells exposed to either DTX, mTORCi, or both. At baseline, β3WT cells incorporated almost 65% more HPG-methionine than β3KO. DTX reduced HPG-methionine incorporation by 25% in β3WT cells, but did not affect *de novo* protein production in β3KO. Importantly, while mTORCi alone had no effect on HPG-methionine incorporation by β3WT cells, combination with DTX resulted in a 60% reduction compared to vehicle, almost twice the reduction observed in β3KO (Fig. 2.6C). Considering previous demonstration of a link between β3 signaling and mTORC1 activity[190, 191], in addition to the clinically approved use of mTORC1 inhibitors in breast cancer patients, we decided to pursue it as a candidate for combination therapy with DTX in breast cancer bone metastases.

To evaluate this combination strategy, we established β3WT PyMT-BO1 bone metastases by i.c. injection. Mice were randomized to receive either vehicle, DTX alone, the mTORC1 inhibitor rapamycin alone (RAPA), or combined treatment (COMBO). While *ex vivo* BLI bone tumor burden in groups receiving DTX or RAPA alone was not significantly different from vehicle, combination therapy synergistically attenuated bone metastases (5.5-fold reduction compared to vehicle, $p<0.01$) (Fig. 2.6D). This effect was not observed in visceral metastases (Fig. S2.6A).

αvβ3-targeted nanoparticles loaded with mTOR inhibitor enhance docetaxel efficacy in bone metastases

To confirm β3-dependent synergy and provide proof of principle for this strategy in a precision

medicine setting, we modified our αvβ3-targeted micelle nanoparticle[175] with a rapamycin cargo (αvβ3-RAPA-NP) to specifically deliver rapamycin to cells expressing activated αvβ3 integrin heterodimers (Fig. 2.7A, Fig. S2.7A). Mice bearing β3WT PyMT-BO1 bone metastases were randomized to receive either cargo-free control nanoparticles (αvβ3-CF-NP), combination αvβ3-CF-NP and free DTX, or combination αvβ3-RAPA-NP and free DTX. By *ex vivo* BLI (Fig. 2.7B), as well as X-ray analysis (Fig. 2.7C), we found that combination αvβ3-RAPA-NP and free DTX was significantly more effective to decrease bone tumor burden and tumor-induced bone loss (osteolysis) than cargo-free nanoparticles and free DTX (Fig 2.7B and 2.7C). As before, the effect on tumor burden was not significant in visceral metastases (Fig. S2.7B). Additionally, rapamycin loading did not increase serum markers of therapy-induced toxicity compared to cargo-free particles in combination with DTX (Fig. S2.7C). Taken together, these data suggest mTORC1 inhibition as a strategy for combination with taxane therapy in the bone metastatic setting.

2.4 Discussion

Bone metastases are a common manifestation of breast cancer, and up to 30% of patients will present with only bone involvement[192]. The biology of bone lesions is fundamentally different from that of either the primary tumor or visceral metastatic sites[70]. Bone-targeted agents such as bisphosphonates and denosumab have improved patient quality of life, but these therapies are not curative and largely spare the tumor itself [24].

Exposure to the bone microenvironment modulates tumor cell phenotype [69, 97]. In previous studies, we found that bone-induced TGF-β signaling upregulates β3 expression in breast cancer cells[175]. The current study expands on this finding, demonstrating that tumoral β3 expression

itself promotes chemoresistance characterized by an alternative metabolic response to DTX. We further showed that combination rapamycin and DTX overcomes β3-mediated resistance. Finally, administration of rapamycin-loaded, αvβ3-targeted nanoparticles specifically improved DTX response in murine bone metastases, providing proof of principle for an effective strategy that might circumvent possible toxicities associated with combination therapy.

β3+ murine breast cancer cells were increased after *in vitro* chemotherapy, corroborating results in human cells reported by Vellon and colleagues[193]. We found that DTX *in vitro* also failed to reduce proliferation in the β3hi population, prompting us to consider that DTX selects for resistant cells with higher β3 expression. This hypothesis was supported by our *in vivo* findings, where β3+ tumor cells were enriched in bone metastases remaining after systemic DTX treatment. In human patients, incomplete response to neoadjuvant chemotherapy is associated with significantly worse outcomes[194], likely driven by selection for and reprogramming toward resistance in the cells that survive[195]. Using publicly available data, we found that β3 expression at diagnosis was associated with a higher recurrence risk in TNBC patients receiving any chemotherapy. Consistent with this, we found populations of β3+ residual tumor cells in 97% of post-chemotherapy tissue specimens we analyzed from high-risk patients with localized TNBC who failed to achieve a pCR after neoadjuvant chemotherapy. While our power to detect survival differences in this TMA cohort was hampered by sample size, we found a trend toward increased risk of recurrence in patients with High β3 expression. This difference was especially pronounced after a curve crossing event ~1.5 years after diagnosis, raising the possibility that β3 expression might be more relevant to recurrence later in the course of TNBC. Studies are planned to recapitulate these analyses in a larger cohort of patient samples chosen with this temporal component in mind.

β3 is an important promoter of bone metastasis[60], is upregulated in bone metastases compared to the primary and visceral sites[175], and has previously been implicated in resistance to therapies across several cancer types[158, 196, 197]. Despite this, direct pharmacological blockade of αvβ3 has not shown significant activity in clinical trials of aggressive and advanced cancers[143], and in some preclinical models actually potentiates pro-tumor neoangiogenesis[198] and immunosuppression[150]. β3 studies in breast cancer have hinged primarily on *in vitro* characterization with pharmacological blockade or on the role of β3 in promoting metastasis[60, 158]. Using CRISPR/Cas9 technology, we performed β3 knock out and retroviral rescue experiments to test the specificity of the chemoresistance phenotype for tumoral β3 and to determine the necessity of β3 signaling for chemoresistance in the setting of an intact immune system. Because manipulation of tumoral integrin β3 could also affect tumor growth[60, 199], we used each genetic line as its own control, normalizing treated samples to their corresponding vehicle-treated group, then comparing differences across genotypes. We show here that bone metastases lacking integrin β3 were significantly more sensitive to docetaxel than wild type metastases.

In vitro, β3WT and β3KO breast cancer cells were both highly sensitive to docetaxel. By contrast, *in vivo* β3WT bone metastases were relatively resistant, and experiments with a signaling-deficient mutant suggested that intact β3 signaling was required for survival. Bone ECM harbors αvβ3 ligands that might be absent from standard tissue culture. *In vitro* survival increased when β3WT cells were plated on BMSCs compared to β3KO, suggesting ligand availability as a potential factor in integrin-mediated resistance. Integrin activation, which induces a conformational change that exposes the ligand binding domain, is typically required for ligand binding and signaling[118]. It is possible that β3 activation in the bone microenvironment

results in easier access to ECM ligands. Moreover, compared to standard cell culture, the bone metastatic microenvironment has a lower pH and oxygen concentration, higher stress modulus, and distinct nutrient and chemical milieu[70], all of which can influence cancer cell reliance on αvβ3 signaling[96, 191, 200].

To further evaluate the role of β3 on chemotherapy resistance in bone, we performed TEM of DTX-treated β3WT and β3KO 4T1 bone metastases. As expected from BLI and histology, tumor cells from DTX-receiving β3KO bone metastases exhibited signs associated with maladaptive stress and cell death. DTX-receiving β3WT tumor cells, by contrast, demonstrated an adaptive increase in endoplasmic reticulum and the appearance of extensive, fibrillar ECM. Dysregulation of the ECM has far-reaching effects on tumor biology, including therapy resistance[178], and is particularly noteworthy for a chemoresistance phenotype driven by integrin binding to ECM ligands. Experiments are ongoing to determine the molecular composition and cellular source of this ECM, as well as the mechanism by which integrin signaling regulates these changes.

We identified endoplasmic reticulum (protein production), ECM enrichment, and OXPHOS as potential downstream targets of β3 signaling in the context of chemotherapy. Although no β3-mediated changes in mitochondrial ultrastructure were evident by TEM, our *in vitro* studies showed that DTX consistently induced increased OCR in β3WT compared to β3KO cells. Live cell imaging of 4T1 cells further demonstrated robust β3-mediated increases in DTX-induced ROS generation, suggestive of an alternative metabolic response. Altered OXPHOS and ROS in malignant cells have been increasingly recognized as drivers of therapeutic resistance[201, 202], suggesting the potential for emerging mitochondrial-targeted agents to sensitize refractory breast cancer bone metastases to chemotherapy.

Consistent with increased ER observed *in vivo*, we found that *in vitro* protein production was higher at baseline and more responsive to docetaxel in β3WT cells. Recent evidence indicates that tumoral ER stress is a common feature of breast cancer bone metastases[203], and others have shown that integrin signaling bolsters *in vitro* protein production during hypoxia[191]. These data raise the possibility that either inability to mount a pro-chemoresistance protein production program or diminished tolerance for ER stress[204] could drive the large chemosensitizing effect we observe from β3KO in the bone compared to more modest effects at other metastatic sites, where tumoral β3 expression is not as high. Future studies are planned to more specifically evaluate the ER stress and unfolded protein responses in β3-mediated chemoresistance. Further, single-cell RNA and ribosomal sequencing of tumor cells collected directly from bone metastases would be invaluable to further dissect the molecular mechanisms of β3 signaling during chemotherapy treatment *in vivo*.

The mTORC1 pathway was enhanced after DTX treatment of β3WT cells and is a demonstrated target of αvβ3 signaling in breast cancer[190, 191]. Given that it also acts as a master regulator of mitochondrial biogenesis and protein translation[189], we selected mTORC1 inhibition for combination therapy with DTX. Administration of the mTORC1 inhibitor rapamycin alone or DTX alone had little effect on the growth of PyMT-BO1 bone metastases, while rapamycin and DTX together significantly attenuated tumor burden in bone. Notably, this synergistic effect was exclusive to bone, where tumor expression of β3 is high; rapamycin had little effect on DTX response in visceral metastases, where β3 expression is significantly lower[175]. mTORC1 inhibition alone has been shown to restrict tumor growth in bone micrometastases[205], suggesting that combination with DTX may be beneficial for adjuvant metastasis prevention[206]. Bone macrometastases, by contrast, are non-responsive[205, 207], though single-agent mTOR inhibition

has been shown to attenuate osteolytic bone loss, which might contribute indirectly to our findings[207].

To test the specific effect of rapamycin inhibition in αvβ3-expressing cells, we co-administered rapamycin-loaded, αvβ3-targeted nanoparticles with free DTX. We have previously shown that αvβ3-NPs preferentially home to breast cancer bone metastases in mice[175]. Combination of mTOR inhibitors and taxane chemotherapy is clinically challenging due to toxicity[208], but αvβ3-NPs can reduce drug availability in the circulation by influencing release kinetics[164, 175]. In the current study, combination therapy with docetaxel and αvβ3-RAPA-NP was more effective than docetaxel alone against PyMT-BO1 bone metastases, demonstrating that the efficacy of mTORC1 inhibition is in part mediated by its specific activity in cells expressing activated αvβ3 integrin. We also found that combination of αvβ3-RAPA-NP with DTX did not significantly affect serum markers of toxicity in mice, a promising initial indicator for potential clinical translation.

Taken together, our data identify β3 as a mediator of docetaxel resistance in breast cancer bone metastases, where it promotes an alternative metabolic response to treatment characterized by perturbations in OXPHOS, ROS, and protein production. mTORC1 inhibitors, given systemically or packaged in αvβ3-targeted nanoparticles, can be leveraged in combination with docetaxel to sensitize β3-expressing bone metastases to therapeutic attenuation. Above all, our findings highlight the need for therapeutic strategies that consider the microenvironmental context of the tumor when targeting metastatic cells.

2.5 Materials and Methods

Animals

All animal studies were performed according to Washington University Institutional Animal Care and Use Committee (WU IACUC, Protocol# 20190104) guidelines. Female C57BL/6J (Jax, RRID:IMSR_JAX:000664) and BALB/c (Jax, RRID:IMSR_JAX:000651) mice were obtained from The Jackson Laboratory and injected at 6-7 weeks of age. All mice were housed under pathogen-free conditions according to the WU IACUC.

Cell lines and constructs

The C57BL/6 background PyMT-BO1-GFP-Luc murine breast tumor cell line was previously developed and validated as described[150]. The BALB/c background 4T1-FL-GFP murine breast tumor cell line (derived from 4T1, RRID:CVCL_0125) was originally from Dr. David Piwnica-Worms (The University of Texas, Houston, TX) as previously described[64]. All cell lines were cultured at low passage (used within 1-3 passages after thaw) and tested regularly for Mycoplasma-specific DNA by PCR amplification of cell or supernatant samples. For in vitro experiments involving coated culture dishes, non-tissue culture-treated plates were coated prior to cell seeding with either poly-L-lysine (Sigma: P4707) or Vitronectin XF (STEMCELL Technologies: 07180) according to manufacturer's recommendations.

CRISPR knockout of the Itgb3 gene in the PyMT-BO1 line was previously described[185]. pMx, pMx-Δβ3, and pMx-hβ3 retroviral vectors used for rescue of β3 expression in the clone #1 β3KO PyMT-BO1 (β3KO1-BO1) line were a gracious gift from Steven Teitelbaum (Washington University School of Medicine, St. Louis, MO). Virus was packaged along with the pCMV-VSVG plasmid using the Plat-E cell line (RRID:CVCL_B488)[209]. Tumor cell lines were transduced with viral supernatant for 12 hours at 37°C in 6-well tissue culture plates. Transduced cells were selected in 2ug/mL blasticidin (Sigma: 203350), and stable protein expression of the wild type (hβ3) and signaling mutant (Δβ3) integrin constructs was validated by western blot.

CRISPR knockout of Itgb3 in the 4T1 cell line was achieved by stable transduction of the Cas9 gene and the following gRNAs: 5'-CACCGCCGGGATAACCTCGTTGTTG-3'; 5'-AAACCAACAACGAGGTTATCCCGGC-3', using the lentiCRISPR v2-Puro vector system (Addgene#: 98290). 293T cells (ATCC, RRID:CVCL_0063) were used for viral packaging with the pCMV-DR8.2 and pCMV-VSVG plasmids. Tumor cell lines were transduced with viral supernatant for 12 hours at 37°C in 6-well tissue culture plates. Transduced cells were selected in 10ug/mL puromycin (Sigma: P8833) and further purified by serial FACS sorting of TGF-β1 (2ng/mL, R&D Systems: 7666-MB-005) stimulated cells based on β3 expression. *Itgb3* knockout cell lines were validated by sequencing and FACS.

Cell viability assays

For cell viability assays, cells were plated in tissue culture-treated multiwell plates (TPP, Trasadingen, Switzerland), left to adhere for 16-24h, treated with serial dilutions of docetaxel, and analyzed at indicated time point for viability by MTT as previously described [62]. Optical density for 570 and 630 was read with either a SpectraMax M5e plate reader (Molecular Devices, Sunnyvale, CA) or a Synergy HT plate reader (BioTek/Agilent), and the OD570-630 of each technical replicate was divided by the average of untreated samples of the same line to obtain % viability. Where indicated, logIC50 was statistically determined using nonlinear fit by least squares regression (four parameter, variable slope) in Prism 8. For apoptosis assays, caspase-3/7 activity was determined using the Caspase-Glo 3/7 Assay System (Promega: G8090) and normalized to cell viability as reported by incubation with CellTiter-Blue (Promega: G8080). Colorimetric and luminescent readouts were measured with a SpectraMax i3 plate reader (Molecular Devices, Sunnyvale, CA).

Murine bone marrow stromal cell co-culture

For co-culture assays, murine bone marrow stromal cells (BMSCs) were harvested from pelvic or leg bones and cultured as previously described[210]. Breast cancer cells (0.5-1x10^4/well) were parachuted on confluent BMSC in 96-well tissue culture-treated plates (TPP) and left to adhere overnight. Co-cultures were then treated with serial dilution of docetaxel (0.8 nM to 1μM in media) and analyzed by MTT after 72h. BMSC alone showed no reduction of formazan fixation at the doses in use, so OD750-630 was normalized by cell line as described.

In vivo modeling of metastasis and therapy

Distant metastases were established in mice by intracardiac (i.c.) inoculation of PyMT-BO1 or 4T1 cells into the left ventricle as previously described[175]. Tumor burden was monitored by *in vivo* bioluminescence imaging (BLI). Mice were assigned randomly by cage to treatment groups; mouse weight and hindlimb tumor burden were compared to ensure no statistical differences between groups prior to treatment initiation. Docetaxel (5mg/kg, LC Laboratories: RP 56976) or equivalent vehicle was freshly prepared and administered by tail vein injection. Freshly prepared working solution of rapamycin (Sigma: R0395) or equivalent vehicle was administered 2mg/kg by i.p. injection. An equimolar equivalent of nanoparticle-encapsulated rapamycin or cargo-free nanoparticle control was administered by tail vein injection for nanoparticle experiments.

A mammary fat pad resection model was utilized for studies involving disseminated tumor cells. For these experiments, orthotopic tumors were established by injection of 1x10^5 cells in 40μL of PBS into the fourth mammary fat pad of 8-week-old female B6 mice. Tumors were then surgically resected after surpassing ~1100mm^3 by caliper measurement. Post-surgery, mice were placed in treatment groups by alternating assignment, adjusted as needed to ensure no statistical difference in mean resected tumor size. ~3 weeks after resection, mice were euthanized, and their

hindlimbs were dissected, disarticulated at the patella, and assessed for tumor burden by bioluminescence imaging as below. Bone marrow was then spun out from all BLI-negative bones and subjected to RNA extraction for qPCR assessment of tumor cell-specific *Luc2* gene expression.

Drug preparation for in vivo studies

Docetaxel (LC Laboratories) was initially solubilized in 100% ethanol and stored at -20°C. A 10mg/mL working solution was freshly prepared on the day of injection by dilution in a Tween 80/PBS solution (final Tween 80 : ethanol : PBS ratio of 20:13:67) to prevent precipitation. Finally, working solution was further diluted to 0.9-1mg/mL in PBS. Vehicle control was prepared and diluted in a similar manner using 100% ethanol without docetaxel.

Rapamycin (Sigma R0395) was solubilized in 100% ethanol, diluted to a 1mg/mL working solution in 5% PEG400, 5% Tween 80, then aliquoted and stored at -20°C. 100% ethanol without rapamycin was prepared and stored in a similar way for mice receiving vehicle control. Aliquots of working solution or equivalent vehicle were freshly thawed on the day of injection and administered 2mg/kg by i.p. injection. An equimolar equivalent of nanoparticle encapsulated rapamycin or cargo-free nanoparticle control was administered by tail vein injection for nanoparticle experiments.

Bioluminescence imaging and radiography

In vivo bioluminescence imaging was performed on the days indicated using an IVIS Lumina (PerkinElmer, Waltham, MA; Living Image 4.2), 5min to 1sec exposure, bin2-8, FOV12.5cm, f/stop1, open filter). Mice were injected intraperitoneally with D-luciferin (150mg/kg in PBS; Gold Biotechnology, St. Louis, MO) and imaged using isoflurane anesthesia (2% vaporized in

O2). Mice were euthanized immediately after *in vivo* confirmation of successful intraperitoneal administration of D-luciferin. Organs of interest were then dissected out and imaged separately. Total photon flux (photons/sec) was measured from fixed regions of interest (ROIs) using Living Image 2.6 (RRID:SCR_014247). Investigators were blinded to treatment groups during BLI analyses.

Osteolytic lesions were imaged by X-Ray imaging system (Faxitron). Tibiofemoral lesion area was quantified using ImageJ (NIH, Bethesda, Maryland; RRID:SCR_003070) with investigators blinded to treatment group.

Immunohistochemical staining

All slides were stained in parallel, using identical staining conditions, with anti-integrin β3 (clone: D7x3P, 1:200, Cell Signaling Technology, RRID:AB_2798136) using previously described protocols[175]. Images were acquired on a NanoZoomer (Hamamatsu Photonics).

Post-chemotherapy biopsies from triple negative breast cancer patients

Primary breast cancer specimens were obtained from M0 patients with localized, triple negative disease at time of surgical resection and subsequently banked, curated, and assembled into a tissue microarray by the St. Louis Breast Tissue Registry. Clinical data were obtained in accordance with the Washington University Institutional Review Board (IRB #201102394) and WAIVER of Elements of Consent per 45 CFR 46.116 (d)., and deidentified prior to investigator access. IRB-directed human research activities were guided by principles set forth in the Belmont Report.

Areas of invasive tumor and tumor cell β3 expression by DAB staining were confirmed in consultation with a board-certified pathologist. β3 expression was scored by a group of

investigators, all blinded to clinical annotation, using a bimodal classification system focused exclusively on positive staining in tumor cells. For each specimen, the percentage of identifiable tumor cells with β3 staining was jointly determined by the scoring group. Based on the range of tumoral β3 staining observed in the cohort as a whole, a cutoff of 10% was determined, with samples below this threshold assigned to the "Low" expressing group and those above assigned to the "High" expressing group. Samples for which the scoring group was not unanimous were referred to a pathologist for resolution.

Survival analysis in human patients

Recurrence-free survival (RFS, defined as date of diagnosis to date of 1st local or distant recurrence, otherwise censored at last known recurrence-free date) of β3 Low versus High triple negative breast cancer (TNBC) core samples after neoadjuvant chemotherapy was determined by Kaplan-Meier analysis using Cox proportional hazards and log rank test in consultation with a statistician in the Siteman Biostatistics Shared Resource. Relevant patient demographic data and tumor characteristics were compared between groups using Wilcoxon rank sum and Fisher's exact tests. RFS in publicly available data was determined by Kaplan-Meier analysis through KM-Plotter[184], comparing TNBC patients receiving any chemotherapy in the lowest quartile of β3 expression to those in the three upper quartiles.

Bone sample preparation for transmission electron microscopy

At Day 15 experimental endpoint, mice were euthanized and perfused with heparin-supplemented PBS, followed with a 2.5% glutaraldehyde, 2% paraformaldehyde fixative solution buffered at pH 7.4 by 0.15M cacodylate with 2mM $CaCl_2$ (TEM fixative). Hindlimb bones were dissected out and submerged in TEM fixative overnight at 4°C. Samples were then decalcified in 14% M EDTA (pH 7.2) for 14 days with mild agitation and periodic switch into

fresh EDTA. Afterwards, samples were rinsed in cacodylate buffer 3 times for 10 minutes each, and subjected to a secondary fixation in 1% osmium tetroxide/1.5% potassium ferrocyanide in cacodylate buffer for one hour, rinsed in ultrapure water 4 times for 10 minutes each, and stained in an aqueous solution of 2% uranyl acetate for one hour. The samples were washed again in ultrapure water 4 times for 10 minutes each and dehydrated in a graded acetone series (10%, 20%, 30%, 50%, 70%, 90%, 100% x4) for 15 minutes in each step. Tissues were then infiltrated with microwave assistance (Pelco BioWave Pro, Redding, CA) into Spurr's resin and cured in an oven at 60˚C for 80 hours.

Transmission electron microscopy of murine bone metastases

Mice bearing 4T1 bone metastases were established, treated, and monitored as described above and in **Fig. 2.2C**. After tissue processing, X-ray microscopy (XRM Versa 520, Zeiss) was performed to identify tumor regions in hindlimb bone samples for thin sectioning. 70nm thin sections were prepared on grids, stained with 2% aqueous uranyl acetate followed by Reynold's lead citrate, and imaged on a TEM (JEOL JEM-1400 Plus) at 120 KeV. Ultrastructural parameters were quantified using ImageJ (NIH, Bethesda, Maryland; RRID:SCR_003070).

RNA sequencing and analysis

RNA-Seq was performed with the Genome Technology Access Center at Washington University School of Medicine.

For transcriptomic profiles of β3KO1-BO1 cells, the pMx, Δβ3, and hβ3 lines were cultured in biological triplicate on tissue culture-treated 6-well plates for 24h in the presence of DMSO or 10nM DTX, followed by lysis and RNA extraction using the RNeasy Plus Mini Kit (QIAGEN: 74134). Total RNA integrity was determined using Agilent Bioanalyzer. Library preparation was

performed with 1ug of total RNA. Ribosomal RNA was removed by a hybridization method using Ribo-ZERO kits (Illumina-EpiCentre). mRNA was then fragmented and reverse transcribed to yield cDNA using SuperScript III RT enzyme (Life Technologies, per manufacturer's instructions) and random hexamers. A second strand reaction was performed to yield ds-cDNA. cDNA was blunt ended, had an A base added to the 3' ends, and then had Illumina sequencing adapters ligated to the ends. Ligated fragments were then amplified for 13 cycles using primers incorporating unique index tags. Fragments were sequenced on an Illumina HiSeq3000 using single end reads extending 50 bases. Sequencing reads were checked for quality using FastQC[211] and aligned to the mouse reference genome (mm10) using the splice-aware alignment tool HISAT2[212] guided by the transcript annotation downloaded from the UCSC genome browser[213]. Subsequently, featureCounts[214] was used to quantify the raw count of reads mapped to the transcripts.

For transcriptomic profiles of 4T1 lines, β3WT and β3KO were cultured in biological triplicate on poly-L-lysine-coated 6-well petri dishes for 24h in the presence of DMSO or 10nM DTX. After a 48h drug-free recovery period, cells were lysed and RNA extracted using the RNeasy Plus Mini Kit (QIAGEN: 74134). Total RNA integrity was determined using Agilent 4200 Tapestation. Library preparation was performed with 1ug of total RNA. Ribosomal RNA was removed by an RNase-H method using RiboErase kits (Kapa Biosystems). mRNA was then fragmented in reverse transcriptase buffer and heated to 94 degrees for 8 minutes. mRNA was reverse transcribed to yield cDNA using SuperScript III RT enzyme (Life Technologies, per manufacturer's instructions) and random hexamers. A second strand reaction was performed to yield ds-cDNA. cDNA was blunt ended, had an A base added to the 3' ends, and then had Illumina sequencing adapters ligated to the ends. Ligated fragments were then amplified for 12

cycles using primers incorporating unique dual index tags. Fragments were sequenced on an Illumina NovaSeq-6000 using paired end reads extending 150 bases. Basecalls and demultiplexing were performed with Illumina's bcl2fastq software and a custom python demultiplexing program with a maximum of one mismatch in the indexing read. RNA-Seq reads were then aligned to the Ensembl release 76 primary assembly with STAR version 2.5.1a[215]. Gene counts were derived from the number of uniquely aligned unambiguous reads by Subread:featureCount version 1.4.6-p5[214]. Isoform expression of known Ensembl transcripts was estimated with Salmon version 0.8.2[216]. Sequencing performance was assessed for the total number of aligned reads, total number of uniquely aligned reads, and features detected. The ribosomal fraction, known junction saturation, and read distribution over known gene models were quantified with RSeQC version 2.6.2[217].

For both projects, gene counts were used for expression normalization and differential expression analysis using edgeR[218]. Ranked lists of normalized expression values were then imported into GSEA v4.0.1 (Broad Institute, RRID:SCR_003199)[219, 220] for hallmark gene set enrichment analysis[187].

qPCR analysis

Total RNA from cells was isolated with the RNeasy Mini Plus Kit (Qiagen). Complementary DNA was made using the SuperScript II first-strand synthesis system for qPCR (Invitrogen). qPCR was performed using SYBR Advantage mix (Bio-Rad) as described previously[150] with the following gene-specific primers: *Luc2* forward 5'-CGG TGT TGG GCG CGT TAT TTA-3'; *Luc2* reverse 5'-TCG ACT GAA ATC CCT GGT AAT C-3'; *Gapdh* forward: 5'-AGG TCG GTG TGA ACG GAT TTG-3', *Gapdh* reverse: 5'-TGT AGA CCA TGT AGT TGA GGT CA-3'.

Flow cytometric analysis

In vitro tumor cells were lifted with 1x Versene (Gibco: 15040066) unless otherwise indicated. For *ex vivo* analysis of murine bone metastases, hindlimb bones were dissected and the tibiofemoral joint isolated and finely crushed with surgical scissors. Manually processed samples were further digested in collagenase A (Roche) and DNase I (Sigma-Aldrich) at 37°C for 1 hour with agitation. Digested samples were strained through 70μm Falcon nylon filters (Corning: 352350) and prepared as single cell suspensions in 5% FBS PBS with 1mM EDTA (Corning). Cells were stained with either PE- or AlexaFluor-647-conjugated anti-mouse integrin β3 (1:200, clone: 2C9.G2, BD Pharmingen; PE RRID:AB_394800; AF647 RRID:AB_2738255), CD45.2, (1:200, clone: 104, BioLegend, RRID:AB_492872) and DAPI (Sigma: D9542) and acquired on the LSRFortessa (BD Biosciences). FlowJo (TreeStar, RRID:SCR_008520) was used for data analysis and representative flow plot generation.

Protein synthesis assays were performed by incubation of cells with the synthetic methionine analog Click-iT® HPG (L-homopropargylglycine) in methionine-free Dulbecco's Modified Eagle Medium (DMEM, Gibco: 21013) supplemented with 200uM L-cyteine (Sigma: 1.02452), 2mM glutamate (Agilent: 103579-100), and 1mM pyruvate (Agilent: 103578-100) for 30 minutes. Cells were lifted with 0.25% trypsin (Gibco: 25200056), and incorporated Click-iT® HPG was further processed for fluorescent readout by flow cytometry using the Invitrogen Click-iT® HPG Alexa Fluor 594 Protein Synthesis Assay Kit (ThermoFisher: C10428) according to manufacturer's recommendations.

For cell proliferation assays using BrdU incorporation, S-phase entry of proliferating cells was assessed by flow cytometry analysis of 5-bromo-2'-deoxyuridine (BrdU) incorporation overnight using the eBioscience BrdU Staining Kit for Flow Cytometry FITC (ThermoFisher: 8811-6600-

42), according to manufacturer's recommendations.

Western blot analysis

Western blot was performed as previously described[150] using anti-integrin β3 (clone: D7x3P, 1:1000, Cell Signaling Technology, RRID:AB_2798136) primary, followed by horseradish peroxidase–conjugated anti-rabbit secondary antibody (Cell Signaling Technology). β-actin (clone: AC15, Sigma, RRID:AB_476744) was used as a loading control. Bands were developed via enhanced chemiluminescence and analyzed by densitometry in ImageJ (NIH, Bethesda, Maryland, RRID:SCR_003070).

Oxygen consumption analyses

Cells were seeded and treated in 6-well plates as indicated, then lifted with trypsin and re-seeded onto Seahorse XF96 V3 PS Cell Culture Microplates (Agilent: 101085-004) overnight at experimentally optimized density. Extracellular flux analysis of oxygen consumption rate (OCR) was performed on the Seahorse Biosciences XF96 Flux Analyzer (Agilent) at baseline and after serial injection of oligomycin (1.5uM), FCCP (0.5 or 1uM), and antimycin A/rotenone (0.5uM) (Seahorse XF Cell Mito Stress Test Kit, Agilent: 103015-100) according to manufacturer's recommendations. After analysis, luciferase activity in tumor cell samples was determined for normalization using a SpectraMax i3 plate reader (Molecular Devices, Sunnyvale, CA). Data normalization, analysis, and calculation of maximum OCR were performed using Wave Desktop v2.6 (Agilent, RRID:SCR_014526).

Galuminox imaging of radical oxygen species

Live cell fluorescence imaging studies were performed at Washington University Center for Cellular Imaging (WUCCI). For imaging studies, β3WT and β3KO 4T1 cells were plated onto

borosilicate 8-well chambered coverglass (Labtek), allowed to grow to approximately 50% confluence at 37°C under 5% CO2 atmosphere in culture media (200μL), and treated with DTX (10nM) for 24h. Following DTX treatments, all wells were rinsed with fresh media. For evaluating impact of ROS, cells were incubated either with Galuminox (20μM), a mitochondrial ROS sensitive metalloprobe[188], or media alone at 37°C for 1h under continuous influx of 5% CO2. After 1h, cellular accumulation studies were performed with an inverted Nikon A1Rsi laser scanning confocal microscope using a 60x oil objective lens (Nikon Instruments Inc., NY, USA). 405 nm lasers were used for the detection of Galuminox. Throughout the data acquisition process, cells were maintained at 37 °C with 5% CO2, controlled by a Tokai Hit stage-top incubation system (Shizuoka, Japan). Acquisition was performed using Nikon NIS-Elements software (Nikon Instruments Inc., NY, USA.). Images were processed and analyzed using the ImageJ software package (NIH, Bethesda, Maryland; RRID:SCR_003070). Regions of interest were manually drawn around cells, the uptake of Galuminox was quantified (wherein corrected total cellular fluorescence (CTCF) = integrated density–(area of selected cell × mean fluorescence of background readings)) using protocols described elsewhere[221, 222].

Integrin αvβ3 antagonist homing ligand

The vitronectin antagonist specific for activated integrin αvβ3 was a quinalone nonpeptide, developed by Bristol-Myers Squibb Medical Imaging (US patent 6,511,648 and related patents) and coupled to phosphatidylethanolamine-polyethylene glycol 2000 (αvβ3-PEG2000-PE, **Fig. S2.7A**). The antagonist was initially characterized as the 111In-DOTA conjugate RP478 and cyan 5.5 homologue TA145[223–225]. The αvβ3 peptidomimetic had a 15-fold preference for the Mn2+-activated receptor[226, 227] and an IC50 for αvβ5, α5β1 and Gp-IIbIIIa of >10 μM (Bristol-Myers Squibb Medical Imaging, unpublished data). Integrin αvβ3-targeted nanoparticles have an

IC50 of 50pM for the Mn22+ activated integrin αvβ3 receptor (Kereos, Inc., unpublished data). Homing specificity to neovascular sprouts was previously demonstrated in a well-defined Matrigel® plug study using the Rag1^{tm1Mom} Tg(TIE-2-lacZ)182-Sato mouse (Jax, RRID:IMSR_JAX:005707)[228].

Synthesis of αvβ3-RAPA nanoparticles

Phospholipid/polysorbate 80 micelle nanoparticles (NP) were prepared as a microfluidized suspension of 20% (v/v) combining polysorbate 80 (NOF America) with a 2.0% (w/v) commixture and 1.7% (w/v) glycerin in pH 6.5 carbonate buffer. The commixture included 2 mole% rapamycin, 0.15 mole% αvβ3-PEG2000-PE, and high-purity phosphatidylcholine (Lipoid). Rapamycin was excluded from commixture for targeted, drug-free nanoparticles. The lipid commixtures were combined with the polysorbate, buffer, and glycerin and homogenized at 20,000 psi for 4 minutes at 4°C with a microfluidics homogenizer (M110s or LV1, Microfluidics, Inc). Nanoparticles were sterile filtered and preserved under inert gas in sterile sealed vials until use. Dynamic light scattering (Zeta Plus, BrookHaven) showed nominal particle size of 23.9 nm, with polydispersity of 0.258 and an average electrophoretic zeta potential of --1.61mv for the αvβ3-RAPA-NPs, which were closely similar to αvβ3-CF-NP control.

Serum chemistry analysis

Blood was obtained by submandibular venous puncture and collected in Microtainer serum separator tubes (BD Biosciences: BD365967) for serum chemistry analysis using the Liasys 330 AMS Diagnostic liquid chemistry analyzer. Investigators were blinded to treatment groups during analysis.

Statistical analysis

All sample sizes reported in the study are the minimum number of samples. For animal studies, sample sizes were decided based on our previous work in these models. Statistical differences were analyzed using either one-tailed unpaired t test with Welch's correction, ANOVA with Tukey or Sidak test for post hoc multiple comparisons, or ANOVA with test for linear trend using Prism 8 (GraphPad Software Inc., RRID:SCR_002798). Results were considered to reach significance at $P \leq 0.05$ and are indicated with asterisks unless otherwise specified (*$P < 0.05$; **$P < 0.01$; ***$P < 0.001$; ****$P < 0.0001$). Data are presented as mean values; error bars represent ± SD.

2.6 Figures

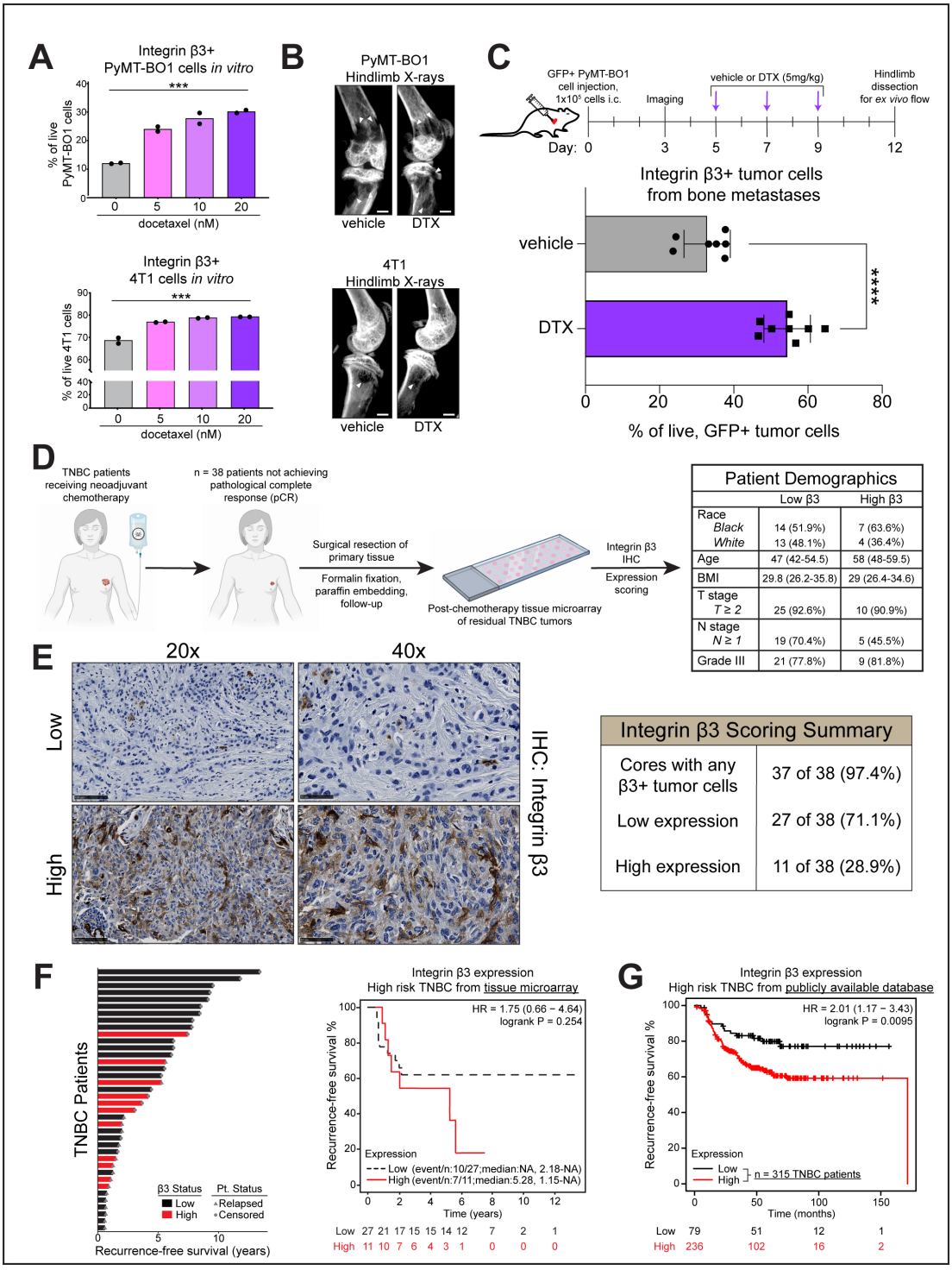
A
Integrin β3+
PyMT-BO1 cells in vitro
***
% of live PyMT-BO1 cells
docetaxel (nM)
Integrin β3+
4T1 cells in vitro
***
% of live 4T1 cells
docetaxel (nM)
B
PyMT-BO1
Hindlimb X-rays
vehicle
DTX
4T1
Hindlimb X-rays
vehicle
DTX
C
GFP+ PyMT-BO1
cell injection,
1x10⁵ cells i.c.
Imaging
vehicle or DTX (5mg/kg)
Hindlimb
dissection
for ex vivo flow
Day: 0 3 5 7 9 12
Integrin β3+ tumor cells
from bone metastases
vehicle
DTX
****
% of live, GFP+ tumor cells
D
TNBC patients
receiving neoadjuvant
chemotherapy
n = 38 patients not achieving
pathological complete
response (pCR)
Surgical resection of
primary tissue
Formalin fixation,
paraffin embedding,
follow-up
Post-chemotherapy tissue microarray
of residual TNBC tumors
Integrin β3
IHC
Expression
scoring
Patient Demographics
Low β3
High β3
Race
Black 14 (51.9%) 7 (63.6%)
White 13 (48.1%) 4 (36.4%)
Age 47 (42-54.5) 58 (48-59.5)
BMI 29.8 (26.2-35.8) 29 (26.4-34.6)
T stage
T ≥ 2 25 (92.6%) 10 (90.9%)
N stage
N ≥ 1 19 (70.4%) 5 (45.5%)
Grade III 21 (77.8%) 9 (81.8%)
E
20x
40x
Low
High
IHC: Integrin β3
Integrin β3 Scoring Summary
Cores with any β3+ tumor cells 37 of 38 (97.4%)
Low expression 27 of 38 (71.1%)
High expression 11 of 38 (28.9%)
F
TNBC Patients
β3 Status
Low
High
Pt. Status
Relapsed
Censored
Recurrence-free survival (years)
Integrin β3 expression
High risk TNBC from tissue microarray
HR = 1.75 (0.66 − 4.64)
logrank P = 0.254
Recurrence-free survival %
Expression
Low (event/n:10/27;median:NA, 2.18-NA)
High (event/n:7/11;median:5.28, 1.15-NA)
Time (years)
Low 27 21 17 15 15 14 12 7 2 1
High 11 10 7 6 4 3 1 0 0 0
G
Integrin β3 expression
High risk TNBC from publicly available database
HR = 2.01 (1.17 − 3.43)
logrank P = 0.0095
Recurrence-free survival %
Expression
Low
High
n = 315 TNBC patients
Time (months)
Low 79 51 12 1
High 236 102 16 2

Figure 2.1 Integrin β3 expression is increased in breast cancer cells after chemotherapy.
A. Flow cytometry of integrin β3 expression in PyMT-BO1 and 4T1 cells harvested 48 hours after overnight treatment with DTX. n = 2 biological replicates per group, one of three independent experiments. **B**. Representative X-ray radiographs of tibiofemoral joints from vehicle and DTX-treated mice bearing either PyMT-BO1 or 4T1 metastases established by i.c. injection. Scale bar = 1.25mm. White arrows indicate areas of significant bone erosion. n = 8-9 mice per group. **C**. *Ex vivo* flow cytometry of live, GFP+ PyMT-BO1 cells harvested from established bone metastases treated with either vehicle or DTX (5mg/kg i.v.). n = 7-8 mice per group. Two-tailed unpaired Welch's t test. **D**. Design of tissue microarray with 38 primary TNBC biopsies obtained after neoadjuvant chemotherapy. Summary of β3-stratified patient demographics (right). **E**. Integrin β3 IHC in human TNBC patients after chemotherapy. Representative images of low and high tumor β3 staining (left), summary of scoring (right, see Materials and Methods). Scale bars = 100 μm (20x) or 50 μm (40x). **F**. Kaplan-Meier analysis of β3-stratified recurrence-free survival in patients from tissue microarray. Swimmer's plot of individual time to recurrence (left), Kaplan-Meier curves and statistics (right). Hazard ratio (HR) and confidence intervals determined by Cox proportional hazards model; significance determined by log rank test. **G**. Kaplan-Meier analysis of β3-stratified recurrence-free survival in 315 high-risk TNBC patients receiving any chemotherapy obtained from publicly available microarray data. Hazard ratio (HR) and confidence intervals determined by Cox proportional hazards model; significance determined by log rank test.

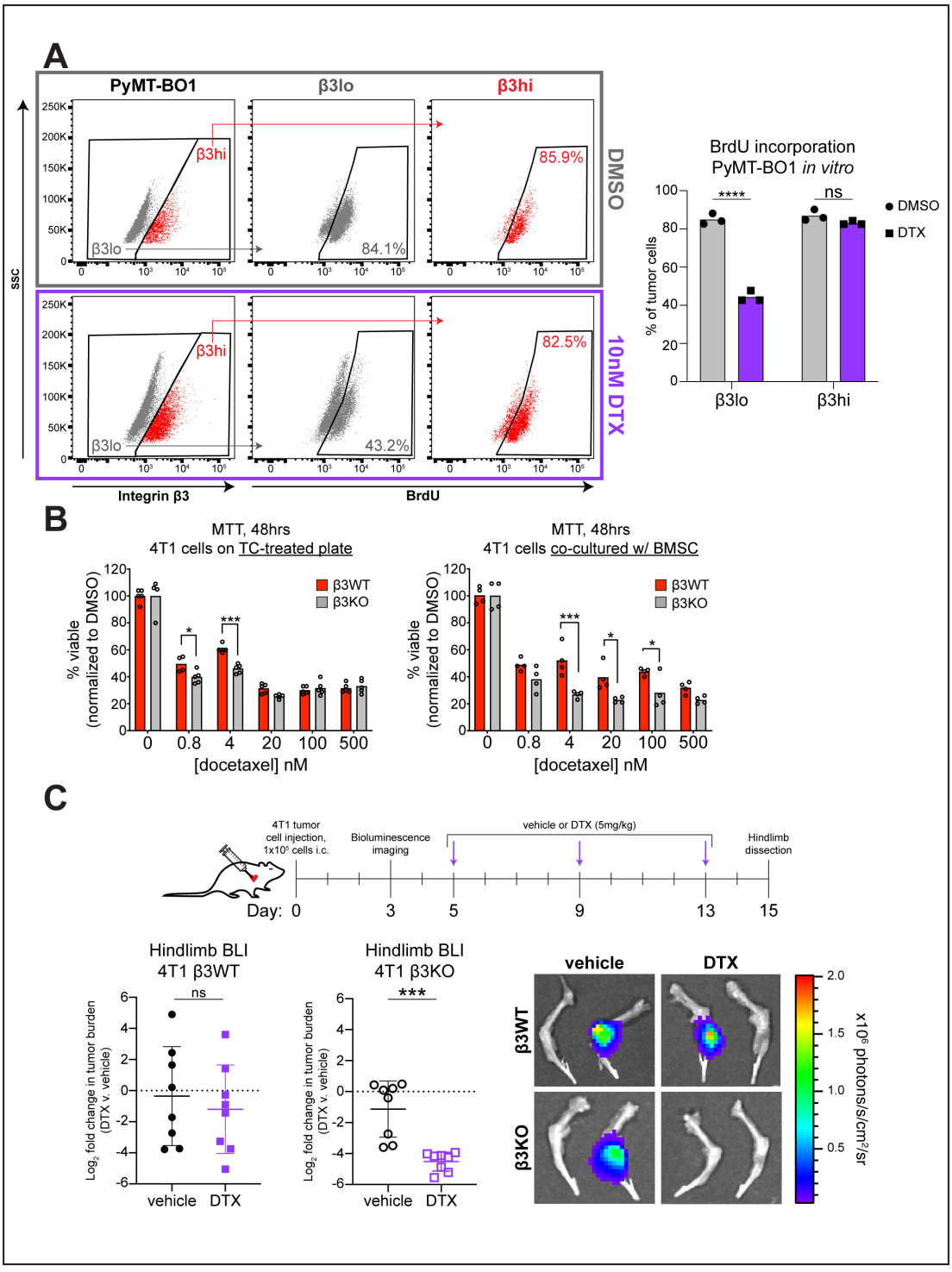

Figure 2.2 Integrin β3 promotes docetaxel resistance in bone metastases.
A. Flow cytometry of overnight BrdU incorporation in β3lo and β3hi PyMT-BO1 cells *in vitro*. Cells were treated with DMSO or 10nM DTX for 24hrs, followed by a 48hr recovery period. Representative samples with integrin β3 gating (left), quantification of

BrdU incorporation in β3lo and β3hi populations (right), n = 3 biological replicates per group, one of two independent experiments. Two-way ANOVA with Tukey *post hoc* test. **B**. MTT viability assay of 4T1 β3KO and β3WT cells treated with DTX for 48hrs. Assay on tissue culture-treated plate (left) and co-cultured with BMSCs (right, see Materials and Methods for details), n = 4 biological replicates per group, one independent experiment. Two-way ANOVA with Sidak *post hoc* test. **C**. *Ex vivo* BLI of 4T1 β3KO and β3WT hindlimb tumor burden from mice receiving either vehicle or DTX (5mg/kg i.v.). Treatment schema (top), quantification of *ex vivo* BLI signal from hindlimbs (bottom left), representative BLI (bottom right), n = 8 mice per group. Data shown are $\log_2$ transformed fold change in photons/s relative to the geometric mean of samples from vehicle treated mice. Each data point represents averaged signaling intensity from hindlimbs of one mouse. β3WT and β3KO experiments were performed independently. One-tailed unpaired t test with Welch's correction.

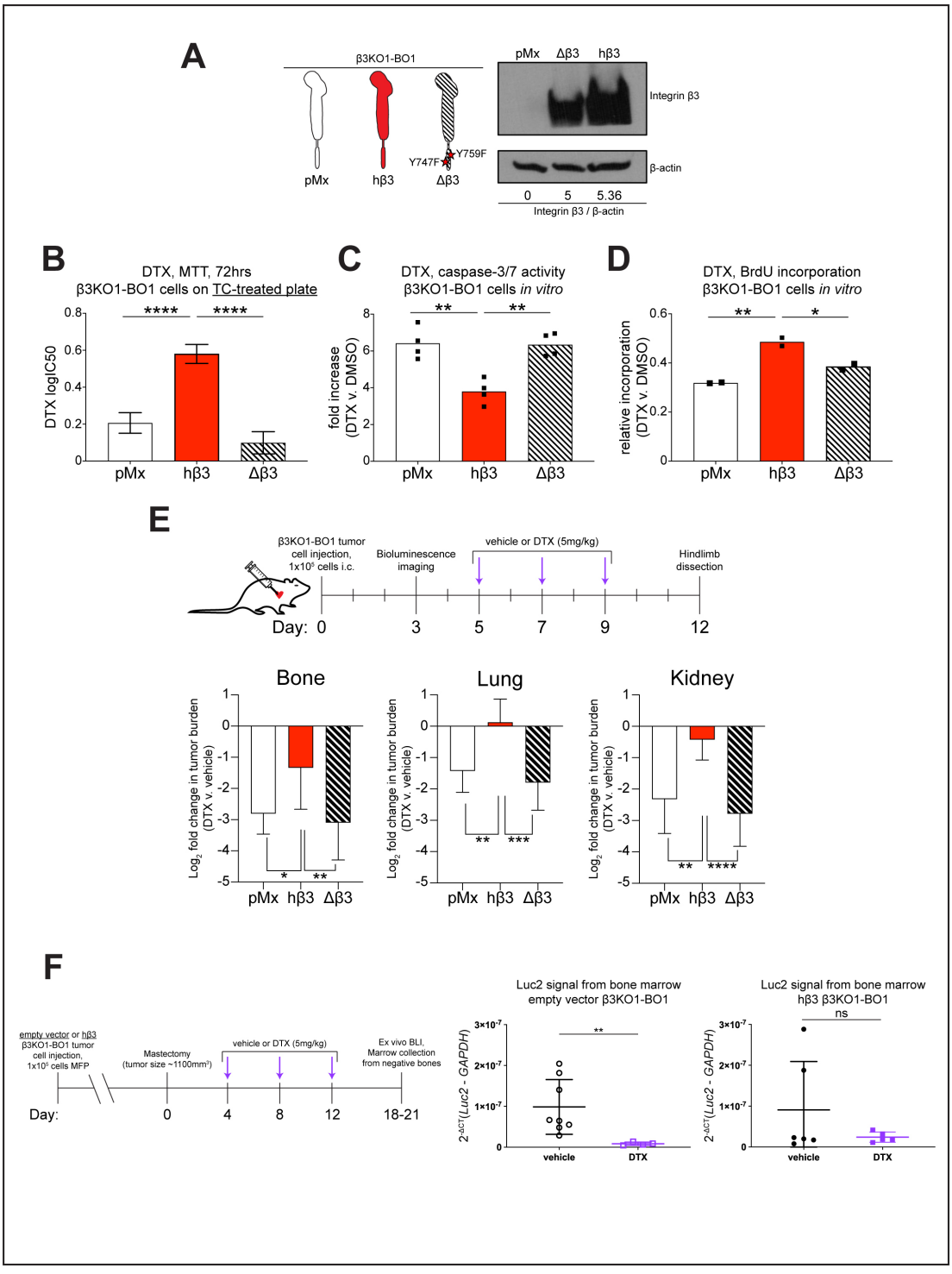

Figure 2.3 Rescue of integrin β3 expression restores chemoresistance in a signaling-dependent manner.

A. Retroviral recue of β3KO1-BO1 cells with empty vector (pMx), functional human β3 (hβ3), or signaling-deficient Δβ3. Construct schematic (left), western blot confirmation of integrin β3 rescue (right). **B**. Docetaxel IC_{50} from 72hr MTT viability assay *in vitro* using pMx, hβ3, and Δβ3 β3KO1-BO1 cells, n =24 per genotype spread across 8 drug concentrations, one of two independent experiments. Data represent mean ± SEM. One-way ANOVA with Tukey *post hoc* test. **C**. Luminometric assessment of caspase-3/7 activity *in vitro*. Cells were treated with DMSO or 30nM DTX for 40hr. Data represent fold increase in luminescent caspase-3/7 activity compared to untreated controls of the same genotype and normalized to cell viability by CellTiter Blue, n = 4 biological replicates per group, one of three independent experiments. One-way ANOVA with Tukey *post hoc* test. **D**. Flow cytometric analysis of BrdU incorporation *in vitro*. Cells were treated with DMSO or 10nM DTX for 40hrs, followed by 2hrs of BrdU incorporation. n = 2 biological replicates per group, one of two independent experiments. One-way ANOVA with Tukey *post hoc* test. **E**. *Ex vivo* bioluminescent tumor burden in hindlimb bone, lung, and kidney of mice bearing pMx, hβ3, or Δβ3 β3KO1-BO1 tumors receiving either vehicle or DTX (5mg/kg i.v.). Tumor establishment by intracardiac injection and treatment schema (top), quantification of *ex vivo* BLI signal from organs (bottom), n = 6-8 mice per group. Data shown are $\log_2$ transformed fold change in photons/s relative to the geometric mean of samples from vehicle-treated mice. pMx, hβ3, and Δβ3 experiments were performed independently. One-way ANOVA with Tukey *post hoc* test. **F**. Assessment of disseminated tumor cell burden in an orthotopic resection model of adjuvant chemotherapy. Tumor establishment, surgical resection, and adjuvant treatment schema (left); qPCR quantification of occult tumor cell burden by *Luc2* expression in flushed marrow from mouse bones without detectable BLI signal (right). Data are $2^{-\Delta CT}$, with ΔC_t representing *Luc2* C_t – *GAPDH* C_t. n = 4-8 mice per group, One-tailed unpaired t test with Welch's correction.

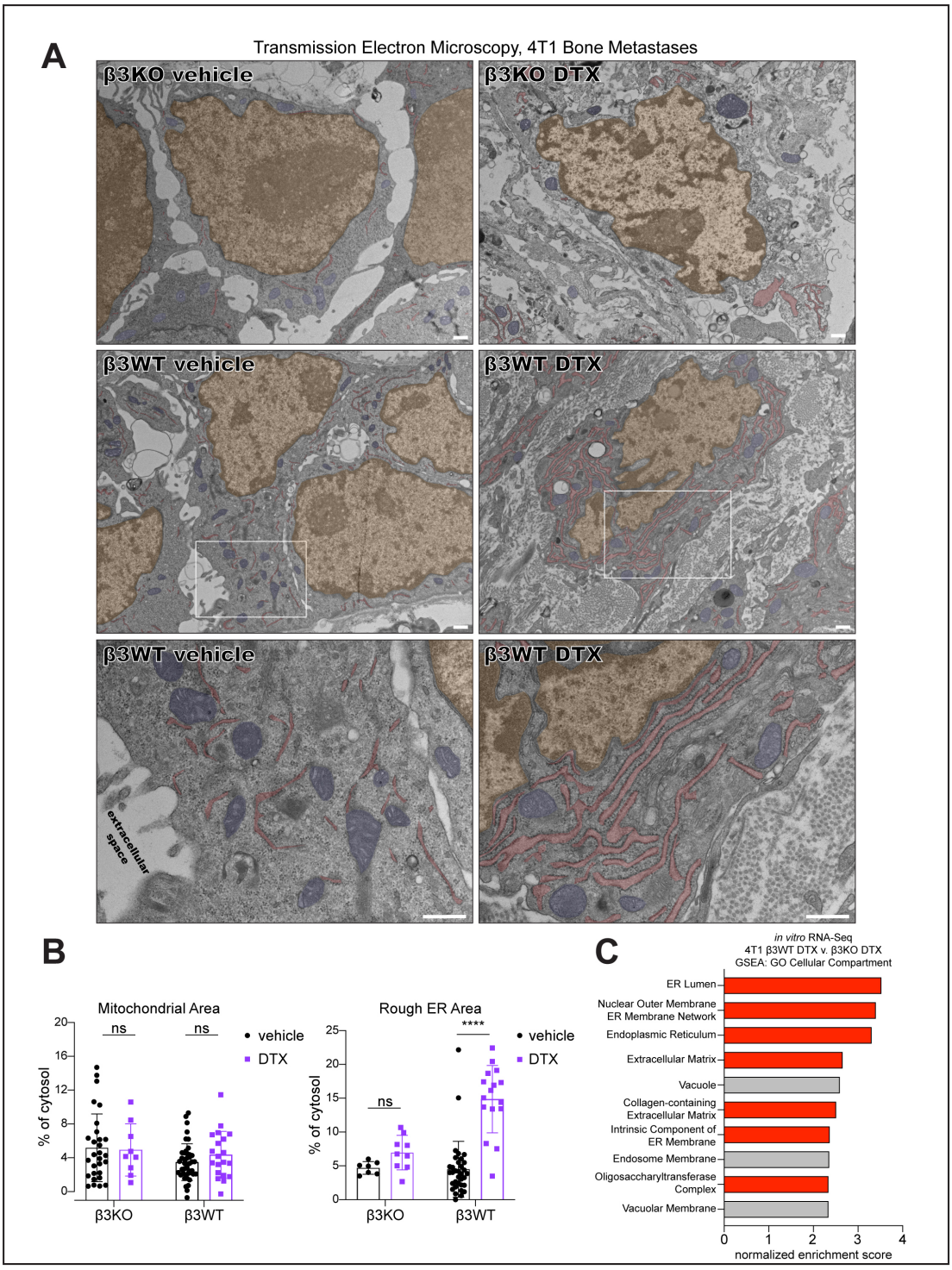

Figure 2.4 Docetaxel treatment elicits rough ER expansion and extracellular matrix production in β3WT bone metastases.

A. Representative transmission electron micrographs of 4T1 β3KO and β3WT bone metastases treated with either vehicle or DTX (5mg/kg). Tumor establishment and i.v. drug administration were performed as indicated in Fig. **2.2C**. Scale bars = 500nm. n = 1-3 tumors per group. Nuclei (orange), mitochondria (blue), rough ER (red). **B**. Quantification of mitochondrial area and rough ER area from individual tumor cells in bone metastases. Data shown as percentage of total cytosolic area per cell, n = 7-43 cells evaluated per group. Two-way ANOVA with Tukey *post hoc* test. **C**. Top 10 normalized enrichment scores from GSEA analysis of GO cellular compartment terms comparing 4T1 β3WT DTX and 4T1 β3KO DTX RNA-Seq samples. Terms related to rough ER and ECM displayed in red.

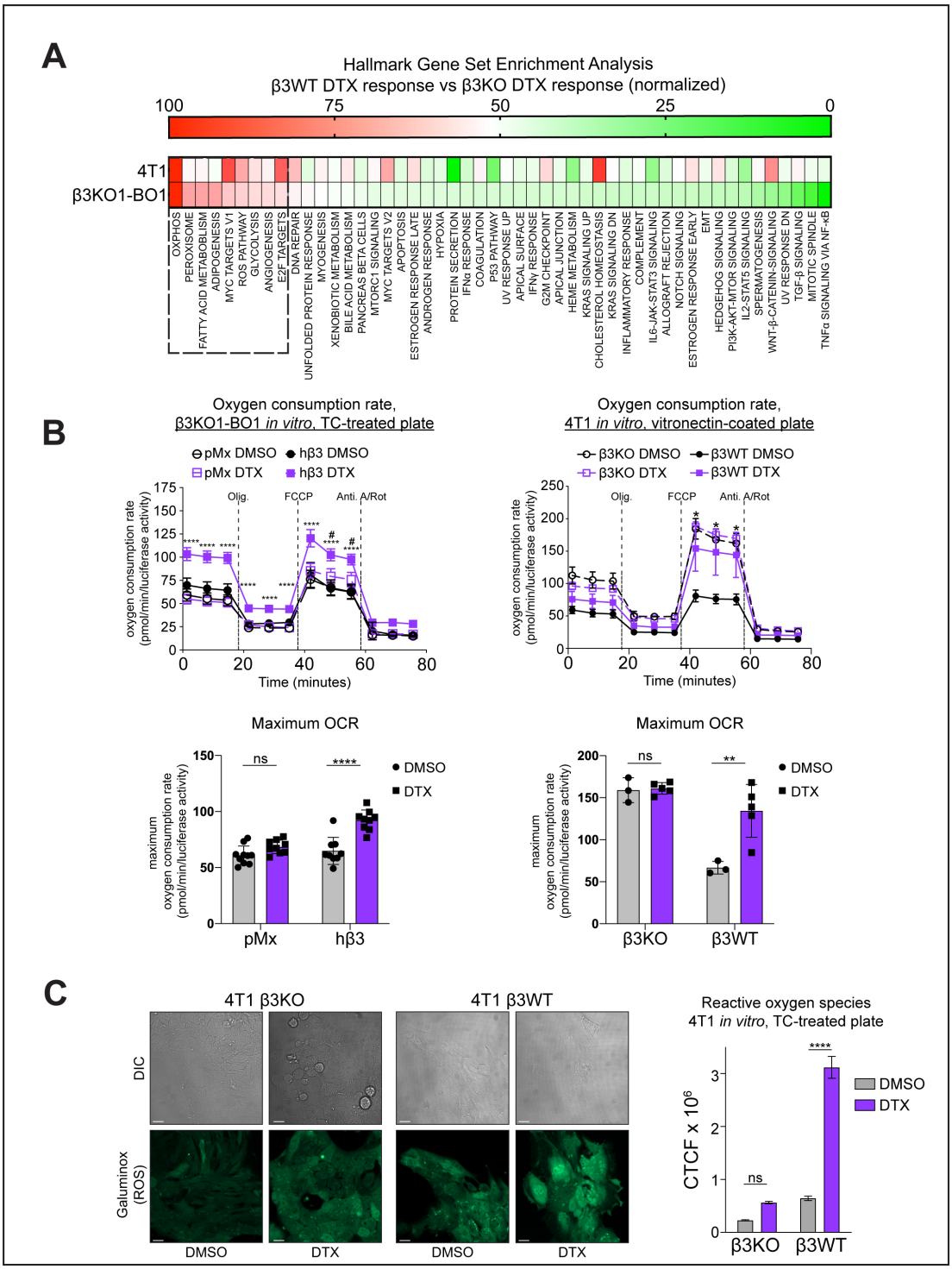

Figure 2.5 Integrin β3 mediates an alternative metabolic response to docetaxel.
A. Comparison of hallmark GSEA results between β3KO1-BO1 and 4T1. For each cell line, normalized enrichment scores (NES) were separately determined for the DTX response (DTX v. DMSO) in β3-expressing and β3KO cells. The difference between

these scores (β3WT response – β3KO response) was calculated, and all values were internally normalized to a 0-100 scale for that line, with 0 corresponding to the smallest NES difference and 100 corresponding to the largest. **B**. Extracellular flux analysis of maximum OCR after serial addition of the indicated drugs (see Materials and Methods). Cells were treated with DMSO or 10nM DTX for 24hrs, followed by a 48hr recovery period. β3KO1-BO1 (left), 4T1 (right), OCR readings over time (top), maximum OCR calculation (bottom, see Materials and Methods). Data shown are pmol O2 consumed per minute, normalized to constitutive luciferase activity measured after assay completion, n = 3-10 biological replicates per group, one of two independent experiments for each cell type. Two-way ANOVA with Tukey *post hoc* test comparing DTX versus DMSO within each genotype; for β3-expressing cells: *, $P<0.05$, **, $P<0.01$; ****, $P<0.0001$; for β3KO cells: #, $P<0.05$. **C**. Fluorescence staining of ROS by Galuminox (see Materials and Methods). β3WT and β3KO 4T1 cells treated with DMSO or 10nM DTX overnight, followed by a 48hr recovery period. Representative DIC and fluorescence images (left), quantitation of Corrected Total Cell Fluorescence (CTCF, see Materials and Methods) (right). Scale bar = 20μm, data are mean ± SEM and represent 3 independent experiments. Two-way ANOVA with Tukey *post hoc* test.

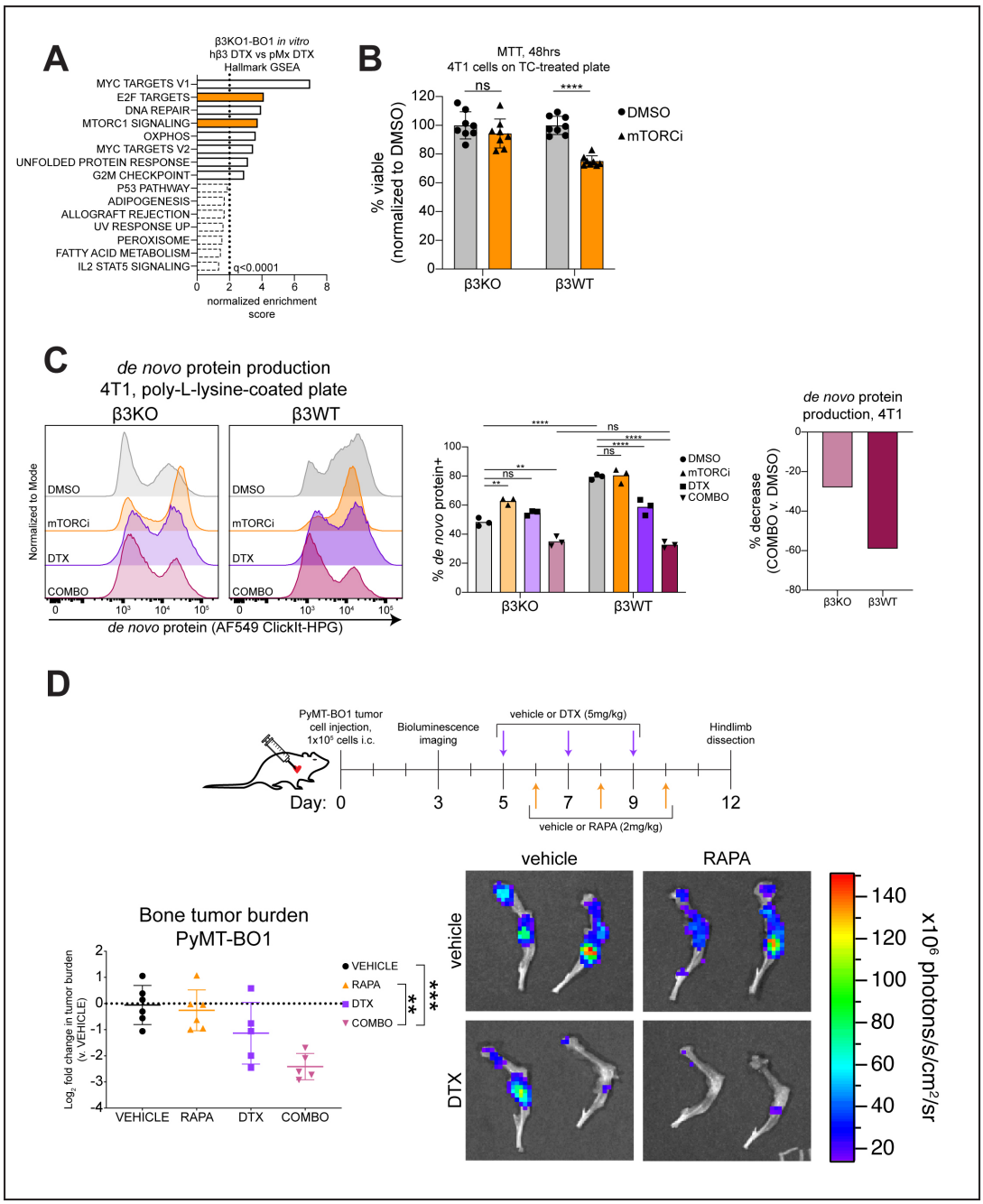

Figure 2.6 mTORC1 inhibition reverses β3-mediated chemoresistance
A. Significantly enriched pathways (FDR q < 0.250) from hallmark GSEA comparing transcriptomic profiles from hβ3 DTX and pMx DTX groups. mTOR and mTOR-associated pathways (orange). **B**. MTT viability assay of 4T1 β3KO and β3WT cells treated with 100nM everolimus (mTORCi) for 48hrs. n = 8 biological replicates per group, one of two independent experiments. Two-way ANOVA with Tukey *post hoc* test. **C**. Flow cytometric analysis of *de novo* protein synthesis in 4T1 β3KO and β3WT cells. Cells were treated with DMSO or 10nM DTX for 24hrs, followed by 48hrs of either DMSO or 100nM everolimus (mTORCi). Representative AF549 ClickIt-HPG histograms (left), quantification of ClickIt-HPG fluorescence positivity (middle), quantification of percentage decrease in positivity between vehicle and combination-treated samples for each genotype (right). n = 3 biological replicates per sample, one of two independent experiments. Three-way ANOVA with Tukey *post hoc* test. **D**. *Ex*

vivo BLI of β3WT PyMT-BO1 hindlimb tumor burden from mice receiving either vehicle, DTX alone (5mg/kg i.v.), rapamycin alone (RAPA, 2mg/kg i.p.), or both combined (COMBO). Treatment schema (top), quantification of *ex vivo* BLI signal from hindlimbs (bottom left), representative BLI (bottom right), n = 5-6 mice per group. Data shown are $\log_2$ transformed fold change in photons/s relative to the geometric mean of samples from vehicle-treated mice. Each data point represents averaged signaling intensity from hindlimbs of one mouse. Two-way ANOVA with Tukey *post hoc* test.

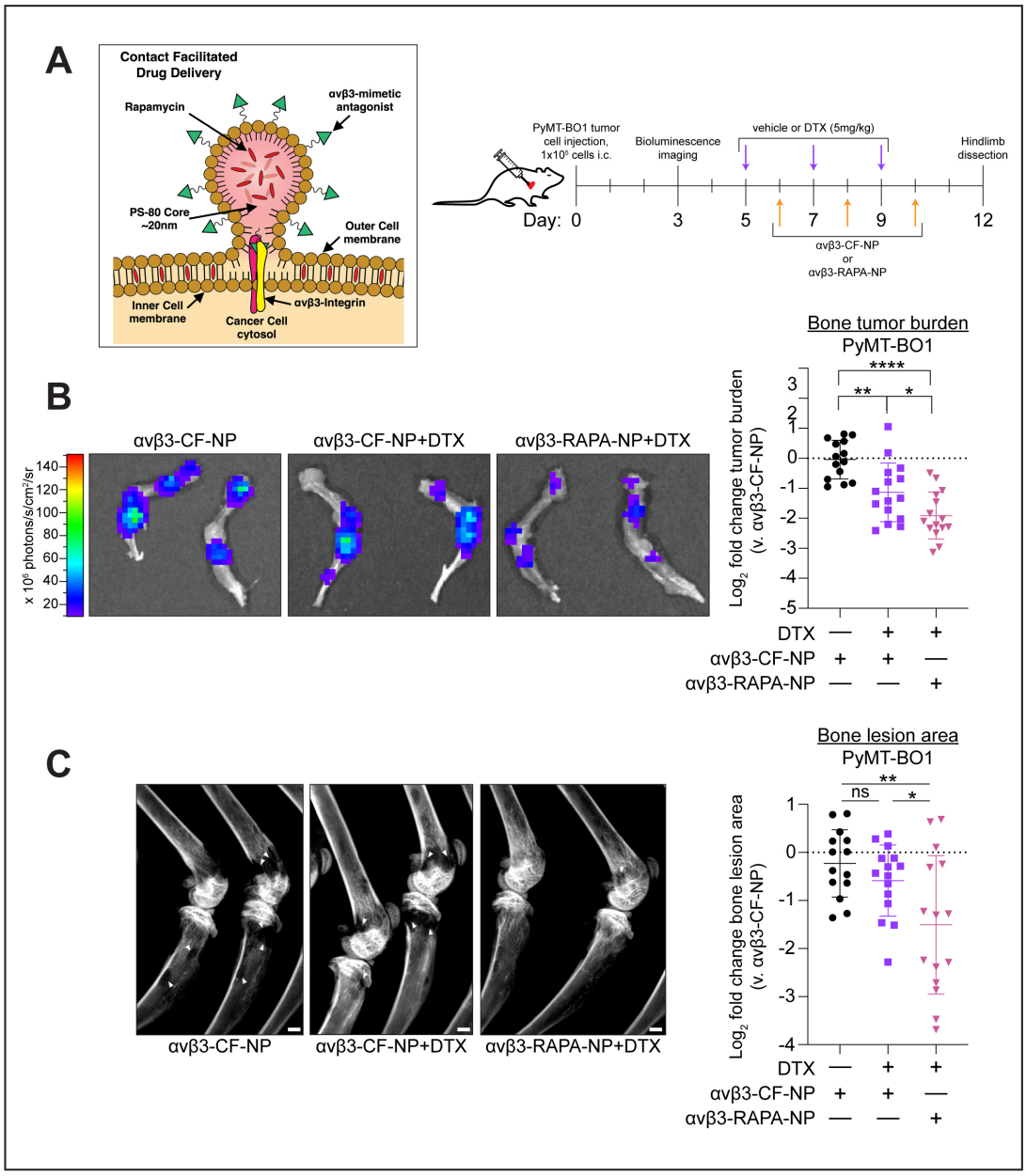

Figure 2.7 αvβ3-targeted nanoparticles loaded with mTOR inhibitor enhance docetaxel efficacy in bone metastases. **A**. Nanoparticle schematic (left), combination treatment strategy (right). **B**. *Ex vivo* BLI of β3WT PyMT-BO1 hindlimb tumor burden from mice receiving either αvβ3-CF-NP, αvβ3-CF-NP and free DTX (5mg/kg i.v.), or αvβ3-RAPA-NP particles (2mg/kg equivalent rapamycin dose) and free DTX. Representative BLI (left), quantification of *ex vivo* BLI signal from hindlimbs (right), n = 14-15 mice per group. Data shown are $\log_2$ transformed fold change in photons/s relative to the geometric mean of samples from αvβ3-CF-NP mice. Each data point represents transformed averaged signaling intensity from hindlimbs of one mouse. One-way ANOVA with Tukey *post hoc* test. **C**. X-ray radiography of osteolytic lesion area in tibiofemoral joints from mice described above. Representative radiographs for each group (left), quantification of osteolytic lesion area (right). Scale bar = 1.25mm. White arrows indicate areas of significant bone erosion. Data shown are $\log_2$ transformed fold change in total lesion area relative to the geometric mean of samples from αvβ3-CF-NP mice. One-way ANOVA with Tukey *post hoc* test.

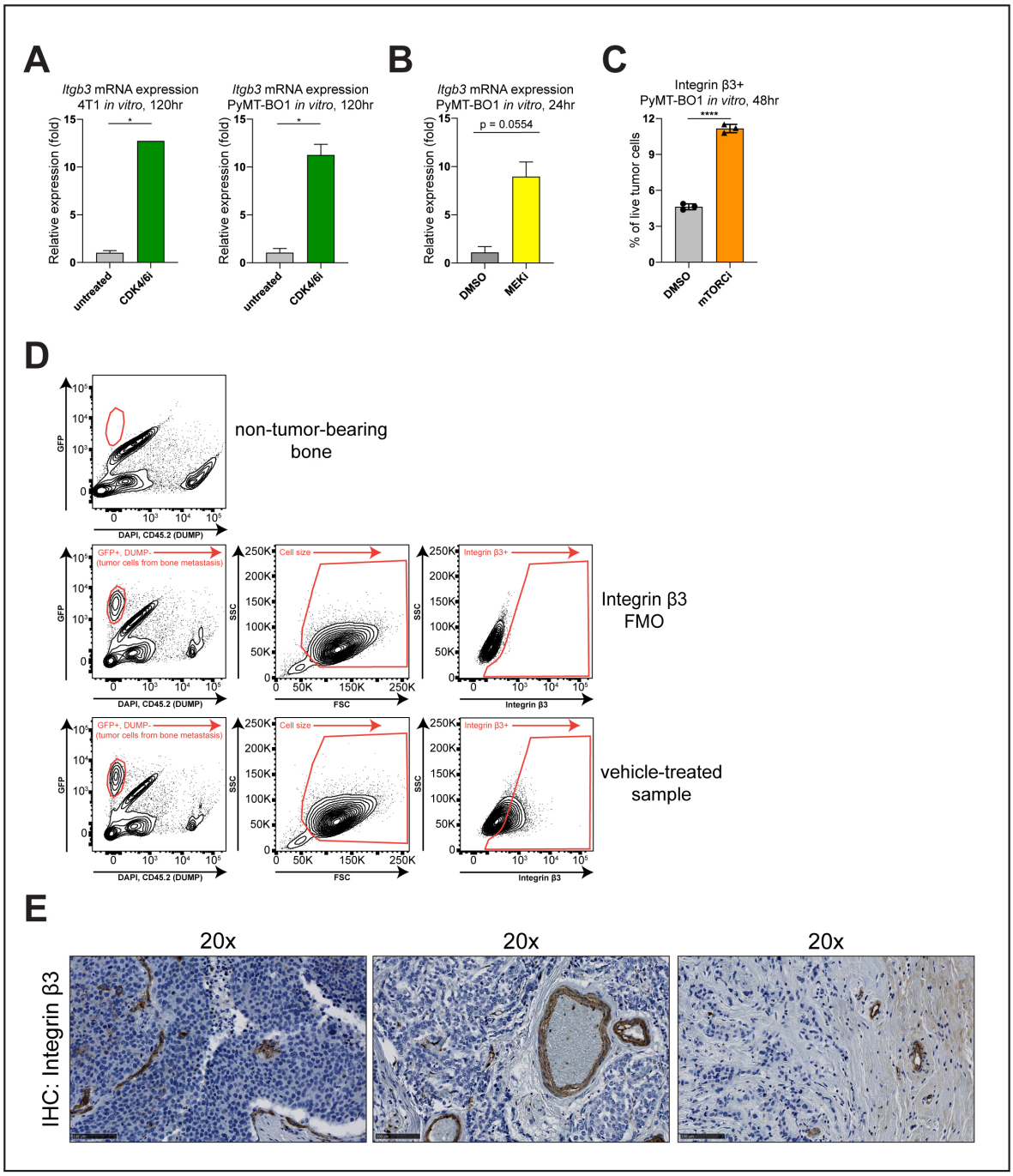

Figure S2.1 Integrin β3 expression on breast cancer cells and vascular endothelium.
A. qPCR analysis of β3 (*Itgb3*) mRNA expression in 4T1 (left) or PyMT-BO1 (right) cells cultured *in vitro*, following 120hr treatment with 10μM CDK4/6i (LEE001). One biological replicate per group, each in technical duplicate. Two-tailed unpaired t test with Welch's correction. **B**. qPCR analysis of β3 (*Itgb3*) mRNA expression PyMT-BO1 cells cultured *in vitro*, following 24hr treatment with 20μM MEKi (U01261). One biological replicate per group, each in technical duplicate. Two-tailed unpaired t test with Welch's correction. **C**. Flow cytometry analysis of integrin β3 expression on PyMT-BO1 cells *in vitro* following 48hr treatment with 100nM mTORCi (RAD001). n = 3 biological replicates per group. Two-tailed unpaired t test with Welch's correction. **D**. Tumor cell gating schema for ex vivo flow cytometry of GFP+DAPI- tumor cells harvested from murine bone metastases. Non-tumor bearing bone with no GFP+DAPI- cells (top), integrin β3 fluorescence minus one (FMO) control

(middle), representative tumoral β3 expression in sample from vehicle-treated mouse (bottom). **C**. Examples of vascular integrin β3 staining by IHC in human TNBC samples.

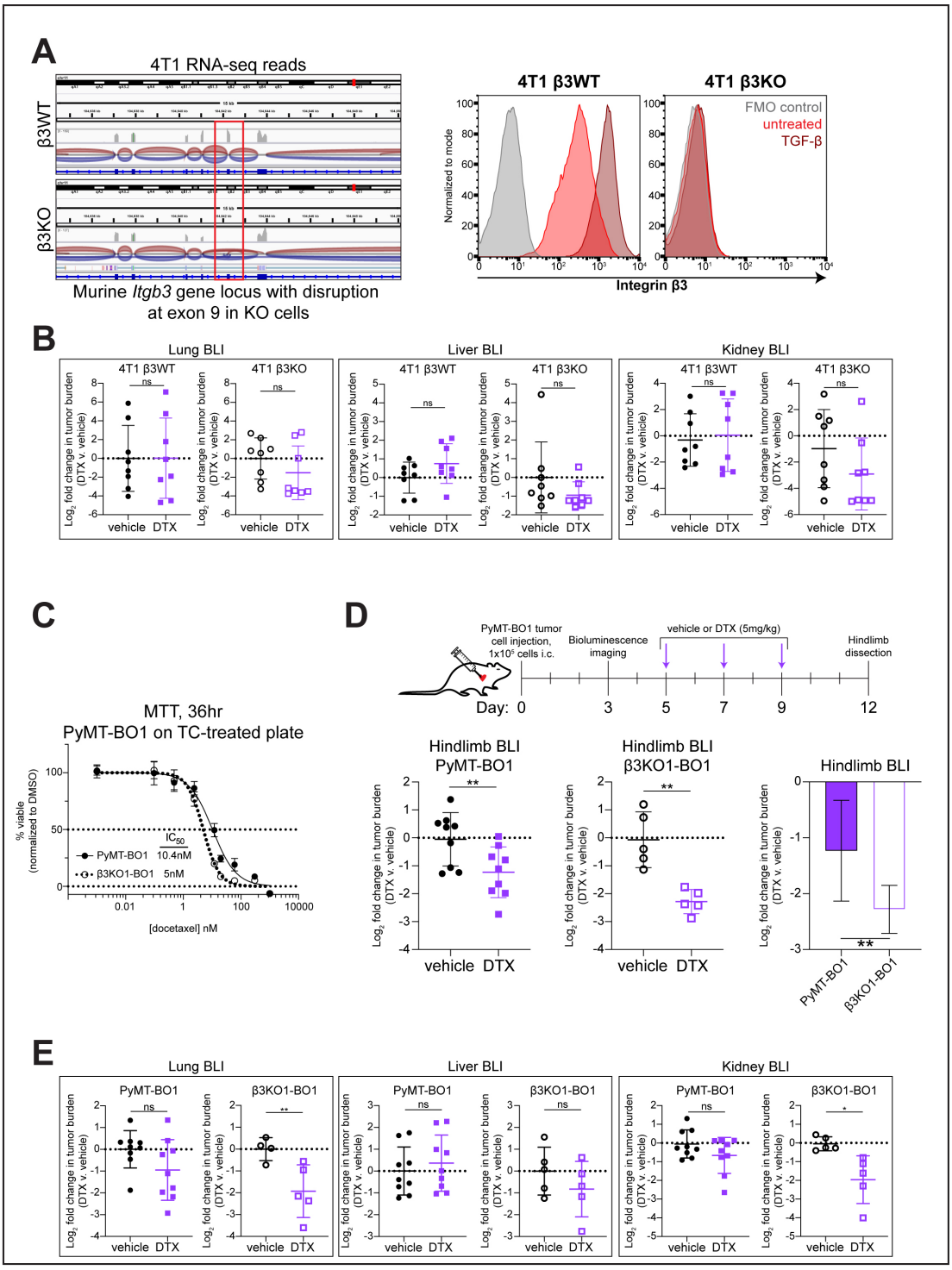

Figure S2.2 Validation of *Itgb3* CRISPR knockout in 4T1 cells and assessment of docetaxel sensitivity *in vitro* and *in vivo*.

A. Genetic deletion of *Itgb3* in murine 4T1 breast cancer cells. Loss of reads aligned to exon 9 of the *Itgb3* locus in a representative RNA-Seq sample in β3KO 4T1 cells (left); representative flow cytometry histograms of integrin β3 expression by β3WT and β3KO 4T1 cells in media and after 48hr of TGF-β (2ng/mL) stimulation (right). n = 3 biological replicates. **B**. *Ex vivo* BLI of 4T1 β3KO and β3WT tumor burden in visceral organs of BALB/c mice described in **Figure 2.2**. Data shown are $\log_2$ transformed fold change in photons/s relative to the geometric mean of samples from vehicle treated mice. Each data point represents averaged signaling intensity from indicated organs of one mouse. n = 8 mice per group. One-tailed unpaired t test with Welch's correction. **C**. MTT viability assay of PyMT-BO1 and β3KO1-BO1 cells treated with DTX for 36hrs. IC50 values determined by nonlinear fit (see Materials and Methods). n = 3 biological replicates per group, one independent experiment. **D**. *Ex vivo* BLI of PyMT-BO1 and β3KO1-BO1 hindlimb tumor burden from mice receiving either vehicle or DTX (5mg/kg i.v.). Establishment of distant metastases and treatment schema (top), quantification and comparison of *ex vivo* BLI signal from hindlimbs (bottom), n = 5-9 mice per group. Data shown are $\log_2$ transformed fold change in photons/s relative to the geometric mean of samples from vehicle treated mice. Each data point represents averaged signaling intensity from hindlimbs of one mouse. β3WT and β3KO experiments were performed independently. One-tailed unpaired t test with Welch's correction. **E**. *Ex vivo* BLI of PyMT-BO1 and β3KO1-BO1 tumor burden in visceral organs of mice described in **D**, n = 4-9 mice per group, one-tailed unpaired t test with Welch's correction.

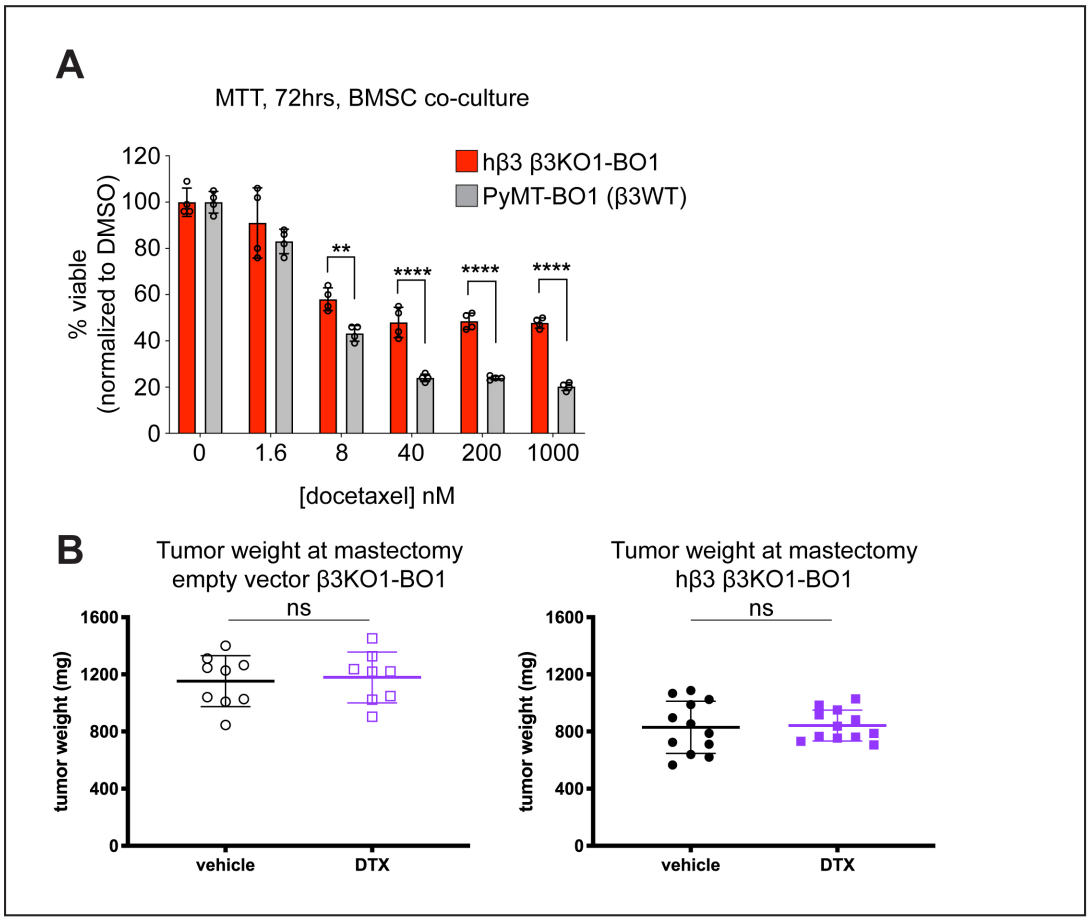

Figure S2.3 BMSC docetaxel viability co-culture and post-mastectomy treatment groups.
A. MTT viability assay of hβ3-rescued β3KO1-BO1 and PyMT-BO1cells treated with DTX for 72hrs in co-culture with BMSCs. n = 4 biological replicates per group, one independent experiment. Two-way ANOVA with Sidak *post hoc* test. **B**. Post-mastectomy weight of MFP tumors in milligrams. n = 8-12 mice per group Two-tailed unpaired t test with Welch's correction.

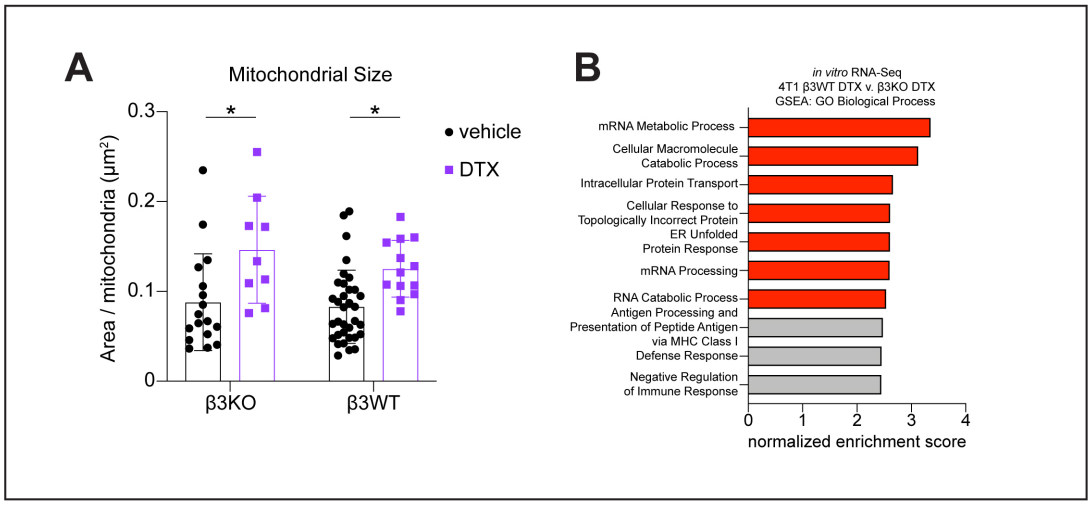

Figure S2.4 TEM quantitation of mitochondrial area and GO Biological Process GSEA in 4T1 cells.
A. Quantification of average area per mitochondria in μm^2 from individual tumor cells in bone metastases. n = 9-34 cells evaluated per group. Two-way ANOVA with Tukey *post hoc* test. **B**. Top 10 normalized enrichment scores from GSEA analysis of GO biological process terms comparing 4T1 β3WT DTX and 4T1 β3KO DTX samples. Terms related to mRNA, ER, and protein metabolism displayed in red.

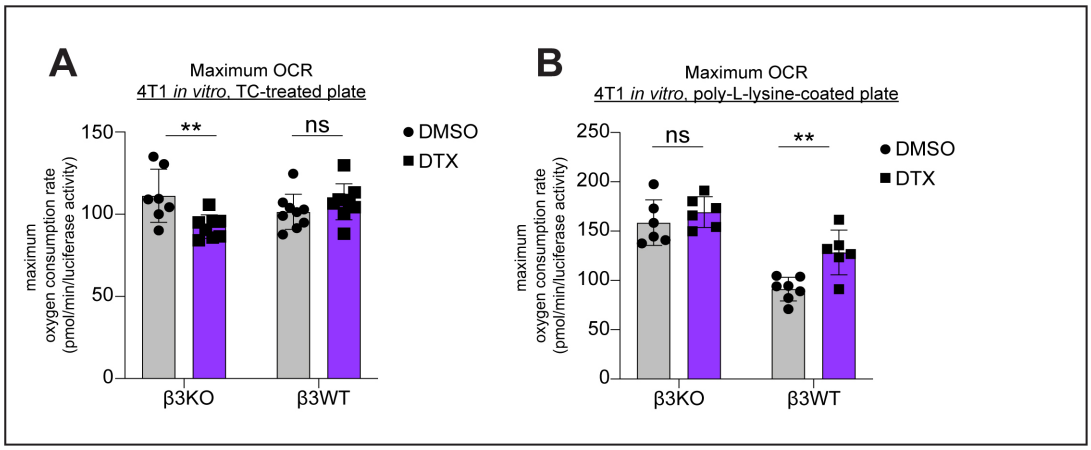

Figure S2.5 4T1 oxygen consumption rate on tissue culture-treated and poly-L-lysine-coated plates.
A. Extracellular flux analysis of maximum oxygen consumption in 4T1 β3KO and β3WT cells. Cells were cultured on tissue culture-treated plates and treated with DMSO or 10nM DTX for 24hrs, followed by a 48hr recovery period. Data shown are pmol O2 consumed per minute, normalized to constitutive luciferase activity measured after assay completion, n = 7-10 biological replicates per group, one independent experiment. Two-way ANOVA with Tukey *post hoc* test comparing DTX versus DMSO within genotypes. **B**. Similar to **A**, but using cells cultured on poly-L-lysine-coated petri dishes. n = 6-7 biological replicates per group, one of two independent experiments. Two-way ANOVA with Tukey *post hoc* test comparing DTX and DMSO within genotypes.

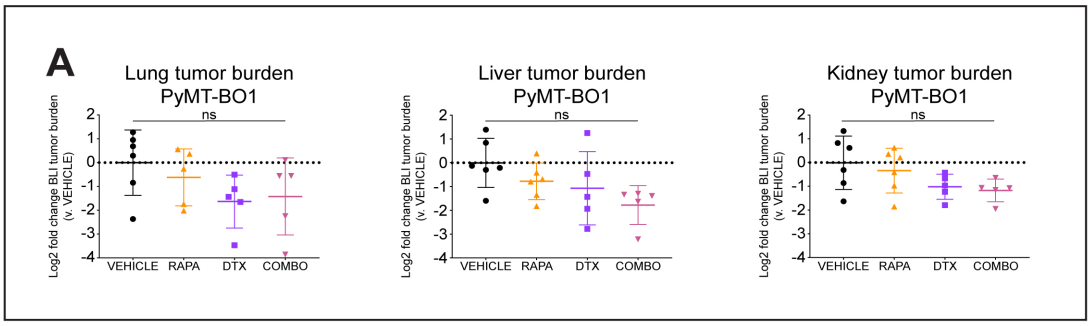

Figure S2.6 Bioluminescence analysis of visceral metastases in PyMT-BO1 tumor-bearing mice treated with DTX and RAPA.

A. *Ex vivo* BLI of β3WT PyMT-BO1 tumor burden in visceral organs of mice described in **Figure 2.6D**. Data shown are $\log_2$ transformed fold change in photons/s relative to the geometric mean of samples from vehicle treated mice. Each data point represents averaged signaling intensity from indicated organs of one mouse. n = 5-6 mice per group. Two-way ANOVA with Tukey *post hoc* test.

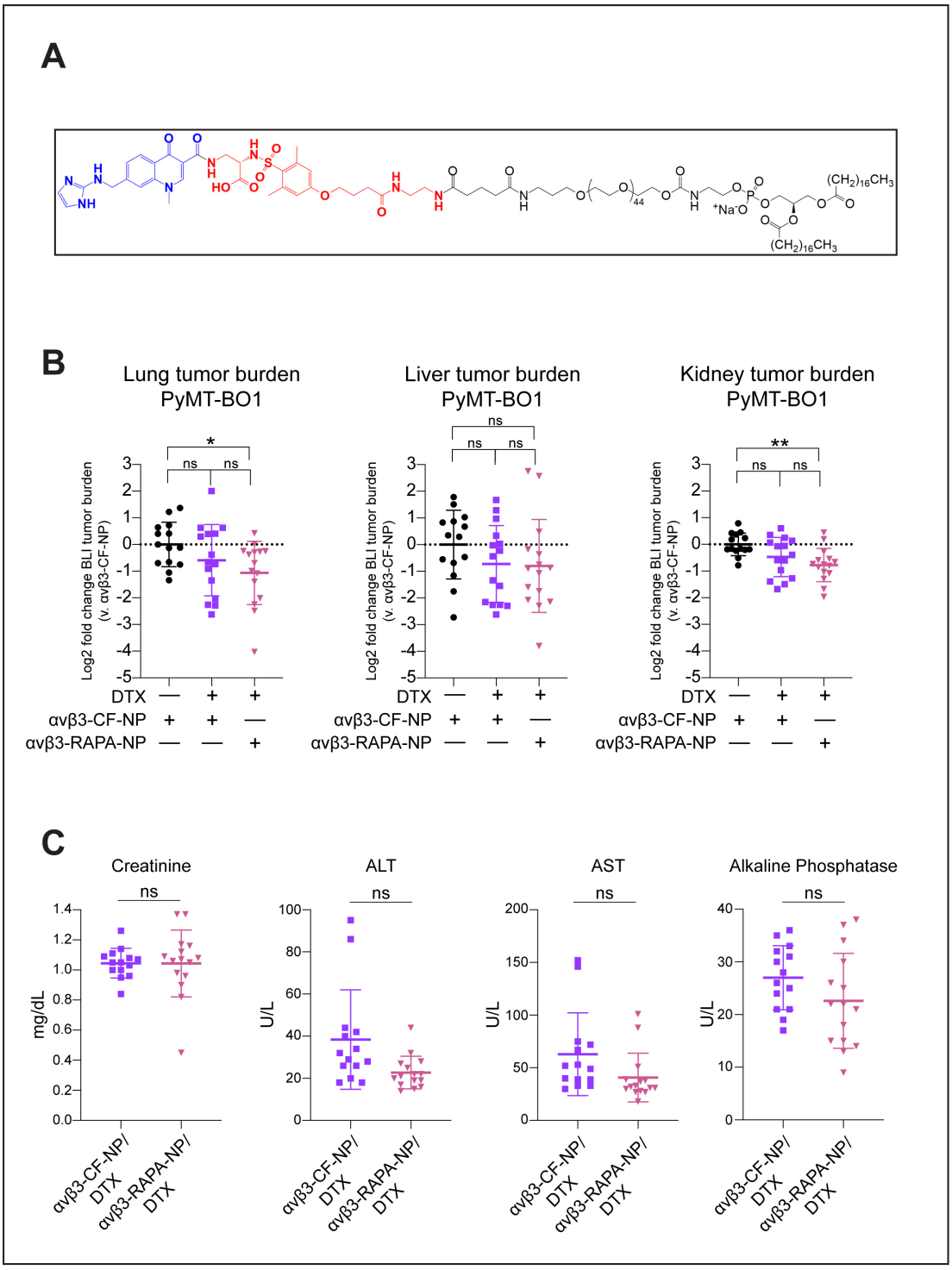

Figure S2.7 αvβ3 targeting ligand schematic and bioluminescence analysis of visceral metastases in PyMT-BO1 tumor-bearing mice treated with free DTX and αvβ3-RAPA-NP.

A. Structure of the αvβ3 homing ligand used for nanoparticle targeting (see Materials and Methods). **B**. *Ex vivo* BLI of β3WT PyMT-BO1 tumor burden in visceral organs of mice described in **Figure 2.7**. Data shown are log2 transformed fold change in photons/s relative to the geometric mean of samples from vehicle treated mice. Each data point represents averaged signaling intensity from indicated organs of one mouse. n = 14-15 mice per group. One-way ANOVA with Tukey *post hoc* test. **C**. Serum chemistry analysis from mice described in **Fig. 2.7**. n = 13-15 mice per group. One-way ANOVA with Tukey *post hoc* test; all three treatment groups tested, only groups receiving DTX shown.

Chapter 3

The role of TGF-β in integrin β3 expression by breast cancer cells *in vitro* and *in vivo*

This chapter combines unpublished work with data from the following publication:

> Ross, M. H., Esser*, A. K., **Fox, G. C.*** et al. Bone-Induced Expression of Integrin β3 Enables Targeted Nanotherapy of Breast Cancer Metastases. *Cancer Res.* **77**, 6299-6312 (2017). *co-second authors

I was involved in planning, executing, and analyzing experiments from this paper pertaining to TGF-β-mediated upregulation of integrin β3. I also contributed extensive edits to the manuscript in both initial preparation and during revision.

3.1 Abstract

Interactions with the bone microenvironment drive unique tumor phenotypes in breast cancer bone metastases, including upregulation of the integrin β3 subunit (β3), a known regulator of metastasis and therapy resistance. In this study, we demonstrate that canonical TGF-β signaling through SMAD2/3 is necessary for β3 induction in breast cancer cells *in vitro*, as well as in bone-resident breast cancer cells *in vivo.* Using a luminescent reporter, we describe a strategy for tracing TGF-β bioavailability in breast cancer cells. Finally, in a genetic mouse model of Marfan syndrome, we show that enhanced TGF-β availability in visceral tissues is sufficient to upregulate tumoral integrin β3 and promote resistance to taxane chemotherapy. Taken together, our results highlight the role of the microenvironment in shaping tumor behavior and therapeutic response.

3.2 Introduction

Bone metastases are common in breast cancer patients[11, 12], where they manifest as osteolytic lesions that are difficult to treat[18] and often associated with substantial increases in morbidity and mortality[12]. Although metastasis to the bone has been well-studied[16], the bone tumor microenvironment is incredibly diverse, exhibiting a range of distinct cellular and molecular characteristics that set it apart from the primary tumor and visceral metastatic sites[88]. As a result, the phenomenological consequences of cross-talk between this heterogeneous microenvironment and tumor cells for various tumor phenotypes, including progression and response to therapy, are still being elucidated[72, 205].

One candidate molecule of special interest with regard to bone tumor microenvironmental crosstalk is integrin αvβ3. Integrins are heterodimeric transmembrane receptors, each comprised of an α and β subunit, that recognize ligand moieties found predominantly in the extracellular

matrix[107]. Integrin signaling is highly tuned to cell type and situational context, with downstream effects on numerous cellular functions, such as survival and proliferation, often hijacked during malignancy[136, 229]. Integrin β3 and αvβ3 expression has been observed on tumor cells in human breast cancer bone metastases[172], and preclinical models have directly implicated tumoral integrin β3 expression in the capacity to metastasize to bone[60, 173]. Much less, by contrast, is understood about how integrin β3 expression is physiologically regulated over the course of the bone metastatic cascade.

The bone is a reservoir for transforming growth factor beta (TGF-β)[67], a pleiotropic signaling molecule that can drive metastasis and resistance to therapy in cancer by activating gene regulatory programs such as EMT and altering cell state [230]. TGF-β signaling has been previously linked with induction of integrin β3[167] and is abundant in the bone tumor microenvironment, where it is converted to its active form by osteoclastic bone resorption[74]. Nevertheless, its role in the regulation of integrin β3 in breast cancer bone metastases is unknown.

Here, we report that the bone microenvironment preferentially induces integrin β3 on breast cancer bone metastases through canonical TGF-β signaling, and describe a luminescent reporter strategy for evaluating canonical TGF-β bioavailability in breast cancer cells. Further, we demonstrate that genetic manipulation of TGF-β availability in non-bone tissues upregulates tumoral integrin β3 on their respective metastases, with consequences for resistance to taxane chemotherapy.

3.3 Results

Integrin β3 is induced in the bone microenvironment and by exposure to TGF-β

In preclinical models and in patient samples, we had previously found that integrin β3 was more highly expressed on breast cancer cells in bone metastases compared to the primary tumor or visceral metastatic sites[175]. As αvβ3 on tumor cells is known to promote bone metastasis[60, 173], we asked if enhanced β3 expression by bone-resident breast cancer cells was a consequence of preferential bone seeding by a $\beta3^{hi}$ subpopulation. To answer this question, we used FACS to sort PyMT-BO1 cells into three populations: low β3 expression (β3-), high β3 expression (β3+), and control sorted (β3-all). These populations were collected, injected i.c. into separate groups of mice to establish bone metastases, and subsequently analyzed by flow cytometry for expression of integrin β3 (Fig. 3.1A). Remarkably, all three of these groups yielded bone metastases with high integrin β3 expression, irrespective of tumor cell β3 status prior to intracardiac injection (Fig. 3.1B). This demonstrated that enrichment for β3hi cells was not required for high tumoral β3 expression in the bone, instead suggesting that interaction with the bone microenvironment itself could potentiate β3 upregulation.

To identify candidate pathways that might mediate this phenotype, we screened a panel of cytokines and growth factors present in the bone microenvironment for their effect on β3 expression in breast cancer cells *in vitro*. Of the 11 factors tested, only TGF-β isoforms were capable of inducing integrin β3 expression in PyMT-BO1 (Fig. 3.1C) and 4T1 (Fig. 3.1D) murine breast cancer cells.

Snail1-mediated epithelial-mesenchymal transition is not required for integrin β3 induction by TGF-β

Integrin β3 has previously been shown to interact with and amplify signal transduction downstream of TGF-β receptors[169, 174], giving it a role in coordinating epithelial-mesenchymal transition (EMT) in a feed-forward manner[167, 176, 231]. As EMT is frequently accompanied by

broad changes in integrin expression[232], we asked whether it was a necessary step for TGF-β-induced upregulation of integrin β3 in breast cancer cells. To first determine if β3 expression was correlated with EMT, we performed immunohistochemistry for E-cadherin (*Cdh1*), an epithelial marker known to be downregulated during EMT in breast cancer cells[233], in murine PyMT-BO1 primary tumors and metastases. While PyMT-BO1 cells exhibited clear positive E-cadherin staining in orthotopic tumors and lung metastases where tumoral β3 is low, bone metastases, where tumoral integrin β3 expression is high, were starkly negative (Fig. 3.2A). *In vitro*, moreover, TGF-β treatment of PyMT-BO1 cells significantly reduced *Cdh1* expression while upregulating fibronectin (*Fn1*), a promoter of EMT and marker of transition to a more mesenchymal phenotype (Fig. 3.2B)[234].

To directly test the necessity of EMT for TGF-β-mediated β3 induction, we performed short hairpin RNA (shRNA) knockdown of *Snail1*, a master regulator of EMT initiation in breast cancer[235], in PyMT-BO1 and 4T1 cells. In both lines, shSNAIL-KD reduced *Snail1* expression by greater than 50% compared to the scrambled control; however, this difference had no significant effect on *Itgb3* induction after TGF-β treatment (Fig. 3.2C), suggesting that a robust EMT might not be required for TGF-β-responsive integrin β3 expression.

Integrin β3 upregulation by TGF-β requires canonical signaling through pSMAD2/3

TGF-β signaling through TGF-β receptor 1 (TGFβRI) canonically phosphorylates the SMAD2 and SMAD3 transcription factors, but has also been associated with "noncanonical" activation of numerous other pathways, most commonly p38 MAP kinase (p38), MAPK/ERK kinase-1 and 2 (MEK1/2), and c-Jun N-terminal kinase (JNK)[236]. To determine the involvement of these pathways in TGF-β-mediated upregulation of integrin β3, we evaluated integrin β3 expression in TGF-β-stimulated breast cancer cells in the presence of pharmacological inhibitors for these

noncanonical pathways, as well as a site-specific inhibitor of canonical SMAD2/SMAD3 phosphorylation by TGFβRI (SMAD2/3i, see Fig. 3.3 for details). In both PyMT-BO1 and 4T1 cell lines, complete blockade of β3 mRNA (Fig. S3.1A) and surface protein (Fig. 3.3A and B) upregulation by TGF-β was only achieved in the context of SMAD2/3i treatment. Western blot analysis demonstrated selective abrogation of SMAD/2/SMAD3 phosphorylation (Fig. 3.3C) and total β3 protein (Fig. 3.3D) upon SMAD2/3i administration in PyMT-BO1 cells. To assess if this was also true of bone metastases *in vivo*, MDA-MB-231 tumor-bearing mice were treated daily with a pharmacologic TGFβRI kinase inhibitor. TGFβRI kinase inhibition significantly suppressed β3 expression on MDA-MB-231 breast cancer bone metastases (Fig. 3.3E), directly confirming the necessity of TGF-β signaling for tumoral β3 upregulation. In keeping with a previous report, TGFβRI kinase inhibition was also associated with a reduction in bone metastatic tumor burden (~1.6-fold, Fig. S3.1B)[68].

A dual luciferase reporter enables breast cancer-specific assessment of TGF-β activity

TGF-β is typically present in the microenvironment in a latent form, which must be activated before receptor binding and signal transduction can take place [230]. We reasoned that this bioavailability requirement might account for the high tumoral β3 expression we had observed in bone metastases compared to the primary tumor or visceral metastatic sites such as the lung.

As a first step toward testing this hypothesis, we developed a dual luciferase reporter derivative of our bone metastatic PyMT-BO1 breast cancer cell line. The p800neoLuc construct, bearing a TGF-β-responsive fragment of the *Pai1* promoter fused to a firefly luciferase reporter gene, has been demonstrated as a sensitive and specific readout of canonical TGF-β activity when stably transfected into mink lung epithelial cells[237]. To assess the relevance of TGF-β-responsive *Pai1* for integrin β3 expression in breast cancer cells, we treated PyMT-BO1 cells with various

concentrations of TGF-β and evaluated *Itgb3* and *Pai1* expression by qPCR. Both genes responded to TGF-β in a dose-dependent manner, and we observed a strong linear correlation in their expression across all doses tested (Fig. 3.4A). As we had previously seen with *Itgb3*, *Pai1* expression was also completely abrogated during inhibition of SMAD2/3 phosphorylation by TGFβRI (Fig. S3.4).

Having confirmed *Pai1* as a TGF-β-responsive gene with *Itgb3*-correlated expression in breast cancer cells, we proceeded with generation of a dual luciferase reporter line (construct strategy in Fig. 3.4B). First, constitutive *Renilla* expression was established in unlabeled PyMT-BO1 cells by lentiviral transduction (see Materials and Methods) and confirmed to correlate with cell number (Fig. 3.4C). The resulting *PGK-Renilla* PyMT-BO1 cells were then transfected with the TGF-β-responsive p800neoLUC plasmid by electroporation, selected in geneticin, and grown as single cell colonies to obtain subclonal lines with stable incorporation of the reporter, as determined by comparison of *Renilla*-normalized luciferase activity before and after TGF-β stimulation (Fig. 3.4D). The resulting candidate clonal derivative, PLR-BO1-X, exhibited a dose-dependent increase in luciferase activity upon TGF-β treatment *in vitro*, with a response profile very similar to what we had observed for *Itgb3* and *Pai1* expression by qPCR (Fig. 3.4A).

Genetic manipulation of TGF-β activity in non-bone organs modulates β3 expression and treatment response

To determine if increased TGF-β bioavailability was indeed sufficient to induce tumoral integrin β3 expression in metastases outside the bone, we turned to a well-characterized fibrillin-1 mutant mouse model of Marfan syndrome (MFS), $Fbn1^{C1039G/+}$. Mice heterozygous for this point mutation (MFS mice) have been demonstrated to exhibit signs of increased TGF-β activity in tissues, particularly elastic organs such as the aorta and the lungs, as a consequence of

diminished fibrillin anchoring of latent TGF-β in the ECM[238, 239, 240] (see schema, Fig. 3.5A). We established systemic metastases by intracardiac injection in wild type (WT) and MFS littermates, allowed them to be conditioned by the metastatic microenvironment for 11 days *in vivo*, then dissected out lungs, kidney, and hindlimb bones for *ex vivo* flow cytometry of integrin β3 expression on GFP+ tumor cells. While tumor cells from kidney and bone metastases exhibited no difference in integrin β3 expression between genotypes, we observed a highly significant increase in the frequency of β3+ tumor cells in the lungs of MFS mice compared to WT (69% vs 41%, $p<0.0001$)(Fig. 3.5B).

Having previously demonstrated that integrin β3 mediates increased resistance to taxane chemotherapy *in vivo*, we wondered if docetaxel treatment would be less effective against β3-expressing lung metastases in MFS mice. To test this, we established systemic PyMT-BO1 metastases by i.c. injection as before and treated mice with either vehicle or an aggressive DTX regimen with demonstrated efficacy against PyMT-BO1 lung metastases (3 doses of 6.67mg/kg each, cumulative 20mg/kg over 11-12 day course)[175]. While growth of lung metastases in WT mice was attenuated by DTX (~8-fold reduction, $p<0.01$), β3-expressing lung metastases in MFS mice failed to exhibit a significant response to therapy (1.6-fold reduction). Moreover, this divergent treatment response was not evident in either hindlimb or kidney metastases, organs where a genotype-driven difference in tumoral integrin β3 expression was also notably absent. Taken together, these data suggest that enhanced TGF-β bioavailability is sufficient to drive integrin β3 expression, and docetaxel resistance, in visceral metastatic sites outside of the bone.

3.4 Discussion

The body's largest natural TGF-β reservoir is the bone, where it is stored in the matrix as an inactive latent complex that must be liberated prior to activation[67]. TGF-β signaling has long

been understood to play an important role in the breast cancer bone metastatic cascade, where its release from the osteoid bone matrix drives a positive feedback loop that promotes tumor proliferation[70], accelerates osteoclast-mediated bone destruction[16, 73], and enhances cancer-related muscle weakness[68, 241]. The integrin β3 subunit, meanwhile, has been shown to promote a bone metastatic phenotype[60, 173] and is upregulated on bone-resident breast cancer cells in both mice and humans[172, 175]. TGF-β had previously been shown to upregulate integrin β3 on normal and transformed mammary epithelial cells[167, 169, 176]; however, the physiological regulation of tumoral β3 expression *in vivo* had not been explored. Here, we demonstrate for the first time that canonical TGF-β signaling through SMAD2/3 promotes upregulation of integrin β3 on tumor cells exposed to the bone microenvironment, likely independent of EMT. We developed a tractable tool for assessment of TGF-β activity in breast cancer cells, and demonstrated that genetic manipulation of environmental TGF-β bioavailability was sufficient to increase β3 expression and resistance to taxane chemotherapy at a visceral metastatic site.

TGF-β activity has been extensively implicated in primary and metastatic breast cancer[171, 230], leading us to wonder why tumoral integrin β3 upregulation appeared limited to the bone microenvironment. In contrast with single-digit pg/mL TGF-β sensitivities described in MLECs[237], *in vitro* characterization of integrin β3 response to TGF-β stimulation using both qPCR and a luminescent reporter of TGF-β activity suggested a threshold effect in breast cancer cells, with TGF-β concentrations of 500pg/mL or higher required before substantial upregulation of β3 could occur. Future *in vivo* experiments using our PLR-BO1-X TGF-β reporter line are planned in order to directly correlate *in vivo* integrin β3 expression with TGF-β bioavailability experienced at various metastatic sites, both at baseline and in the context of chemotherapy. Establishment of PLR reporter derivatives of other syngeneic, immunocompetent mouse models

of bone metastatic breast cancer (e.g. 4T1) would also be useful to determine if such a threshold effect is generalizable beyond the PyMT-BO1 line. If it is not—that is, if breast cancer cells generally exhibit a broad range of sensitivities to TGF-β stimulation—this would suggest an intriguing new hypothesis in which *in vivo* integrin β3 expression is actually the product of two tunable factors: intrinsic tumor cell sensitivity to TGF-β signaling, and TGF-β bioavailability in the microenvironment. Such a mechanism, if borne out, would be particularly interesting in terms of its potential consequences for induction of β3-mediated chemoresistant phenotypes outside of the bone.

Despite identifying canonical signaling through SMAD2/3 as a requirement for TGF-β-mediated induction of integrin β3 in breast cancer cells, we were unable to isolate the effector pathways or genes that more immediately control β3 expression downstream of TGF-β ligand binding and receptor signaling. While we provide evidence against a regulatory role for EMT through experiments in *Snail1* knockdown PyMT-BO1 and 4T1 cells, *Snail1* expression was not completely abrogated in our hands, and EMT programs are known to exhibit substantial redundancy that withstands genetic insult[242]. More holistic evaluation of the TGF-β-mediated gene regulatory events that contribute to integrin β3 upregulation in breast cancer cells, possibly through chromatin accessibility profiling or mass spectrometry aided by promoter trapping, will likely be necessary for progress in this area to be made.

Genetic and pharmacological inhibition of TGF-β signaling has been demonstrated to have anti-tumor activity in preclinical models of breast cancer bone metastasis [68, 76]. Moreover, other groups have shown that TGF-β inhibition can synergize with broad spectrum anti-mitotic chemotherapeutic agents such as paclitaxel[243, 244] to restrain breast cancer growth. Our observation of enhanced docetaxel resistance in lung metastases in Marfan syndrome mice lends

additional support to this paradigm and implicates upregulated tumoral integrin β3 as a possible molecular mediator. Future studies using β3 and TGF-β receptor knockout cell lines are needed to definitively demonstrate the causal relationship between enhanced TGF-β bioavailability, integrin β3 expression, and therapeutic resistance in bone and at visceral metastatic sites. Reciprocal studies in MFS mice treated with a pan-neutralizing antibody against TGF-β ligands would also be helpful to cement fully the role that increased active microenvironmental TGF-β appears to play in regulating tumoral expression of integrin β3.

Taken together, we demonstrate that integrin β3 is upregulated on bone-resident breast cancer cells in a TGF-β-dependent fashion that requires canonical signaling through SMAD2/3. Using a mouse model of Marfan Syndrome, we further show that enhanced TGF-β bioavailability is sufficient to induce tumoral integrin β3 expression and chemoresistance in visceral metastatic sites, emphasizing the importance of dynamic TGF-β bioavailability for signaling and therapeutic response in breast cancer.

3.5 Materials and Methods

Animals

Animal studies were performed according to the guidelines established by the Washington University Institutional Animal Care and Use Committee. Tumor cells were implanted into female C57BL/6 mice. All mice were obtained from The Jackson Laboratory, and injected at 6−7 weeks of age. All rodents were housed according to the guidelines of the Division of Comparative Medicine, Washington University School of Medicine (St. Louis, MO). In collaboration with Dr. T.A. Guise, histologic bone sections from female athymic nude mice injected with MDA-MB-231 human breast cancer cells were obtained from an experiment

described previously[68].

Cell lines and constructs

The murine C57BL/6 PyMT-Bo1 luminal B breast cancer cell line (stably expressing GFP and firefly luciferase genes) was originally isolated from a transgenic MMTV-PyMT breast tumor, as validated and described previously[150]. The murine BALB/c 4T1 triple-negative breast cancer cell line was purchased from ATCC, as described previously[62]. All cells were maintained at sub-confluence in DMEM with 10% FBS and 0.5% penicillin-streptomycin, in a humidified chamber at standard culture conditions. Low-passage stocks were used and regularly tested for *Mycoplasma* and maintenance of growth characteristics.

Stable knockdown of *Snai1* in PyMT-BO1 and 4T1 cell lines was achieved by transduction of shRNA constructs with the following sequences: *Snai1* 1: 5'-GCCACCTTCTTTGAGGTACAA-3', *Snai1* 2: 5'-GCGGAAGATCTTCAACTGCAA-3', scrambled control (SCRAM-CTRL): CCTAAGGTTAAGTCGCCCTCGCTC using pLKO.1 vectors, as previously described[245].

Constitutive *Renilla* expression in PyMT-BO1 cells was achieved using the pLenti.PGK.blast-Renilla_Luciferase vector system (Addgene#: 74444). 293T cells (ATCC, RRID:CVCL_0063) were used for viral packaging with the pCMV-DR8.2 and pCMV-VSVG plasmids. Tumor cell lines were transduced with viral supernatant for 12 hours at 37°C in 6-well tissue culture plates. Transduced cells were selected in 2ug/mL blasticidin (Sigma: 203350). *Renilla*-expressing cells were subsequently transfected by electroporation with 2µg of the TGF-β-responsive p800neoLUC reporter construct[237], selected in 500ug/mL geneticin (Gibco: G418), and single-cell cloned by seeding at limiting dilution to select for robust luciferase response to TGF-β stimulation.

In vivo modeling of metastasis and therapy

To establish orthotopic mammary fat pad (MFP) tumors, $0.1x10^6$ tumor cells in 50-uL PBS were injected into MFP tissue of 7-week-old female mice. To establish experimental secondary metastases, $0.05x10^6$ tumor cells in 50uL PBS were intracardially injected into the left ventricular chamber of 6-week-old female, with one exception; in collaboration with Dr. T.A. Guise, human MDA-MB-231 tumor cells were intracardially injected ($0.1\ 10^6$ tumor cells in 100uL PBS) into 4-week-old female athymic nude mice, as described previously[68].

Docetaxel (5mg/kg, LC Laboratories: RP 56976) or equivalent vehicle was freshly prepared and administered by tail vein injection. Docetaxel was initially solubilized in 100% ethanol and stored at -20°C. A 10mg/mL working solution was freshly prepared on the day of injection by dilution in a Tween 80/PBS solution (final Tween 80 : ethanol : PBS ratio of 20:13:67) to prevent precipitation. Finally, working solution was further diluted to 0.9-1mg/mL in PBS. Vehicle control was prepared and diluted in a similar manner using 100% ethanol without docetaxel.

Bioluminescence imaging

In vivo bioluminescence imaging was performed on the days indicated using an IVIS Lumina (PerkinElmer, Waltham, MA; Living Image 4.2), 5min to 1sec exposure, bin2-8, FOV12.5cm, f/stop1, open filter). Mice were injected intraperitoneally with D-luciferin (150mg/kg in PBS; Gold Biotechnology, St. Louis, MO) and imaged using isoflurane anesthesia (2% vaporized in O2). Mice were euthanized immediately after *in vivo* confirmation of successful intraperitoneal administration of D-luciferin. Organs of interest were then dissected out and imaged separately. Total photon flux (photons/sec) was measured from fixed regions of interest (ROIs) using Living Image 2.6 (RRID:SCR_014247). Investigators were blinded to treatment groups during BLI

analyses.

In vitro elicitation of Renilla and firefly luciferase activity in PLR-BO1 cells was achieved using the Dual-Glo® Luciferase Assay System (Promega: E2920) according to manufacturer's instructions and read out on a SpectraMax i3 plate reader (Molecular Devices, Sunnyvale, CA).

Immunohistologic staining

Freshly removed tissue was fixed in 10% neutral buffered formalin for 24 hours. Bone was decalcified in 14% EDTA for 10 days. Tissue was paraffin embedded and sectioned 5-mm thick at the histology core of the Washington University Musculoskeletal Research Center.

For IHC, all slides were stained in parallel, using identical staining conditions. Paraffin tissue slides were prepared by immersing slides in xylene and rehydrating tissue in 100% ethanol, 95% ethanol, 70% ethanol, 50% ethanol, and deionized water washing steps. Slides were immersed in EDTA antigen retrieval buffer (1 mmol/L EDTA, 0.05% Tween 20, PH 8.0) at 50°C overnight. Slides were treated with dual endogenous enzyme block (Dako), TBS/0.1% Tween-20 (TBST) wash buffer, and 10 minutes of serum-free protein block (Dako). Slides were stained with the following primary antibodies: anti-integrin β3 antibody (D7X3P, 1:200, Cell Signaling Technology), anti-e-cadherin (24E10, 1:200, Cell Signaling Technology), or isotype control rabbit IgG (ab27472, Abcam) antibody. Following primary antibody incubation, slides were extensively washed in TBST. Either Anti-Rabbit EnVision+ System-HRP (Dako) or Vectastain Elite ABC HRP kit (Vector Laboratories) was used as the secondary antibody, followed by Liquid DAB+ (3,30 -Diaminobenzidine) Substrate system (Dako), according to the manufacturer's protocol. Nuclear hematoxylin counterstain was applied, followed by dehydration through 70% ethanol, 95% ethanol, 100% ethanol, and xylene. Slides were mounted with

Cytoseal XYL (Thermo Scientific).

Histologic imaging and analysis

Histologic slides were imaged on either an Olympus NanoZoomer 2.0-HT System or on a Zeiss AxioScan.Z1. In each experiment, post-imaging analysis was limited to changes in brightness or contrast, gamma 1⁄4 1, which were applied equally to all images. Sections stained with integrin β3 were quantified using Visiopharm software, which allows for recognition and quantification of DAB-stained tissue areas. A supervised Bayesian pixel classifier was used to classify an image based on three distinct categories: DAB staining, hematoxylin staining (nuclei), and unstained tissue and other background structures. Integrin β3 expression from each sample was calculated within 5-10 random high-powered fields of 100-200 cells within the tumors. Values expressed as the percentage of integrin β3 expression (area of total DAB-positive staining) divided by the tumor area in the high-powered field.

Flow cytometry and FACS

In vitro tumor cells were lifted with 1x Versene (Invitrogen). *Ex vivo* tumor cells were collected from the MFP, kidney, lung, or bone, and prepared into single-cell suspensions for flow cytometry analysis as described previously[150]. For some experiments, *ex vivo* cells were stained with PE-conjugated anti-mouse integrin β3 (1:200, clone: 2C9.G2, BD Pharmingen), fixed, and permeabilized using the Cytofix/Cytoperm kit (BD Biosciences) according to the manufacturer's protocol, and then with AlexaFluor488–conjugated anti-human/mouse cytokeratin 18 (1:100, clone LDK18, eBioscience). For live analysis, cells were stained with either PE- or AlexaFluor-647-conjugated anti-mouse integrin β3 (1:200, clone: 2C9.G2, BD Pharmingen; PE RRID:AB_394800; AF647 RRID:AB_2738255), CD45.2, (1:200, clone: 104, BioLegend, RRID:AB_492872) and DAPI (Sigma: D9542). Data acquisition was performed on the

LSRFortessa (BD Biosciences) and FlowJo software version 10.1 (Tree Star) was used for analysis and fluorescence compensation using UltraComp eBeads (eBioscience) according to the manufacturer's protocol. All flow cytometry data are presented as median fluorescent intensity.

For FACS, in vitro tumor cells were lifted with 1x Versene (Invitrogen) and stained for surface expression of integrin β3 as described above. Tumor cells were sorted into two populations using a BD FACSAria-II cell sorter (BD Biosciences): integrin β3 negative (β3-) cells (based on the fluorescent intensity of unstained cells) and integrin β3-expressing (β3+) cells. Control cells sorted without β3 discrimination were also collected (β3-all). After sorting, each population was counted for live/dead cells, and $0.05x10^6$ live tumor cells in 50uL PBS were intracardially injected into the 6-week-old female mice.

Pharmacologic inhibition of signaling pathways

Tumor cells were pretreated for 1 hour with pharmacologic inhibitors: cells were pretreated for 1 hour with the following pharmacologic inhibitors: TGF-β receptor I kinase inhibitor, specific for the site necessary for SMAD2/SMAD3 phosphorylation (SMAD2/3i, SB431542, 20 umol/L, Sigma-Aldrich); p38 MAP kinase (MAPK) inhibitor (p38i, SB203580, 20 umol/L, Cell Signaling Technology); MEK1/2 (MAPK/ERK Kinase) inhibitor (MEK1/2i, U0126, 20 umol/L, Cell Signaling Technology); c-Jun N-terminal kinase (JNK) inhibitor (JNKi, SP600125, 50 umol/L, Sigma-Aldrich). After 1 hour of pre- treatment, cells were treated with 2 ng/mL of murine TGF-β1 (R&D Systems) or vehicle treatment. Cells were all cultured in 0.1% DMSO.

Western blot analysis

Whole cell lysates from tumor cells were collected in RIPA buffer (Cell Signaling Technology) in the presence of Halt phosphatase inhibitor cocktail (Thermo Scientific) at 4°C . Protein

samples were separated on 10% Mini-PROTEAN TGX polyacrylamide gels (Bio-Rad) and transferred onto an Immobilon-P polyvinylidene difluoride membrane (EMD Millipore). Membranes were incubated with phosphorylated-SMAD2/phosphorylated-SMAD3 (pSMAD2/pSMAD3, D27F4), total SMAD2/SMAD3 (D7G7), integrin β3 (D7X3P), or β-actin (13E5), followed by horseradish peroxidase-conjugated anti-rabbit secondary antibody (all from Cell Signaling Technology). All antibodies were diluted and used according to the manufacturer's protocol. Bands were developed by enhanced chemiluminescence.

qPCR analysis

Total RNA from cells was isolated with the RNeasy Mini Plus Kit (Qiagen). Complementary DNA was made using the SuperScript II first-strand synthesis system for qPCR (Invitrogen). qPCR was performed using SYBR Advantage mix (Bio-Rad) as described previously[150], with mouse-specific primers for mRNA genes of interest: *Itgb3* forward: 5'-TTC AAT GCC ACC TGC CTC AAC AAC-3', *Itgb3* reverse: 5'-ACG CAC CTT GGC CTC GAT ACT AAA-3', *Fn1* forward: 5'-TCC TGT CTA CCT CAC AGA CTA C-3', *Fn1* reverse: 5'-GTC TAC TCC ACC GAA CAA CAA-3', *Pai1* forward: 5'-GGG ACG AAA CTG GAG ATG TTA T-3', *Pai1* reverse: 5'-GAG GAG TTG CCT TCT CTT TCT C-3', *Snai1* forward: 5'-GCT GAT GGA GTG CCT TTG TA-3', *Snai1* reverse: 5'-CCA GTG GGT TGG CTT TAG TT-3', *Cdh1* forward: 5'-AAC AAC AAC AGA GAG TCG TAA G-3', *Cdh1* reverse: 5'-GTC CTG CCA ATC CTG ATG AA-3', *Gapdh* forward: 5'-AGG TCG GTG TGA ACG GAT TTG-3', *Gapdh* reverse: 5'-TGT AGA CCA TGT AGT TGA GGT CA-3'. Target gene expression was normalized against the housekeeping gene GAPDH (*Gapdh*), and data were analyzed using the $\Delta\Delta C_t$ method.

Panel of cytokines and growth factors

Tumor cells were cultured for 24 hours with the following murine factors: 2 ng/mL TGF-β1

(R&D Systems), 2 ng/mL TGF-β2 (R&D Systems), 50 ng/mL Sonic Hedgehog (Shh; Pepro-Tech, #315-22), 50 ng/mL WNT-3A (PeproTech, #315-20), 100 ng/mL insulin-like growth factor 1 (IGF-1; PeproTech, #250-19), 50 ng/mL epidermal growth factor (EGF; PeproTech, #315-09), 50 ng/mL fibroblast growth factor 2 (FGF2 or bFGF; PeproTech, #450-33), 100 ng/mL osteopontin (OPN; Leinco, #O121), 10 ng/mL IL4 (R&D Systems), 200 ng/mL stromal cell-derived factor 1a (SDF-1α or CXCL12; Biolegend), 10 ng/mL IL6 (R&D Systems).

3.6 Figures

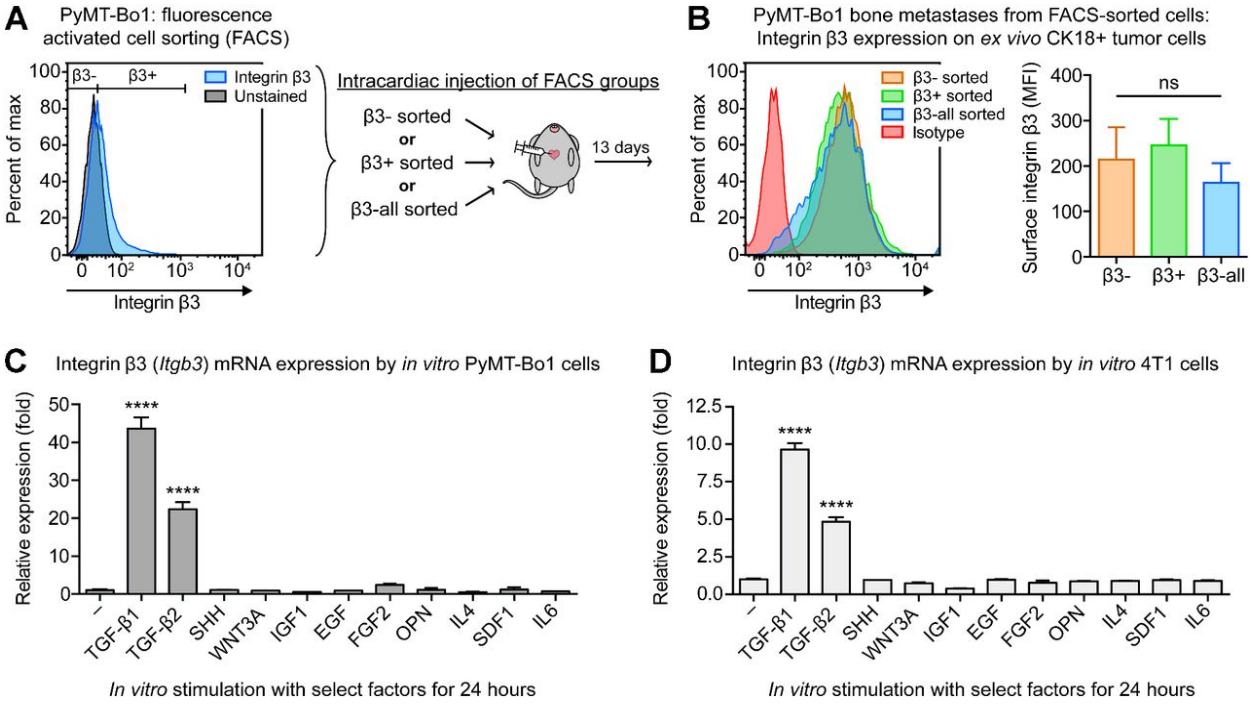

Figure 3.1 Integrin β3 is induced in the bone microenvironment and by exposure to TGF-β.
A. *In vitro* PyMT-BO1 cells were FACS sorted into three groups based on basal β3 expression: β3-, β3+, and β3-all. Immediately after collection, cells were injected i.c. into separate groups of mice. **B**. Thirteen days post-injection, isolated bone metastatic PyMT-BO1 cells were identified by CK18+ and evaluated by flow cytometry for surface β3 expression. Left, representative samples. Right, n = 4 β3-; n = 4 β3-all; n = 5 β3+. One-way ANOVA with Tukey *post hoc* test. **C**. and **D**. qPCR analysis of β3 (*Itgb3*) mRNA expression by PyMT-BO1 or 4T1 cells cultured *in vitro*, following 24hr stimulation with the listed factors (see Materials and Methods for details). One of two biological replicates, each in technical duplicate. One-way ANOVA with Tukey *post hoc* test. Data presented as mean ± SEM.

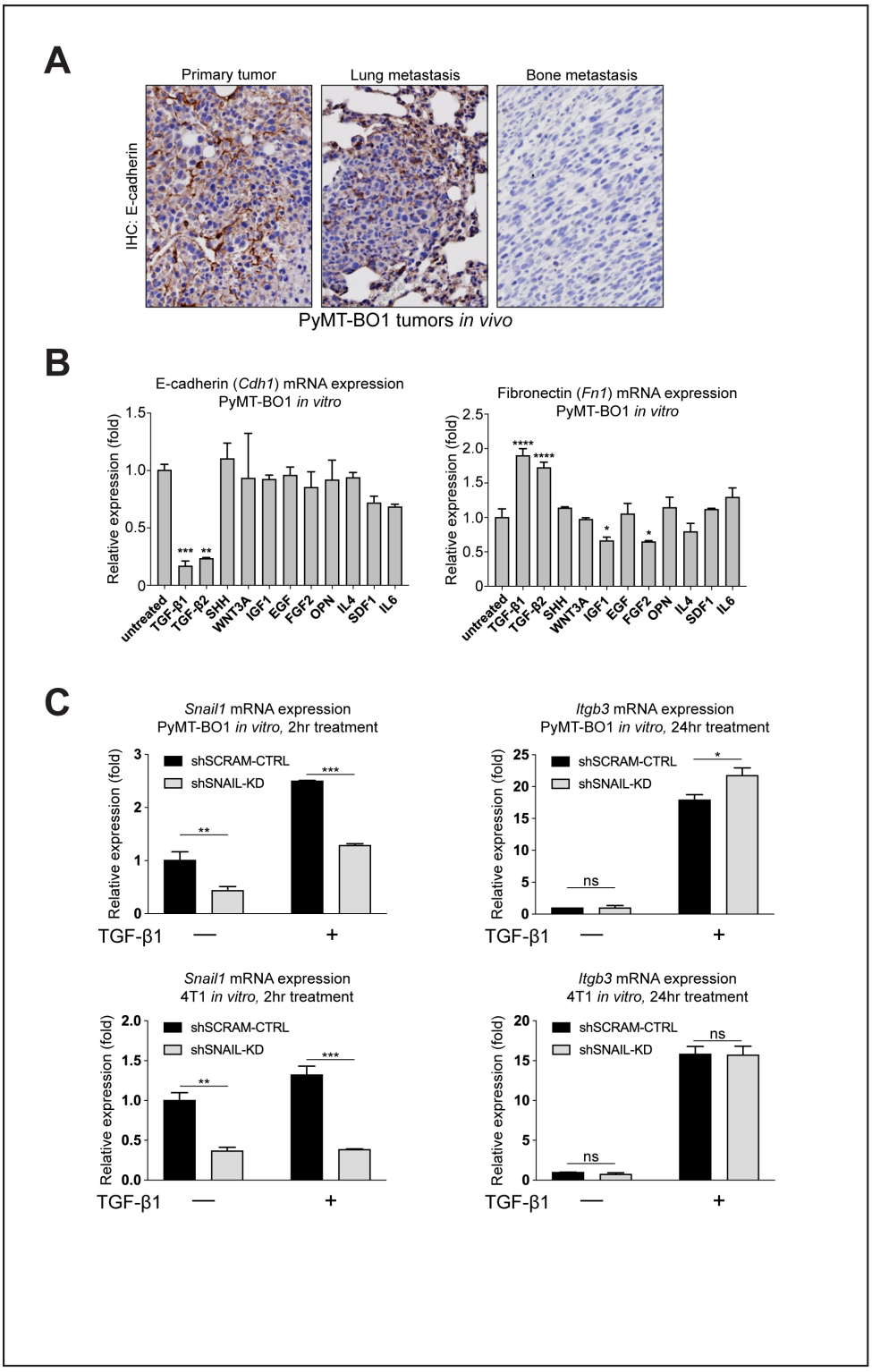

Figure 3.2 Snail1-mediated epithelial-mesenchymal transition is not required for integrin β3 induction by TGF-β

A. Immunohistochemical staining for E-cadherin in PyMT-BO1: orthotopic mammary fat pad tumor (left), lung metastasis (middle), and bone metastasis (right). **B**. qPCR analysis of E-cadherin (*Cdh1*, left) and fibronectin (*Fn1*, right) in PyMT-BO1 cells cultured *in vitro*, following 24hr stimulation with the listed factors (see Materials and Methods for details). One biological replicate per group, each in technical duplicate. One-way ANOVA with Tukey *post hoc* test. **C**. qPCR analysis of *Snail1* (left) and integrin β3 (*Itgb3*, right) in PyMT-BO1 (top) and 4T1 (bottom) cells with SNAIL (gray) or SCRAM-CTRL (black) shRNA knockdown. Cells cultured *in vitro*, following 2hr (*Snail1*) or 24hr (*Itgb3*) stimulation with 2ng/mL TGF-β1. One biological replicate per group, each in technical duplicate. Two-way ANOVA with Tukey *post hoc* test. Data presented as mean ± SD.

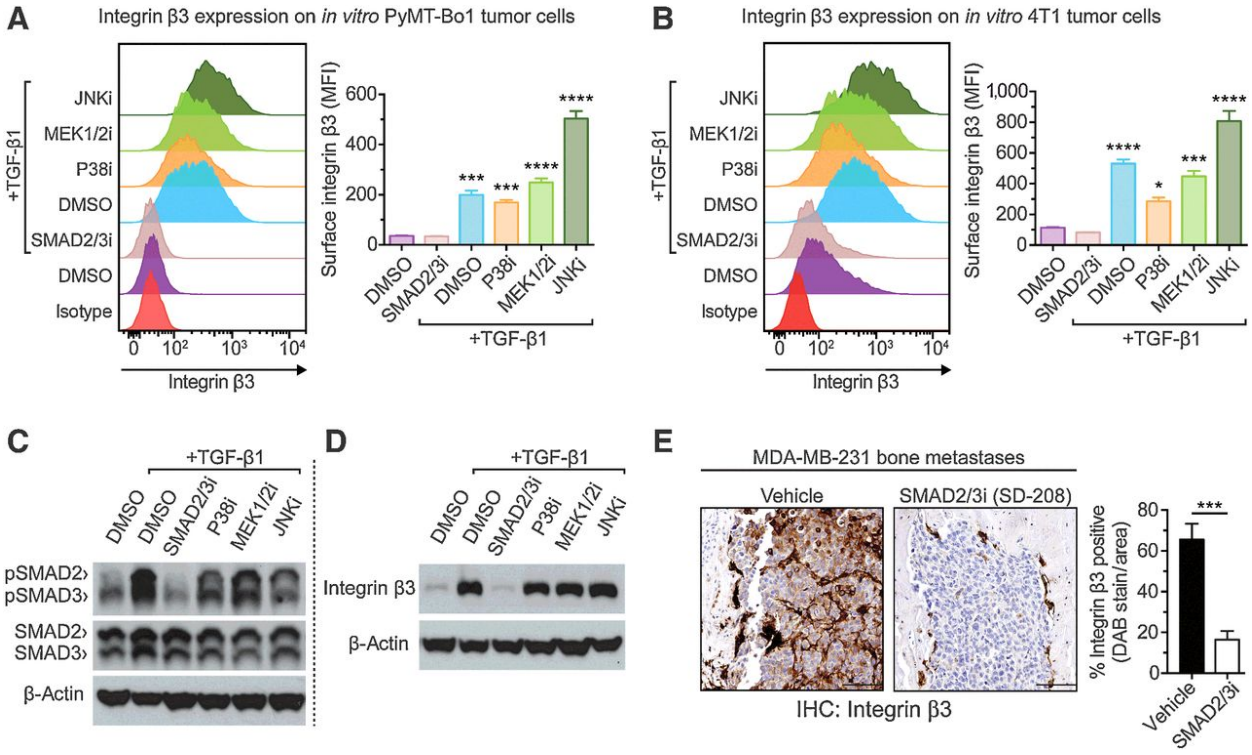

Figure 3.3 Integrin β3 upregulation by TGF-β requires canonical signaling through pSMAD2/3.
A. and **B**. *In vitro* tumor cells treated with either 2ng/mL TGF-β1 or DMSO control in the presence of a pharmacologic inhibitor SMAD2/3i (20μM, SB431542), MEK1/2i (20μM U0126), p38i (20μM SB203580), or JNKi (50μM, SP600125). After 48 hours, flow cytometry for surface β3 expression was evaluated on PyMT-BO1 cells (**A**) or 4T1 cells (**B**). Left, representative experiment; right, n = 3 biological replicates. One-way ANOVA with Tuckey *post hoc* test, with denoted significance in relation to DMSO control. **C**. and **D**. Western blot analysis of *in vitro* PyMT-BO1 cells treated as described previously, for 3 hours (**C**) or 24 hours (**D**). **E**. Mice injected i.c. with MDA-MD-235 cells were treated daily with a TGFβRI kinase inhibitor of SMAD2/3 phosphorylation (SD-208, 60mg/kg/d) or vehicle control (1% methylcellulose for 28 days. IHC for β3 with representative images (left) and quantification of DAB-stained bone metastases, n = 4 (right). Scale bar, 100μm. Two-tailed unpaired t test. Data presented as mean ± SEM.

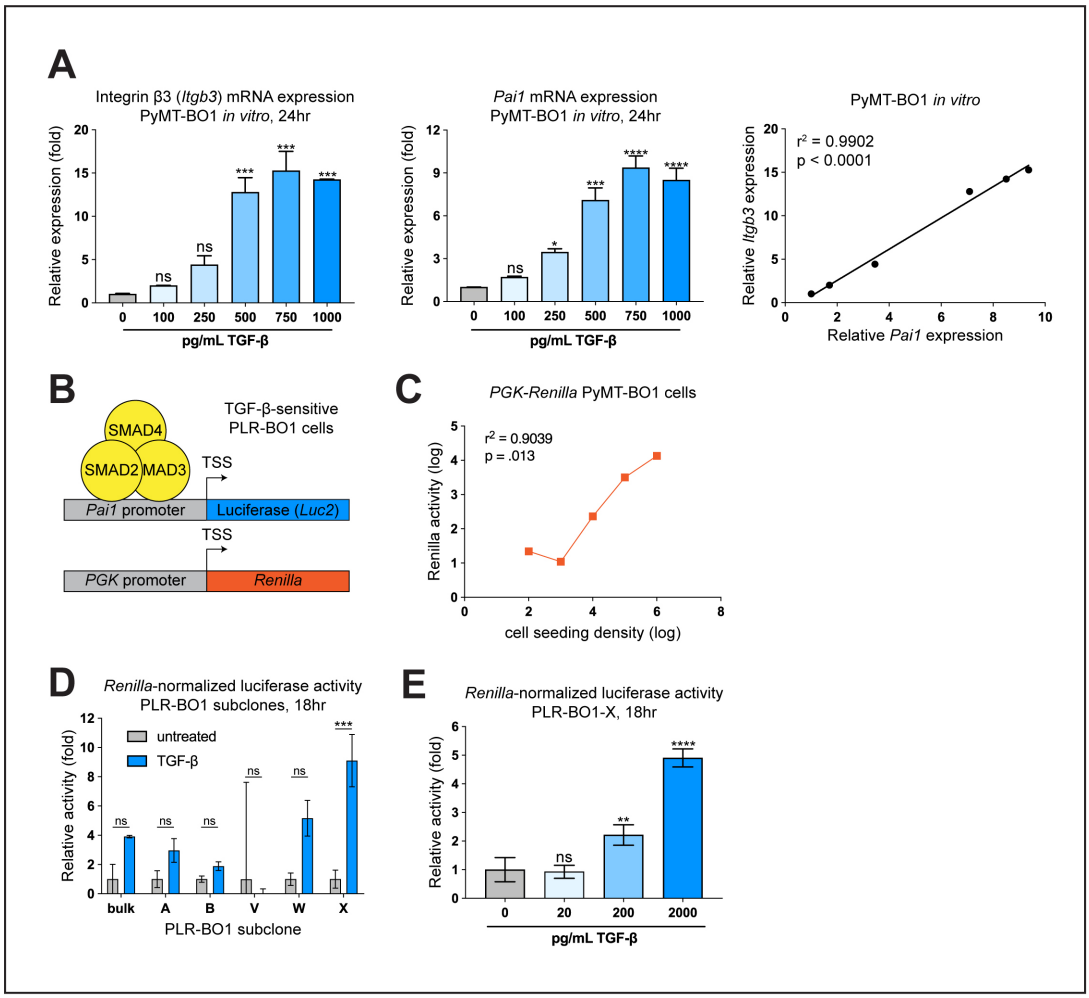

Figure 3.4 A dual luciferase reporter enables breast cancer-specific assessment of TGF-β activity
A. qPCR analysis of integrin β3 (*Itgb3*, left) and *Pai1* (middle) in PyMT-BO1 cells cultured *in vitro*, following 24hr stimulation with the indicated concentrations of TGF-β1. Correlation between *Itgb3* and *Pai1* expression with increasing concentrations of TGF-β1 stimulation. One biological replicate, in technical duplicate. One-way ANOVA with Tukey *post hoc* test; Pearson correlation coefficient. **B**. Schematic of constitutive *Renilla* and TGF-β-responsive luciferase (*Luc2*) reporter constructs. **C**. Correlation between overnight cell seeding density and measured *Renilla* activity in *PGK-Renilla* PyMT-BO1 cells, n = 2 biological replicates per group. Pearson correlation coefficient **D**. Luciferase activity in PLR-BO1 subclones treated with 2000pg/mL TGF-β1 for 18hr, normalized to constitutive *Renilla* activity, n = 3 biological replicates per group. Two-way ANOVA with Tuckey *post hoc* test. **E**. Luciferase activity in PLR-BO1-X cells treated with the indicated concentrations of TGF-β1 for 18hr, normalized to constitutive *Renilla* activity, n = 3 biological replicates. One-way ANOVA with Dunnet's multiple comparisons test, with denoted significance in relation to untreated control. Data presented as mean ± SD.

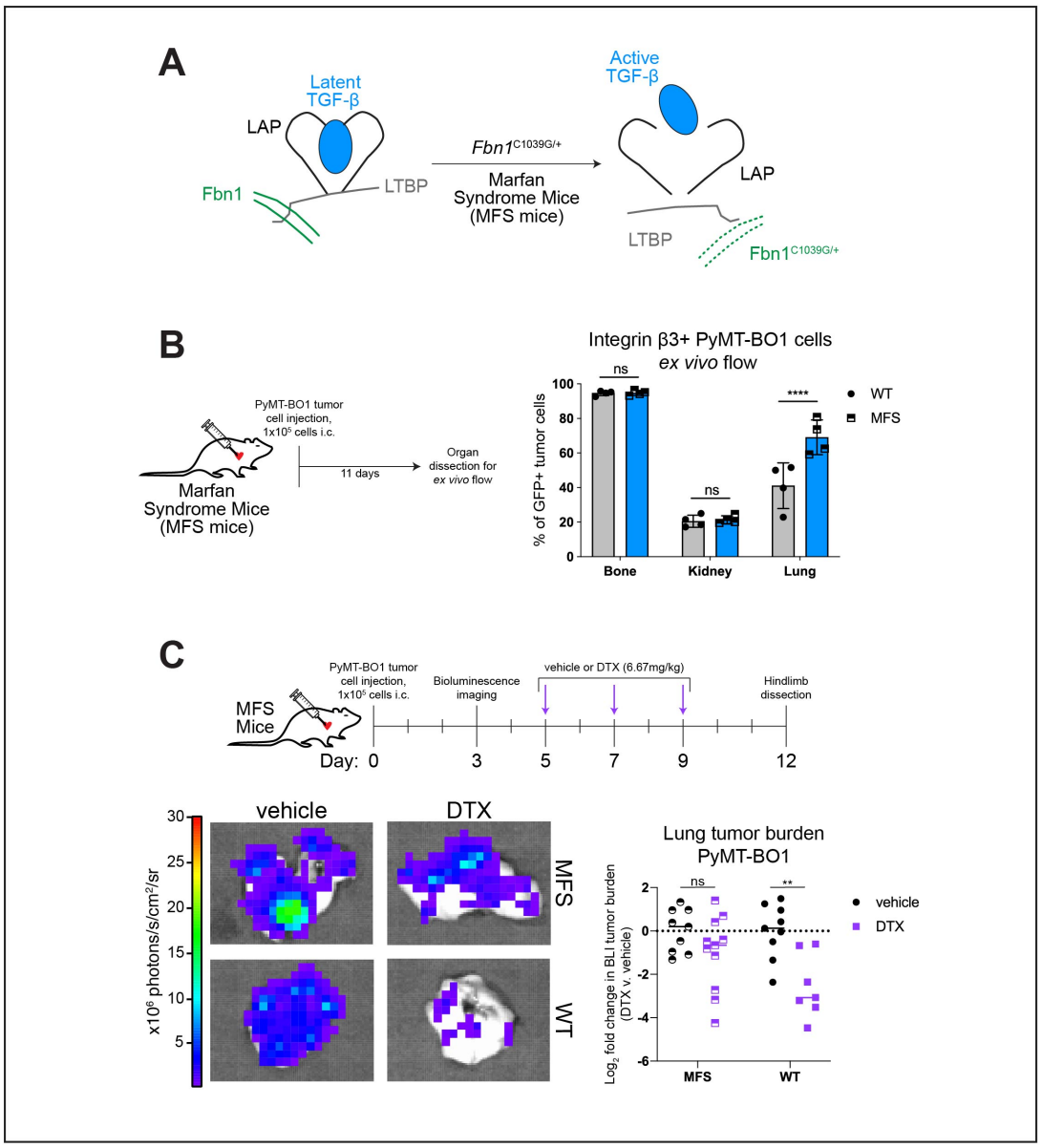

Figure 3.5 Genetic manipulation of TGF-β activity in non-bone organs modulates β3 expression and treatment response
A. Schematic detailing the effect of *Fbn1*$^{C1039G/+}$ on TGF-β availability in affected tissues of Marfan syndrome (MFS) mice. **B**. *Ex vivo* flow cytometry analysis of integrin β3 expression on live, GFP+ PyMT-BO1 cells harvested from established metastases in the indicated organs, n = 4 mice per group. Two-way ANOVA with Tuckey *post hoc* test. **C**. *Ex vivo* BLI of β3WT PyMT-BO1 lung tumor burden from WT or MFS mice receiving either vehicle or DTX (6.67mg/kg i.v.). Treatment schema (top), representative BLI (bottom left), quantification of *ex vivo* BLI signal from lungs (bottom right). n = 7-11 mice per group, pooled from two independent experiments. Data shown are $\log_2$ transformed fold change in photons/s relative to the geometric mean of samples from vehicle-treated mice of the same genotype. Two-way ANOVA with Tukey *post hoc* test.

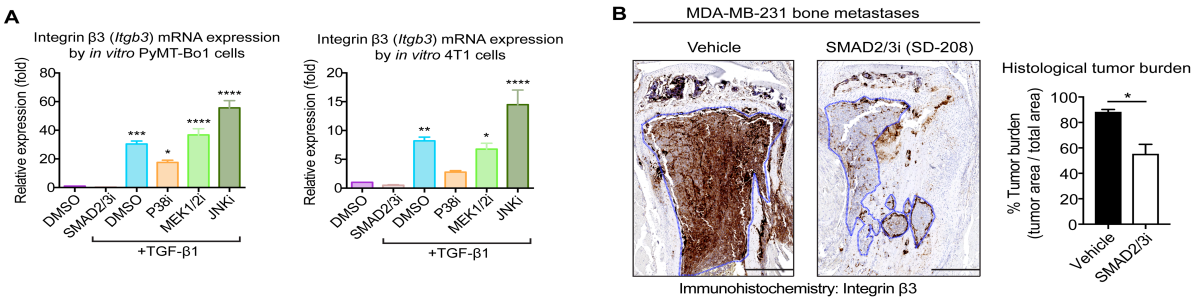

Figure S3.1 Tumoral changes following TGF-β stimulation and pharmacological inhibition of TGFβRI-mediated phosphorylation of SMAD2/SMAD3.
A. qPCR analysis of integrin β3 mRNA (*Itgb3)* expression in PyMT-BO1 or 4T1 cells, following 24hr stimulation with 2ng/mL TGF-β1 or DMSO control, in the presence or absence of a pharmacological inhibitor: SMAD2/3i (20μM SB431542), MEK1/2i (20 μM U0126), p38i (20μM SB203580), or JNKi (50μM SP600125). N=3 biological replicates per group, in technical duplicate. One-way ANOVA with Tukey's post-hoc test, with denoted significance in relation to the DMSO control, **B**. Mice intracardiac injected with MDA-MB-231 cells were treated daily with a TGFβRI kinase inhibitor of SMAD2/3 phosphorylation (SD-208, 60 mg/kg/d) or vehicle control (1% methylcellulose) for 28 days. Histological analysis of tumor burden within the tibiofemoral joint, identified based on histological sections staining for β3, n=4 (right). Representative images (left). Scale=500 μm. Two-tailed Mann–Whitney *U*-test. All data are presented as mean ± SEM.

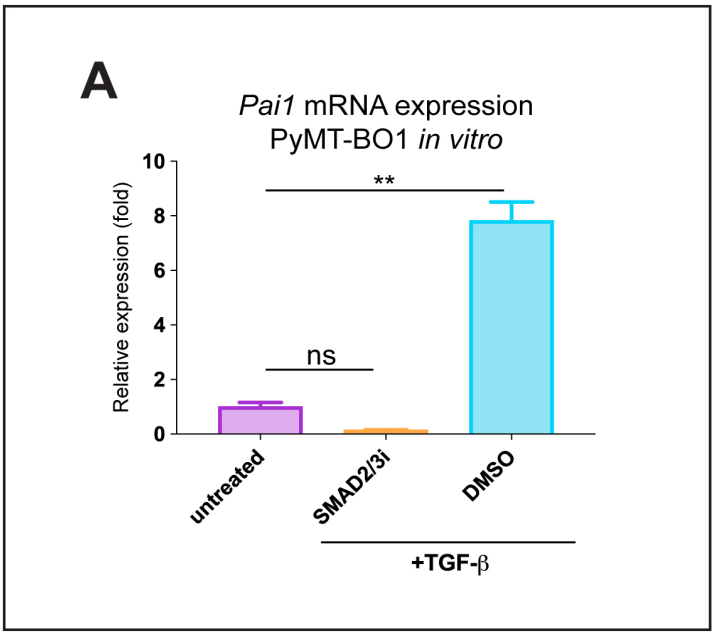

Figure S3.2 SMAD2/3i inhibits *Pai1* expression in TGF-β-treated PyMT-BO1 cells.
A. qPCR analysis of integrin β3 mRNA (*Itgb3)* expression within PyMT-BO1 or 4T1 cells, following 24 hrs stimulation with 2 ng/mL TGF-β1 or DMSO control, in the presence or absence of SMAD2/3i (20μM SB431542). n=1 biological replicate per group, in technical duplicate. One-way ANOVA with Tukey's post-hoc test, with denoted significance in relation to the DMSO control

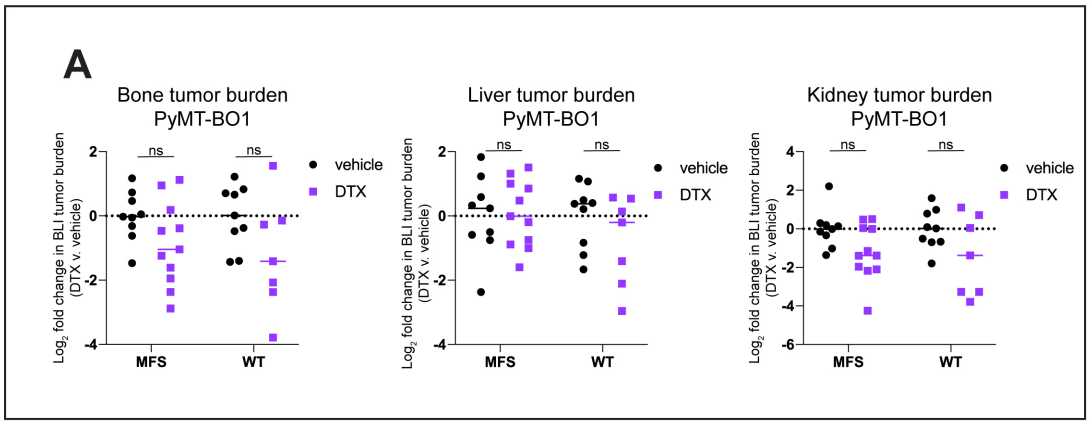

Figure S3.3 Tumor burden in other organs after docetaxel is unchanged between WT and MFS mice.
A. *Ex vivo* BLI of β3WT PyMT-BO1 hindlimb bone (left), liver (middle), and kidney (right) tumor burden from WT or MFS mice receiving either vehicle or DTX (5mg/kg i.v.), as detailed in **Fig. 3.5**. n = 7-11 mice per group, pooled from two independent experiments. Data shown are $\log_2$ transformed fold change in photons/s relative to the geometric mean of samples from vehicle-treated mice of the same genotype. In hindlimb bone and kidneys each data point represents averaged signaling intensity from organs of one mouse. Two-way ANOVA with Tukey *post hoc* test.

Chapter 4

Summary and Future Directions

4.1 Summary

Breast cancer bone metastases are common, incurable lesions that contribute to substantial morbidity and mortality in patients. Though the advent of bone-targeted therapies such as the bisphosphonate zoledronic acid and the anti-RANKL monoclonal antibody denosumab has been associated with diminished adverse skeletal-related events, survival benefit from these agents is confined to a subset of patients, and traditional treatments inevitably fail.

The malignant phenotype of breast cancer bone metastases is aided and abetted by their unique interaction with the bone microenvironment, which contributes to enhanced bone destruction, invasion, and resistance to therapy. Our lab had previously observed that tumor cells in breast cancer bone metastases exhibit higher expression of the β3 integrin subunit (β3) compared to their counterparts in primary tumors or visceral metastases. Based on *in vitro* evidence linking β3 expression to poor treatment response, we evaluated the functional role of tumoral integrin β3 in breast cancer bone metastases in the setting of systemic chemotherapy.

In vitro and in bone metastases *in vivo*, populations of β3+ tumor cells were enriched after exposure to docetaxel chemotherapy (DTX). 97% of post-chemotherapy clinical samples obtained from human patients with localized triple negative breast cancer (TNBC) exhibited populations of β3+ tumor cells, and a subset of patients with high β3 expression exhibited a trend toward increased risk of recurrence that was reinforced by survival analysis in a publicly available data set of TNBC patients receiving any chemotherapy. Genetic deletion of β3 in two immunocompetent murine breast cancer models greatly enhanced the activity of DTX chemotherapy, particularly in bone metastases, while genetic β3 rescue could reverse sensitivity in bone and visceral metastatic sites.

Using a combination of transmission electron microscopy in bone metastases and transcriptomic and functional studies *in vitro*, we demonstrated that β3 expression mediated an alternative metabolic response to chemotherapy characterized by increased protein production, oxygen consumption, and reactive oxygen species generation. Inhibition of the metabolic regulatory pathway mTORC1, either delivered as free drug or targeted to cells expressing activated αvβ3 integrin, could interrupt this response *in vivo* and synergistically attenuate bone metastases in combination with DTX. These studies highlight the importance of the metastatic microenvironment when designing combination treatments and provide evidence for mTOR inhibitors as a means to specifically sensitize resistant breast cancer bone metastases to chemotherapy.

To better understand what signals were driving the acquisition of this β3-mediated chemoresistance phenotype in bone metastases, we evaluated a panel of bone-relevant cytokines and growth factors for their ability to induce β3 expression in breast cancer cells, finding that only TGF-β isoforms were capable of doing so. While TGF-β-mediated epithelial-mesenchymal transition appeared to be dispensable for β3 upregulation, canonical signal transduction through phospho-SMAD2/3 was absolutely required *in vitro* and in breast cancer bone metastases *in vivo*. Furthermore, enhanced TGF-β bioavailability in the lungs of a mouse model of Marfan syndrome was sufficient to upregulate β3 on lung metastatic tumor cells and decrease their *in vivo* sensitivity to docetaxel, bringing our initial functional findings full circle.

Taken together, our data provide mechanistic evidence for a β3-mediated chemoresistance phenotype in breast cancer that is induced by interaction with the bone microenvironment and can be specifically reversed with targeted combination therapy. This paradigm has the potential to be clinically informative, particularly for the up to 40% of breast cancer patients who present

with bone-only metastatic disease. More than anything, our findings reinforce the profound role of the bone microenvironment in sculpting tumor phenotypes and clarify the remarkable specificity required for effective targeting and personalization of cancer therapy.

4.2 Future Directions

Our findings demonstrate that integrin β3 expression drives chemoresistance in breast cancer bone metastases. β3-expressing cells respond differently to DTX across a variety of metabolic parameters, including protein production, oxygen consumption, and reactive oxygen species. We found that combination of DTX and mTOR inhibition could reverse β3-mediated resistance, potentially through effects on protein production. Moreover, genetic manipulation of TGF-β bioavailability could induce tumoral β3 expression and chemoresistance in the lungs, suggesting integrin β3 as a causal link connecting TGF-β to resistant phenotypes. While we have traveled a fair way towards unraveling the nature of β3-mediated chemoresistance in the bone, our data have also raised an abundance of questions that we have yet to explore, particularly with regard to the nature and purpose of the β3-mediated alternative metabolic response to chemotherapy.

4.2.1 Is the β3-mediated alternative metabolic response necessary for chemoresistance?

We identified three main components of the β3-mediated alternative metabolic response--1) enhanced protein production / ER stress; 2) enhanced OXPHOS / oxygen consumption; and 3) enhanced generation of reactive oxygen species—all of which have been implicated in therapy resistance in malignancy [202, 246, 247], and all of which can be, tantalizingly, regulated by mTORC1 signaling[248–250]. Beyond this phenomenological characterization, however, we still know relatively little about the actual molecular specifics of this response that we have identified, nor can we say for certain whether it is an active contributor to β3-mediated resistance or a mere

bystander, perhaps turned on incidentally by other pathways farther up the signal transduction chain.

I have two main ideas to address this issue. First, we need to move "down the stack" of the metabolic phenomenon and see if directly targeting its component elements sensitizes breast cancer bone metastases to chemotherapy. We focused on mTOR inhibition for the paper because it is already in wide clinical use in breast cancer patients, was novel as combination therapy in our context, and had favorable chemistry for loading into the αvβ3-targeted micelle nanoparticles. Going forward, however, it will be beneficial to test docetaxel in combination with agents such as the small molecule electron transport chain complex I inhibitor IACS-010759 [251] to inhibit OXPHOS and translation inhibitors such as cycloheximide to target protein production, as well as both the ROS-generating proteasome inhibitor bortezomib[252] and, paradoxically, ROS inhibitors like N-acetyl-cysteine. Until we actually test the causal relationship between these metabolic phenomena and the chemoresistance phenotype we observe in bone metastases, we cannot know if they represent an interesting opportunity or a convenient distraction.

Second, as much as possible, we need to go *in vivo*, and stay there. One of the more striking aspects of the β3-mediated chemoresistance phenotype is, to my mind, its dependence on the bone microenvironment. Some *in vitro* differences between the docetaxel response in β3KO compared to β3WT cells have, thankfully, been durable. That said, it is again not clear the extent to which even the differences that we do see *in vitro* are actually representative of the reality *in vivo*. As an example. we observed clear changes in mitochondrial and oxygen-related parameters in cells on a dish, but mitochondria in bone metastases did not exhibit detectable, β3-dependent differences in ultrastructure. This is not to say that these changes don't mean anything, *per s*e, but rather that we need better ways to ascertain their meaning for the *in vivo* context going

forward.

To this end, in addition to the suggestions for combination therapy listed above, more needs to be done to specifically characterize what is happening metabolically in β3-expressing tumor cells in the bone when they are faced with chemotherapeutic challenge. *In vivo* visualization of ROS after systemic DTX treatment of β3WT and β3KO bone metastases using Galimunox would be a wonderful first experiment in this vein, giving us *in vitro* and *in vivo* data using the same reagent to directly compare and build our understanding of the phenotype. A similar one-to-one comparison could be obtained by using the de novo protein assay kit employed in Chapter 2 to bone metastases, either as part of an *ex vivo* flow cytometry experiment or via fluorescence microscopy of cytospun cells from bone metastases. There also appear to be a number of reporter constructs, both fluorescent and luminescent, for reading out aspects of the ER stress and unfolded protein responses [253]. Depending on what we find from the investigations recommended in 4.2.2 below, these or something similar might prove to be a reasonably quick way of narrowing down exactly what is going on from a mechanistic standpoint.

4.2.2 ECM and ER responses to DTX treatment in β3-WT tumors

Philosophically, one of the most striking findings from my dissertation work has been the transmission electron microscopy images of resistant tumor cells responding to chemotherapy. When I think about therapy-resistant cells, I often imagine them shrugging off chemotherapy completely, either through rapid efflux or as a function of complete uncoupling from what should be their normal responses to toxic stress. What I never imagined, until seeing these images, was cells that were barely struggling to get by, cells that were certainly surviving, but being forced to scrape and claw to do so. Of course, these images also immediately called to mind a number of questions of great relevance to the phenotypes and phenomena described in

this dissertation. What proteins are β3-expressing tumor cells in bone metastases producing normally, and how is this altered in the setting of chemotherapy? Are the tumor cells themselves the source of the extensive fibrillar matrix that appears around DTX-treated β3-WT cells, and if so, why do we *not* see the same thing in TEM images taken *in vitro*? Of greatest urgency, perhaps: are the ER and ECM phenotypes causally relevant for chemoresistance?

In light of the fact that integrin β3 is itself a receptor for ECM ligands, it is very tempting to speculate a feed-forward loop phenomenon, wherein β3-expressing cells might respond to chemotherapy in the bone microenvironment by producing ligand for themselves, or even other tumor-expressed integrin heterodimers, to bind, stabilizing a resistant phenotype. To get at whatever the answer actually is, however, we will need to molecularly profile *in vivo* treated tumor cells. RNA-Seq, whether single-cell or of specific populations of sorted cells, would be useful for identification of cell populations that change or exhibit divergent responses to chemotherapy. Perhaps even more useful, in light of the ultrastructural phenotype, would be tumor cell ribosomal profiling, which could give us a clear sense as to the proteins being actively translated in the dramatically expanded rough ER that we observe by TEM. More difficult, but potentially the most rewarding, would be metabolomic profiling of treated breast cancer bone metastases to identify flux through metabolic pathways, metabolite enrichment and de-enrichment, and potential opportunities for synthetic lethality.

4.2.3 Finishing the TGF-β story

The β3 expression and chemoresistance phenotypes that we observe in the lungs of tumor-bearing Marfan syndrome mice are exciting, tying an elegant bow on the initial hypothesis that TGF-β could drive chemoresistance through upregulation of integrin β3. To finish up this story for publication, we need two main things. First, we will need to show that the PLR-BO1-X

reporter works *in vivo* and that it exhibits increased luciferase activity in the lungs of MFS mice. As a formality, we will probably also need to show that this activity is responsive to a pharmacological inhibitor of TGF-β, similar to what Yibin Kang's group demonstrated using a different TGF-β reporter[74]. Second, we will need to show that β3 and TGF-β receptor knockout lines 1) do not exhibit increased reistance in the MFS lung, and 2) in the case of the TGF-β receptor knockout, that it does not exhibit increased integrin β3 expression in the MFS lung. If we can show those two things, I think we could have a small, publishable report pretty quickly.

Going forward from there, I am very taken by the idea of integrin β3 expression in the primary and metastatic site as a biomarker for possible combination treatment with chemotherapy and TGF-β inhibitors. If the paradigm established in MFS mice holds, it is possible to envision integrin β3 expression being used as a surrogate for "actual" TGF-β bioavailability at a tumor site, with implications for treatment. While canonical TGF-β signaling is clearly not the only input into integrin β3 (see the increased expression with JNKi from Chapter 3) this would be an interesting direction to take this data, using insights gleaned from mouse models to better understand why integrin β3 is upregulated where it is, and possibly even what to do about it.

References

1. Group USCSW. U.S. Cancer Statistics Data Visualizations Tool, based on 2019 submission data (1999-2017): U.S. Department of Health and Human Services, Centers for Disease Control and Prevention and National Cancer Institute. 2020

2. Welch HG, Prorok PC, O'Malley AJ, Kramer BS. Breast-cancer tumor size, overdiagnosis, and mammography screening effectiveness. N Engl J Med. 2016;375:1438-47.

3. Narod SA, Iqbal J, Miller AB. Why have breast cancer mortality rates declined. Journal of Cancer Policy. 2015;5:8-17.

4. Beau AB, Andersen PK, Vejborg I, Lynge E. Limitations in the effect of screening on breast cancer mortality. J Clin Oncol. 2018;36:2988-94.

5. Weigelt B, Peterse JL, Van't Veer LJ. Breast cancer metastasis: markers and models. Nature Reviews Cancer. 2005;5:591-602.

6. Paget S. The distribution of secondary growths in cancer of the breast. Lancet. 1889;571-3.

7. Braun S, Vogl FD, Naume B, Janni W, Osborne MP, Coombes RC et al. A pooled analysis of bone marrow micrometastasis in breast cancer. N Engl J Med. 2005;353:793-802.

8. Hüsemann Y, Geigl JB, Schubert F, Musiani P, Meyer M, Burghart E et al. Systemic spread is an early step in breast cancer. Cancer Cell. 2008;13:58-68.

9. Wang R, Zhu Y, Liu X, Liao X, He J, Niu L. The clinicopathological features and survival outcomes of patients with different metastatic sites in stage IV breast cancer. BMC Cancer. 2019;19:1091.

10. Coleman RE, Rubens RD. The clinical course of bone metastases from breast cancer. Br J Cancer. 1987;55:61-6.

11. Body JJ, Quinn G, Talbot S, Booth E, Demonty G, Taylor A et al. Systematic review and meta-analysis on the proportion of patients with breast cancer who develop bone metastases. Crit Rev Oncol Hematol. 2017;115:67-80.

12. Coleman RE. Clinical features of metastatic bone disease and risk of skeletal morbidity. Clin Cancer Res. 2006;12:6243s-9s.

13. Clark GM, Sledge GW, Osborne CK, McGuire WL. Survival from first recurrence: relative importance of prognostic factors in 1,015 breast cancer patients. J Clin Oncol. 1987;5:55-61.

14. Kennecke H, Yerushalmi R, Woods R, Cheang MC, Voduc D, Speers CH et al. Metastatic behavior of breast cancer subtypes. J Clin Oncol. 2010;28:3271-7.

15. Rueda OM, Sammut S-J, Seoane JA, Chin S-F, Caswell-Jin JL, Callari M et al. Dynamics of breast-cancer relapse reveal late-recurring ER-positive genomic subgroups. Nature. 2019;567:399-404.

16. Mundy GR. Metastasis to bone: causes, consequences and therapeutic opportunities. Nat Rev Cancer. 2002;2:584-93.

17. Jones SJ, Boyde A, Ali NN, Maconnachie E. A review of bone cell and substratum interactions: An illustration of the role of scanning electron microscopy. Scanning. 1985;7:5-24.

18. Niikura N, Liu J, Hayashi N, Palla SL, Tokuda Y, Hortobagyi GN et al. Treatment outcome and prognostic factors for patients with bone-only metastases of breast cancer: a single-institution retrospective analysis. The Oncologist. 2011;16:155.

19. Ahn SG, Lee HM, Cho SH, Lee SA, Hwang SH, Jeong J et al. Prognostic factors for patients with bone-only metastasis in breast cancer. Yonsei Med J. 2013;54:1168-77.

20. Gonzalez-Angulo AM, Morales-Vasquez F, Hortobagyi GN. Overview of resistance to systemic therapy in patients with breast cancer. Breast Cancer Chemosensitivity. Springer; 2007. p. 1-22.

21. Selvaggi G, Scagliotti GV. Management of bone metastases in cancer: a review. Crit Rev Oncol Hematol. 2005;56:365-78.

22. Briasoulis E, Karavasilis V, Kostadima L, Ignatiadis M, Fountzilas G, Pavlidis N. Metastatic breast carcinoma confined to bone: portrait of a clinical entity. Cancer. 2004;101:1524-8.

23. Coleman RE. Bone cancer in 2011: Prevention and treatment of bone metastases. Nat Rev Clin Oncol. 2011;9:76-8.

24. Ottewell P, Wilson C. Bone-targeted agents in breast cancer: do we now have all the answers. Breast Cancer (Auckl). 2019;13:1178223419843501.

25. Kimmel DB. Mechanism of action, pharmacokinetic and pharmacodynamic profile, and clinical applications of nitrogen-containing bisphosphonates. J Dent Res. 2007;86:1022-33.

26. Luckman SP, Hughes DE, Coxon FP, Russell RGG, Rogers MJ. Nitrogen-containing bisphosphonates inhibit the mevalonate pathway and prevent post-translational prenylation of GTP-binding proteins, including Ras. Journal of Bone and Mineral Research. 1998;13:581-9.

27. Saad F. Zoledronic acid: past, present and future roles in cancer treatment. Future Oncology. 2005; 1.

28. Boyle WJ, Simonet WS, Lacey DL. Osteoclast differentiation and activation. Nature. 2003;423:337-42.

29. Delmas PD. Clinical potential of RANKL inhibition for the management of postmenopausal osteoporosis and other metabolic bone diseases. J Clin Densitom. 2008;11:325-38.

30. Cummings SR, San Martin J, McClung MR, Siris ES, Eastell R, Reid IR et al. Denosumab for prevention of fractures in postmenopausal women with osteoporosis. N Engl J Med. 2009;361:756-65.

31. Rosen LS, Gordon D, Tchekmedyian S, Yanagihara R, Hirsh V, Krzakowski M et al. Zoledronic acid versus placebo in the treatment of skeletal metastases in patients with lung cancer and other solid tumors: a phase III, double-blind, randomized trial--the Zoledronic Acid Lung Cancer and Other Solid Tumors Study Group. J Clin Oncol. 2003;21:3150-7.

32. Stopeck AT, Lipton A, Body J-J, Steger GG, Tonkin K, De Boer RH et al. Denosumab compared with zoledronic acid for the treatment of bone metastases in patients with advanced breast cancer: a randomized, double-blind study. Journal of Clinical Oncology. 2010;28:5132-9.

33. Lipton A, Cook R, Saad F, Major P, Garnero P, Terpos E et al. Normalization of bone markers is associated with improved survival in patients with bone metastases from solid tumors and elevated bone resorption receiving zoledronic acid. Cancer. 2008;113:193-201.

34. Aft R, Naughton M, Trinkaus K, Watson M, Ylagan L, Chavez-MacGregor M et al. Effect of zoledronic acid on disseminated tumour cells in women with locally advanced breast cancer: an open label, randomised, phase 2 trial. Lancet Oncol. 2010;11:421-8.

35. Coleman RE, Finkelstein D, Barrios CH, Martin M, Iwata H, Glaspy JA et al. Adjuvant denosumab in early breast cancer: First results from the international multicenter randomized phase III placebo controlled D-CARE study. Journal of Clinical Oncology. 2018;36:15_suppl, 501.

36. Gnant M, Mlineritsch B, Stoeger H, Luschin-Ebengreuth G, Heck D, Menzel C et al. Adjuvant endocrine therapy plus zoledronic acid in premenopausal women with early-stage breast cancer: 62-month follow-up from the ABCSG-12 randomised trial. The Lancet Oncology. 2011;12:631-41.

37. Coleman R, Cameron D, Dodwell D, Bell R, Wilson C, Rathbone E et al. Adjuvant zoledronic acid in patients with early breast cancer: final efficacy analysis of the AZURE (BIG 01/04) randomised open-label phase 3 trial. The Lancet Oncology. 2014;15:997-1006.

38. Hanahan D, Weinberg RA. Hallmarks of cancer: the next generation. Cell. 2011;144:646-74.

39. Pan H, Gray R, Braybrooke J, Davies C, Taylor C, McGale P et al. 20-Year risks of breast-cancer recurrence after stopping endocrine therapy at 5 years. N Engl J Med. 2017;377:1836-46.

40. Aslakson CJ, Miller FR. Selective events in the metastatic process defined by analysis of the sequential dissemination of subpopulations of a mouse mammary tumor. Cancer Research. 1992;52:1399-405.

41. Talmadge JE, Fidler IJ. AACR centennial series: the biology of cancer metastasis: historical perspective. Cancer Res. 2010;70:5649-69.

42. Hanahan D, Weinberg RA. Hallmarks of cancer: the next generation. Cell. 2011;144:646-74.

43. Brabletz T, Kalluri R, Nieto MA, Weinberg RA. EMT in cancer. Nature Reviews Cancer. 2018;18:128.

44. Ocaña OH, Córcoles R, Fabra Á, Moreno-Bueno G, Acloque H, Vega S et al. Metastatic colonization requires the repression of the epithelial-mesenchymal transition inducer Prrx1. Cancer Cell. 2012;22:709-24.

45. Tsai JH, Donaher JL, Murphy DA, Chau S, Yang J. Spatiotemporal regulation of epithelial-mesenchymal transition is essential for squamous cell carcinoma metastasis. Cancer Cell. 2012;22:725-36.

46. Stankic M, Pavlovic S, Chin Y, Brogi E, Padua D, Norton L et al. TGF-β-Id1 signaling opposes Twist1 and promotes metastatic colonization via a mesenchymal-to-epithelial transition. Cell Reports. 2013;5:1228-42.

47. Lu H, Clauser KR, Tam WL, Fröse J, Ye X, Eaton EN et al. A breast cancer stem cell niche supported by juxtacrine signalling from monocytes and macrophages. Nat Cell Biol. 2014;16:1105-17.

48. Labelle M, Begum S, Hynes RO. Direct signaling between platelets and cancer cells induces an epithelial-mesenchymal-like transition and promotes metastasis. Cancer Cell. 2011;20:576-90.

49. Hiratsuka S, Watanabe A, Sakurai Y, Akashi-Takamura S, Ishibashi S, Miyake K et al. The S100A8–serum amyloid A3–TLR4 paracrine cascade establishes a pre-metastatic phase. Nature Cell Biology. 2008;10:1349-55.

50. Kaplan RN, Riba RD, Zacharoulis S, Bramley AH, Vincent L, Costa C et al. VEGFR1-positive haematopoietic bone marrow progenitors initiate the pre-metastatic niche. Nature. 2005;438:820-7.

51. Karagiannis GS, Poutahidis T, Erdman SE, Kirsch R, Riddell RH, Diamandis EP. Cancer-associated fibroblasts drive the progression of metastasis through both paracrine and mechanical pressure on cancer tissue. Mol Cancer Res. 2012;10:1403-18.

52. Liao D, Luo Y, Markowitz D, Xiang R, Reisfeld RA. Cancer associated fibroblasts promote tumor growth and metastasis by modulating the tumor immune microenvironment in a 4T1 murine breast cancer model. PLoS One. 2009;4:e7965.

53. Fidler IJ. Metastasis: quantitative analysis of distribution and fate of tumor emboli labeled with 125I-5-iodo-2′-deoxyuridine. Journal of the National Cancer Institute. 1970;45:773-82.

54. Weiss L. Metastatic inefficiency: causes and consequences. Cancer Rev. 1986;3:1-24.

55. Plaks V, Koopman CD, Werb Z. Circulating tumor cells. Science. 2013;341:1186-8.

56. Butler TP, Gullino PM. Quantitation of cell shedding into efferent blood of mammary adenocarcinoma. Cancer Research. 1975;35:512-6.

57. Kang Y, Siegel PM, Shu W, Drobnjak M, Kakonen SM, Cordón-Cardo C et al. A multigenic program mediating breast cancer metastasis to bone. Cancer Cell. 2003;3:537-49.

58. Minn AJ, Gupta GP, Siegel PM, Bos PD, Shu W, Giri DD et al. Genes that mediate breast cancer metastasis to lung. Nature. 2005;436:518-24.

59. Bos PD, Zhang XH, Nadal C, Shu W, Gomis RR, Nguyen DX et al. Genes that mediate breast cancer metastasis to the brain. Nature. 2009;459:1005-9.

60. Zhao Y, Bachelier R, Treilleux I, Pujuguet P, Peyruchaud O, Baron R et al. Tumor alphavbeta3 integrin is a therapeutic target for breast cancer bone metastases. Cancer Res. 2007;67:5821-30.

61. Korah R, Boots M, Wieder R. Integrin α5β1 promotes survival of growth-arrested breast cancer cells: an in vitro paradigm for breast cancer dormancy in bone marrow. Cancer Research. 2004;64:4514-22.

62. Xiang J, Hurchla MA, Fontana F, Su X, Amend SR, Esser AK et al. CXCR4 protein epitope mimetic antagonist POL5551 disrupts metastasis and enhances chemotherapy effect in triple-negative breast cancer. Mol Cancer Ther. 2015;14:2473-85.

63. Shiozawa Y, Pedersen EA, Havens AM et al. Human prostate cancer metastases target the hematopoietic stem cell niche to establish footholds in mouse bone marrow. J Clin Invest. 2011;121:1298-1312.

64. Smith MCP, Luker KE, Garbow JR, Prior JL, Jackson E, Piwnica-Worms D et al. CXCR4 regulates growth of both primary and metastatic breast cancer. Cancer Res. 2004;64:8604-12.

65. Phan TG, Croucher PI. The dormant cancer cell life cycle. Nat Rev Cancer. 2020;20:398-411.

66. Lawson MA, McDonald MM, Kovacic N, Hua Khoo W, Terry RL, Down J et al. Osteoclasts control reactivation of dormant myeloma cells by remodelling the endosteal niche. Nat Commun. 2015;6:8983.

67. Carrington JL, Roberts AB, Flanders KC, Roche NS, Reddi AH. Accumulation, localization, and compartmentation of transforming growth factor beta during endochondral bone development. J Cell Biol. 1988;107:1969-75.

68. Waning DL, Mohammad KS, Reiken S, Xie W, Andersson DC, John S et al. Excess TGF-β mediates muscle weakness associated with bone metastases in mice. Nat Med. 2015;21:1262-71.

69. Wang H, Tian L, Liu J, Goldstein A, Bado I, Zhang W et al. The osteogenic niche is a calcium reservoir of bone micrometastases and confers unexpected therapeutic vulnerability. Cancer Cell. 2018;34:823-839.e7.

70. Weilbaecher KN, Guise TA, McCauley LK. Cancer to bone: a fatal attraction. Nat Rev Cancer. 2011;11:411-25.

71. Guise TA, Yin JJ, Taylor SD, Kumagai Y, Dallas M, Boyce BF et al. Evidence for a causal role of parathyroid hormone-related protein in the pathogenesis of human breast cancer-mediated osteolysis. J Clin Invest. 1996;98:1544-9.

72. Sethi N, Dai X, Winter CG, Kang Y. Tumor-derived JAGGED1 promotes osteolytic bone metastasis of breast cancer by engaging notch signaling in bone cells. Cancer Cell. 2011

73. Yin JJ, Selander K, Chirgwin JM, Dallas M, Grubbs BG, Wieser R et al. TGF-beta signaling blockade inhibits PTHrP secretion by breast cancer cells and bone metastases development. J Clin Invest. 1999;103:197-206.

74. Korpal M, Yan J, Lu X, Xu S, Lerit DA, Kang Y. Imaging transforming growth factor-beta signaling dynamics and therapeutic response in breast cancer bone metastasis. Nat Med. 2009;15:960-6.

75. Kang Y, He W, Tulley S, Gupta GP, Serganova I, Chen CR et al. Breast cancer bone metastasis mediated by the Smad tumor suppressor pathway. Proc Natl Acad Sci. 2005;102:13909-14.

76. Dunn LK, Mohammad KS, Fournier PG, McKenna CR, Davis HW, Niewolna M et al. Hypoxia and TGF-beta drive breast cancer bone metastases through parallel signaling pathways in tumor cells and the bone microenvironment. PLoS ONE. 2009;4:e6896.

77. Butcher DT, Alliston T, Weaver VM. A tense situation: forcing tumour progression. Nat Rev Cancer. 2009;9:108-22.

78. Netti PA, Berk DA, Swartz MA, Grodzinsky AJ, Jain RK. Role of extracellular matrix assembly in interstitial transport in solid tumors. Cancer Res. 2000;60:2497-503.

79. Page JM, Merkel AR, Ruppender NS, Guo R, Dadwai UC, Connonier SA et al. Matrix rigidity induces osteolytic gene expression of metastatic breast cancer cells. PloS one. 2010;64:33-44.

80. Liu S, Goldstein RH, Scepansky EM, Rosenblatt M. Inhibition of rho-associated kinase signaling prevents breast cancer metastasis to human bone. Cancer research. 2009;69:8742-8751.

81. Holle AW, Engler AJ. More than a feeling: discovering, understanding, and influencing mechanosensing pathways. Curr Opin Biotechnol. 2011;22:648-54.

82. Tannock IF. The relation between cell proliferation and the vascular system in a transplanted mouse mammary tumour. Br J Cancer. 1968;22:258-73.

83. Spencer JA, Ferraro F, Roussakis E, Klein A, Wu J, Runnels JM et al. Direct measurement of local oxygen concentration in the bone marrow of live animals. Nature. 2014;508:269-73.

84. Zhong H, De Marzo AM, Laughner E, Lim M, Hilton DA, Zagzag D et al. Overexpression of hypoxia-inducible factor 1alpha in common human cancers and their metastases. Cancer Res. 1999;59:5830-5.

85. Carcereri de Prati A, Butturini E, Rigo A, Oppici E, Rossin M, Boriero D et al. Metastatic breast cancer cells enter into dormant state and express cancer stem cells phenotype under chronic hypoxia. J Cell Biochem. 2017;118:3237-48.

86. Hiraga T, Kizaka-Kondoh S, Hirota K, Hiraoka M, Yoneda T. Hypoxia and hypoxia-inducible factor-1 expression enhance osteolytic bone metastases of breast cancer. Cancer Res. 2007;67:4157-63.

87. Blair HC, Robinson LJ, Huang CL, Sun L, Friedman PA, Schlesinger PH et al. Calcium and bone disease. Biofactors. 2011;37:159-67.

88. Zhang W, Bado I, Wang H, Lo HC, Zhang XH. Bone metastasis: find your niche and fit in. Trends Cancer. 2019;5:95-110.

89. Joeckel E, Haber T, Prawitt D, Junker K, Hampel C, Thüroff JW et al. High calcium concentration in bones promotes bone metastasis in renal cell carcinomas expressing calcium-sensing receptor. Mol Cancer. 2014;13:42.

90. Liao J, Schneider A, Datta NS, McCauley LK. Extracellular calcium as a candidate mediator of prostate cancer skeletal metastasis. Cancer Res. 2006;66:9065-73.

91. Teitelbaum SL, Ross FP. Genetic regulation of osteoclast development and function. Nat Rev Genet. 2003;4:638-49.

92. Honore P, Luger NM, Sabino MA, Schwei MJ, Rogers SD, Mach DB et al. Osteoprotegerin blocks bone cancer-induced skeletal destruction, skeletal pain and pain-related neurochemical reorganization of the spinal cord. Nat Med. 2000;6:521-8.

93. Colegio OR, Chu NQ, Szabo AL, Chu T, Rhebergen AM, Jairam V et al. Functional polarization of tumour-associated macrophages by tumour-derived lactic acid. Nature. 2014;513:559-63.

94. Balgi AD, Diering GH, Donohue E, Lam KK, Fonseca BD, Zimmerman C et al. Regulation of mTORC1 signaling by pH. PLoS One. 2011;6:e21549.

95. Webb BA, Chimenti M, Jacobson MP, Barber DL. Dysregulated pH: a perfect storm for cancer progression. Nat Rev Cancer. 2011;11:671-7.

96. Paradise RK, Lauffenburger DA, Van Vliet KJ. Acidic extracellular pH promotes activation of integrin α(v)β(3). PLoS One. 2011;6:e15746.

97. Zheng H, Bae Y, Kasimir-Bauer S, Tang R, Chen J, Ren G et al. Therapeutic antibody targeting tumor- and osteoblastic niche-derived Jagged1 sensitizes bone metastasis to chemotherapy. Cancer Cell. 2017;32:731-747.e6.

98. Corcoran KE, Trzaska KA, Fernandes H, Bryan M, Taborga M, Srinivas V et al. Mesenchymal stem cells in early entry of breast cancer into bone marrow. PLoS One. 2008;3:e2563.

99. Jackson W, Sosnoski DM, Ohanessian SE, Chandler P, Mobley A, Meisel KD et al. Role of megakaryocytes in breast cancer metastasis to bone. Cancer Res. 2017;77:1942-54.

100. Zhao E, Xu H, Wang L, Kryczek I, Wu K, Hu Y et al. Bone marrow and the control of immunity. Cell Mol Immunol. 2012;9:11-9.

101. Tulotta C, Groenewoud A, Snaar-Jagalska BE, Ottewell P. Animal models of breast cancer bone metastasis. Methods Mol Biol. 2019;1914:309-30.

102. Ottewell PD, Wang N, Brown HK, Reeves KJ, Fowles CA, Croucher PI et al. Zoledronic acid has differential antitumor activity in the pre- and postmenopausal bone microenvironment in vivo. Clin Cancer Res. 2014;20:2922-32.

103. Lelekakis M, Moseley JM, Martin TJ, Hards D, Williams E, Ho P et al. A novel orthotopic model of breast cancer metastasis to bone. Clin Exp Metastasis. 1999;17:163-70.

104. Jinnah AH, Zacks BC, Gwam CU, Kerr BA. Emerging and established models of bone metastasis. Cancers (Basel). 2018;10

105. Wright LE, Ottewell PD, Rucci N, Peyruchaud O, Pagnotti GM, Chiechi A et al. Murine models of breast cancer bone metastasis. Bonekey Rep. 2016;5:804.

106. Wetterwald A, van der Pluijm G, Que I, Sijmons B, Buijs J, Karperien M et al. Optical imaging of cancer metastasis to bone marrow: a mouse model of minimal residual disease. Am J Pathol. 2002;160:1143-53.

107. Hynes RO. Integrins: bidirectional, allosteric signaling machines. cell. 2002;110:673-87.

108. Hynes RO. Integrins: a family of cell surface receptors. Cell. 1987;48:549-54.

109. Whittaker CA, Hynes RO. Distribution and evolution of von Willebrand/integrin A domains: widely dispersed domains with roles in cell adhesion and elsewhere. Mol Biol Cell. 2002;13:3369-87.

110. Elices MJ, Osborn L, Takada Y, Crouse C, Luhowskyj S, Hemler ME et al. VCAM-1 on activated endothelium interacts with the leukocyte integrin VLA-4 at a site distinct from the VLA-4/fibronectin binding site. Cell. 1990;60:577-84.

111. Pytela R, Pierschbacher MD, Ruoslahti E. Identification and isolation of a 140 kd cell surface glycoprotein with properties expected of a fibronectin receptor. Cell. 1985;40:191-8.

112. van der Flier A, Sonnenberg A. Function and interactions of integrins. Cell Tissue Res. 2001;305:285-98.

113. Humphries JD, Byron A, Humphries MJ. Integrin ligands at a glance. Journal of cell science. 2006

114. Xiong JP, Stehle T, Diefenbach B, Zhang R, Dunker R, Scott DL et al. Crystal structure of the extracellular segment of integrin alpha Vbeta3. Science. 2001;294:339-45.

115. Xiong YM, Haas TA, Zhang L. Identification of functional segments within the beta2I-domain of integrin alphaMbeta2. J Biol Chem. 2002;277:46639-44.

116. Shattil SJ, Kim C, Ginsberg MH. The final steps of integrin activation: the end game. Nat Rev Mol Cell Biol. 2010;11:288-300.

117. Beer JH, Springer KT, Coller BS. Immobilized Arg-Gly-Asp (RGD) peptides of varying lengths as structural probes of the platelet glycoprotein IIb/IIIa receptor. Blood. 1992;79:117-28.

118. Kim C, Ye F, Ginsberg MH. Regulation of integrin activation. Annu Rev Cell Dev Biol. 2011;27:321-45.

119. Shattil SJ, Kashiwagi H, Pampori N. Integrin signaling: the platelet paradigm. Blood. 1998;91:2645-57.

120. Packham MA. Role of platelets in thrombosis and hemostasis. Can J Physiol Pharmacol. 1994;72:278-84.

121. O'Toole TE, Mandelman D, Forsyth J, Shattil SJ, Plow EF, Ginsberg MH. Modulation of the affinity of integrin alpha IIb beta 3 (GPIIb-IIIa) by the cytoplasmic domain of alpha IIb. Science. 1991;254:845-7.

122. Tadokoro S, Shattil SJ, Eto K, Tai V, Liddington RC, de Pereda JM et al. Talin binding to integrin beta tails: a final common step in integrin activation. Science. 2003;302:103-6.

123. Critchley DR. Biochemical and structural properties of the integrin-associated cytoskeletal protein talin. Annu Rev Biophys. 2009;38:235-54.

124. Katsumi A, Orr AW, Tzima E, Schwartz MA. Integrins in mechanotransduction. J Biol Chem. 2004;279:12001-4.

125. Galbraith CG, Yamada KM, Sheetz MP. The relationship between force and focal complex development. J Cell Biol. 2002;159:695-705.

126. Sun Z, Guo SS, Fässler R. Integrin-mediated mechanotransduction. J Cell Biol. 2016;215:445-56.

127. Cooper J, Giancotti FG. Integrin signaling in cancer: mechanotransduction, stemness, epithelial plasticity, and therapeutic resistance. Cancer Cell. 2019;35:347-67.

128. Schwartz MA. Integrin signaling revisited. Trends Cell Biol. 2001;11:466-70.

129. Giancotti FG, Tarone G. Positional control of cell fate through joint integrin/receptor protein kinase signaling. Annu Rev Cell Dev Biol. 2003;19:173-206.

130. Miyamoto S, Teramoto H, Gutkind JS, Yamada KM. Integrins can collaborate with growth factors for phosphorylation of receptor tyrosine kinases and MAP kinase activation: roles of integrin aggregation and occupancy of receptors. J Cell Biol. 1996;135:1633-42.

131. Assoian RK. Control of the G1 phase cyclin-dependent kinases by mitogenic growth factors and the extracellular matrix. Cytokine Growth Factor Rev. 1997;8:165-70.

132. Sieg DJ, Hauck CR, Ilic D, Klingbeil CK, Schaefer E, Damsky CH et al. FAK integrates growth-factor and integrin signals to promote cell migration. Nat Cell Biol. 2000;2:249-56.

133. Frisch SM, Ruoslahti E. Integrins and anoikis. Curr Opin Cell Biol. 1997;9:701-6.

134. Montgomery AM, Reisfeld RA, Cheresh DA. Integrin alpha v beta 3 rescues melanoma cells from apoptosis in three-dimensional dermal collagen. Proc Natl Acad Sci USA. 1994;91:8856-60.

135. Mamidi A, Prawiro C, Seymour PA, de Lichtenberg KH, Jackson A, Serup P et al. Mechanosignalling via integrins directs fate decisions of pancreatic progenitors. Nature. 2018

136. Desgrosellier JS, Cheresh DA. Integrins in cancer: biological implications and therapeutic opportunities. Nat Rev Cancer. 2010;10:9-22.

137. Guo W, Giancotti FG. Integrin signalling during tumour progression. Nat Rev Mol Cell Biol. 2004;5:816-26.

138. Stupack DG, Teitz T, Potter MD, Mikolon D, Houghton PJ, Kidd VJ et al. Potentiation of neuroblastoma metastasis by loss of caspase-8. Nature. 2006;439:95-9.

139. Kren A, Baeriswyl V, Lehembre F, Wunderlin C, Strittmatter K, Antoniadis H et al. Increased tumor cell dissemination and cellular senescence in the absence of beta1-integrin function. EMBO J. 2007;26:2832-42.

140. Seguin L, Kato S, Franovic A, Camargo MF, Lesperance J, Elliott KC et al. An integrin β_3-KRAS-RalB complex drives tumour stemness and resistance to EGFR inhibition. Nat Cell Biol. 2014;16:457-68.

141. Desgrosellier JS, Barnes LA, Shields DJ, Huang M, Lau SK, Prévost N et al. An integrin alpha(v)beta(3)-c-Src oncogenic unit promotes anchorage-independence and tumor progression. Nat Med. 2009;15:1163-9.

142. Trusolino L, Bertotti A, Comoglio PM. A signaling adapter function for alpha6beta4 integrin in the control of HGF-dependent invasive growth. Cell. 2001;107:643-54.

143. Hariharan S, Gustafson D, Holden S, McConkey D, Davis D, Morrow M et al. Assessment of the biological and pharmacological effects of the alpha nu beta3 and alpha nu beta5 integrin receptor antagonist, cilengitide (EMD 121974), in patients with advanced solid tumors. Ann Oncol. 2007;18:1400-7.

144. Brooks PC, Clark RA, Cheresh DA. Requirement of vascular integrin alpha v beta 3 for angiogenesis. Science. 1994;264:569-71.

145. Mahabeleshwar GH, Feng W, Phillips DR, Byzova TV. Integrin signaling is critical for pathological angiogenesis. J Exp Med. 2006;203:2495-507.

146. Robinson SD, Hodivala-Dilke KM. The role of β3-integrins in tumor angiogenesis: context is everything. Curr Opin Cell Biol. 2011;23:630-7.

147. Goetz JG, Minguet S, Navarro-Lérida I, Lazcano JJ, Samaniego R, Calvo E et al. Biomechanical remodeling of the microenvironment by stromal caveolin-1 favors tumor invasion and metastasis. Cell. 2011;146:148-63.

148. Jin H, Aiyer A, Su J, Borgstrom P, Stupack D, Friedlander M et al. A homing mechanism for bone marrow-derived progenitor cell recruitment to the neovasculature. J Clin Invest. 2006;116:652-62.

149. Jin H, Su J, Garmy-Susini B, Kleeman J, Varner J. Integrin alpha4beta1 promotes monocyte trafficking and angiogenesis in tumors. Cancer Res. 2006;66:2146-52.

150. Su X, Esser AK, Amend SR, Xiang J, Xu Y, Ross MH et al. Antagonizing integrin β3 increases immunosuppression in cancer. Cancer Res. 2016;76:3484-95.

151. Hoshino A, Costa-Silva B, Shen TL, Rodrigues G, Hashimoto A, Tesic Mark M et al. Tumour exosome integrins determine organotropic metastasis. Nature. 2015;527:329-35.

152. Pytela R, Pierschbacher MD, Ruoslahti E. A 125/115-kDa cell surface receptor specific for vitronectin interacts with the arginine-glycine-aspartic acid adhesion sequence derived from fibronectin. Proc Natl Acad Sci U S A. 1985;82:5766-70.

153. Yokosaki Y, Tanaka K, Higashikawa F, Yamashita K, Eboshida A. Distinct structural requirements for binding of the integrins alphavbeta6, alphavbeta3, alphavbeta5, alpha5beta1 and alpha9beta1 to osteopontin. Matrix Biol. 2005;24:418-27.

154. Adair BD, Xiong JP, Maddock C, Goodman SL, Arnaout MA, Yeager M. Three-dimensional EM structure of the ectodomain of integrin {alpha}V{beta}3 in a complex with fibronectin. J Cell Biol. 2005;168:1109-18.

155. Huang J, Roth R, Heuser JE, Sadler JE. Integrin alpha(v)beta(3) on human endothelial cells binds von Willebrand factor strings under fluid shear stress. Blood. 2009;113:1589-97.

156. Gillan L, Matei D, Fishman DA, Gerbin CS, Karlan BY, Chang DD. Periostin secreted by epithelial ovarian carcinoma is a ligand for alpha(V)beta(3) and alpha(V)beta(5) integrins and promotes cell motility. Cancer Res. 2002;62:5358-64.

157. Oskarsson T, Acharyya S, Zhang XH, Vanharanta S, Tavazoie SF, Morris PG et al. Breast cancer cells produce tenascin C as a metastatic niche component to colonize the lungs. Nat Med. 2011;17:867-74.

158. Menendez JA, Vellon L, Mehmi I, Teng PK, Griggs DW, Lupu R. A novel CYR61-triggered 'CYR61-alphavbeta3 integrin loop' regulates breast cancer cell survival and chemosensitivity through activation of ERK1/ERK2 MAPK signaling pathway. Oncogene. 2005;24:761-79.

159. Wang MY, Chen PS, Prakash E, Hsu HC, Huang HY, Lin MT et al. Connective tissue growth factor confers drug resistance in breast cancer through concomitant up-regulation of Bcl-xL and cIAP1. Cancer Res. 2009;69:3482-91.

160. McHugh KP, Hodivala-Dilke K, Zheng MH, Namba N, Lam J, Novack D et al. Mice lacking beta3 integrins are osteosclerotic because of dysfunctional osteoclasts. J Clin Invest. 2000;105:433-40.

161. Bakewell SJ, Nestor P, Prasad S, Tomasson MH, Dowland N, Mehrotra M et al. Platelet and osteoclast β3 integrins are critical for bone metastasis. Proceedings of the National Academy of Sciences. 2003;100:14205-10.

162. Uluçkan O, Becker SN, Deng H, Zou W, Prior JL, Piwnica-Worms D et al. CD47 regulates bone mass and tumor metastasis to bone. Cancer Res. 2009;69:3196-204.

163. Atkinson SJ, Gontarczyk AM, Alghamdi AAA, Ellison TS, Johnson RT, Fowler WJ et al. The β3-integrin endothelial adhesome regulates microtubule-dependent cell migration. EMBO Reports. 2018;19

164. Pan D, Pham CTN, Weilbaecher KN, Tomasson MH, Wickline SA, Lanza GM. Contact-facilitated drug delivery with Sn2 lipase labile prodrugs optimize targeted lipid nanoparticle drug delivery. Wiley Interdisciplinary Reviews: Nanomedicine and Nanobiotechnology. 2016;8:85-106.

165. Kouros-Mehr H, Bechis SK, Slorach EM, Littlepage LE, Egeblad M, Ewald AJ et al. GATA-3 links tumor differentiation and dissemination in a luminal breast cancer model. Cancer Cell. 2008;13:141-52.

166. Yeo SK, Wen J, Chen S, Guan JL. Autophagy differentially regulates distinct breast cancer stem-like cells in murine models via EGFR/Stat3 and Tgfβ/Smad signaling. Cancer Res. 2016;76:3397-410.

167. Desgrosellier JS, Lesperance J, Seguin L, Gozo M, Kato S, Franovic A et al. Integrin v 3 drives slug activation and stemness in the pregnant and neoplastic mammary gland. Developmental Cell. 2014;30:295-308.

168. Sun Q, Lesperance J, Wettersten H, Luterstein E, DeRose YS, Welm A et al. Proapoptotic PUMA targets stem-like breast cancer cells to suppress metastasis. J Clin Invest. 2018;128:531-44.

169. Parvani JG, Galliher-Beckley AJ, Schiemann BJ, Schiemann WP. Targeted inactivation of β1 integrin induces β3 integrin switching, which drives breast cancer metastasis by TGF-β. Mol Biol Cell. 2013;24:3449-59.

170. Lo PK, Kanojia D, Liu X, Singh UP, Berger FG, Wang Q et al. CD49f and CD61 identify Her2/neu-induced mammary tumor-initiating cells that are potentially derived from luminal progenitors and maintained by the integrin-TGFβ signaling. Oncogene. 2012;31:2614-26.

171. Wendt MK, Tian M, Schiemann WP. Deconstructing the mechanisms and consequences of TGF-β-induced EMT during cancer progression. Cell Tissue Res. 2012;347:85-101.

172. Liapis H, Flath A, Kitazawa S. Integrin alpha V beta 3 expression by bone-residing breast cancer metastases. Diagn Mol Pathol. 1996;5:127-35.

173. Sloan EK, Pouliot N, Stanley KL, Chia J, Moseley JM, Hards DK et al. Tumor-specific expression of alphavbeta3 integrin promotes spontaneous metastasis of breast cancer to bone. Breast Cancer Res. 2006;8:R20.

174. Page JM, Merkel AR, Ruppender NS, Guo R, Dadwal UC, Cannonier SA et al. Matrix rigidity regulates the transition of tumor cells to a bone-destructive phenotype through integrin 3 and TGF- receptor type II. Biomaterials. 2015;64:33-44.

175. Ross MH, Esser AK, Fox GC, Schmieder AH, Yang X, Hu G et al. Bone-induced expression of integrin β3 enables targeted nanotherapy of breast cancer metastases. Cancer Res. 2017;77:6299-312.

176. Galliher AJ, Schiemann WP. Beta3 integrin and Src facilitate transforming growth factor-beta mediated induction of epithelial-mesenchymal transition in mammary epithelial cells. Breast Cancer Res. 2006;8:R42.

177. Fox GC, Su X, Davis JL, Xu Y, Kwakwa KA, Ross MH et al. Targeted therapy to β3 integrin reduces chemoresistance in breast cancer bone metastases. Mol Cancer Ther. 2021;20:1183-98.

178. Correia AL, Bissell MJ. The tumor microenvironment is a dominant force in multidrug resistance. Drug Resist Updat. 2012;15:39-49.

179. Croucher PI, McDonald MM, Martin TJ. Bone metastasis: the importance of the neighbourhood. Nat Rev Cancer. 2016;16:373.

180. Seguin L, Desgrosellier JS, Weis SM, Cheresh DA. Integrins and cancer: regulators of cancer stemness, metastasis, and drug resistance. Trends in Cell Biology. 2015;25:234-40.

181. Esser AK, Schmieder AH, Ross MH, Xiang J, Su X, Cui G et al. Dual-therapy with αvβ3-targeted Sn2 lipase-labile fumagillin-prodrug nanoparticles and zoledronic acid in the Vx2 rabbit tumor model. Nanomedicine: Nanotechnology, Biology and Medicine. 2016;12:201-11.

182. Morgan EA, Schneider JG, Baroni TE, Uluçkan O, Heller E, Hurchla MA et al. Dissection of platelet and myeloid cell defects by conditional targeting of the beta3-integrin subunit. FASEB J. 2010;24:1117-27.

183. Weis SM, Cheresh DA. Tumor angiogenesis: molecular pathways and therapeutic targets. Nat Med. 2011;17:1359-70.

184. Győrffy B, Lanczky A, Eklund AC, Denkert C, Budczies J, Li Q et al. An online survival analysis tool to rapidly assess the effect of 22,277 genes on breast cancer prognosis using microarray data of 1,809 patients. Breast Cancer Research and Treatment. 2010;123:725-31.

185. Esser AK, Ross MH, Fontana F, Su X, Gabay A, Fox GC et al. Nanotherapy delivery of c-myc inhibitor targets protumor macrophages and preserves antitumor macrophages in breast cancer. Theranostics. 2020;10:7510-26.

186. Nefedova Y, Landowski TH, Dalton WS. Bone marrow stromal-derived soluble factors and direct cell contact contribute to de novo drug resistance of myeloma cells by distinct mechanisms. Leukemia. 2003;17:1175-82.

187. Liberzon A, Birger C, Thorvaldsdóttir H, Ghandi M, Mesirov JP, Tamayo P. The molecular signatures database hallmark gene set collection. Cell Systems. 2015;1:417-25.

188. Sivapackiam J, Liao F, Zhou D, Shoghi KI, Gropler RJ, Gelman AE et al. Galuminox: Preclinical validation of a novel PET tracer for non-invasive imaging of oxidative stress in vivo. Redox Biol. 2020;37:101690.

189. Morita M, Gravel S-P, Hulea L, Larsson O, Pollak M, St-Pierre J et al. mTOR coordinates protein synthesis, mitochondrial activity and proliferation. Cell Cycle. 2015;14:473-80.

190. Bui T, Rennhack J, Mok S, Ling C, Perez M, Roccamo J et al. Functional redundancy between β1 and β3 integrin in activating the IR/Akt/mTORC1 signaling axis to promote ErbB2-driven breast cancer. Cell Rep. 2019;29:589-602.e6.

191. Pola C, Formenti SC, Schneider RJ. Vitronectin-αvβ3 integrin engagement directs hypoxia-resistant mTOR activity and sustained protein synthesis linked to invasion by breast cancer cells. Cancer Res. 2013;73:4571-8.

192. Diessner J, Wischnewsky M, Stüber T, Stein R, Krockenberger M, Häusler S et al. Evaluation of clinical parameters influencing the development of bone metastasis in breast cancer. BMC Cancer. 2016;16:307.

193. Vellon L, Menendez JA, Liu H, Lupu R. Up-regulation of alphavbeta3 integrin expression is a novel molecular response to chemotherapy-induced cell damage in a heregulin-dependent manner. Differentiation. 2007;75:819-30.

194. von Minckwitz G, Untch M, Blohmer JU, Costa SD, Eidtmann H, Fasching PA et al. Definition and impact of pathologic complete response on prognosis after neoadjuvant chemotherapy in various intrinsic breast cancer subtypes. J Clin Oncol. 2012;30:1796-804.

195. Marusyk A, Janiszewska M, Polyak K. Intratumor heterogeneity: the rosetta stone of therapy resistance. Cancer Cell. 2020;37:471-84.

196. Zhu X, Tao X, Lu W, Ding Y, Tang Y. Blockade of integrin β3 signals to reverse the stem-like phenotype and drug resistance in melanoma. Cancer Chemotherapy and Pharmacology. 20191-10.

197. Christmann M, Diesler K, Majhen D, Steigerwald C, Berte N, Freund H et al. Integrin αVβ3 silencing sensitizes malignant glioma cells to temozolomide by suppression of homologous recombination repair. Oncotarget. 2017;8:27754.

198. Reynolds AR, Hart IR, Watson AR, Welti JC, Silva RG, Robinson SD et al. Stimulation of tumor growth and angiogenesis by low concentrations of RGD-mimetic integrin inhibitors. Nat Med. 2009;15:392-400.

199. Abu-Tayeh H, Weidenfeld K, Zhilin-Roth A, Schif-Zuck S, Thaler S, Cotarelo C et al. 'Normalizing' the malignant phenotype of luminal breast cancer cells via alpha(v)beta(3)-integrin. Cell Death & Disease. 2016;7:e2491-e2491.

200. Page JM, Merkel AR, Ruppender NS, Guo R, Dadwal UC, Cannonier S et al. Matrix rigidity regulates the transition of tumor cells to a bone-destructive phenotype through integrin β3 and TGF-β receptor type II. Biomaterials. 2015;64:33-44.

201. Kim E-K, Jang M, Song M-J, Kim D, Kim Y, Jang HH. Redox-mediated mechanism of chemoresistance in cancer cells. Antioxidants. 2019;8:471.

202. Echeverria GV, Ge Z, Seth S, Zhang X, Jeter-Jones S, Zhou X et al. Resistance to neoadjuvant chemotherapy in triple-negative breast cancer mediated by a reversible drug-tolerant state. Sci Transl Med. 2019;11

203. Xu L, Zhang W, Zhang XH-F, Chen X. Endoplasmic reticulum stress in bone metastases. Frontiers in Oncology. 2020;10

204. Clarke R, Cook KL, Hu R, Facey CO, Tavassoly I, Schwartz JL et al. Endoplasmic reticulum stress, the unfolded protein response, autophagy, and the integrated regulation of breast cancer cell fate. Cancer Res. 2012;72:1321-31.

205. Wang H, Yu C, Gao X, Welte T, Muscarella AM, Tian L et al. The osteogenic niche promotes early-stage bone colonization of disseminated breast cancer cells. Cancer Cell. 2015;27:193-210.

206. Carlson P, Dasgupta A, Grzelak CA, Kim J, Barrett A, Coleman IM et al. Targeting the perivascular niche sensitizes disseminated tumour cells to chemotherapy. Nat Cell Biol. 2019

207. Hussein O, Tiedemann K, Murshed M, Komarova SV. Rapamycin inhibits osteolysis and improves survival in a model of experimental bone metastases. Cancer Lett. 2012;314:176-84.

208. Moulder S, Gladish G, Ensor J, Gonzalez-Angulo AM, Cristofanilli M, Murray JL et al. A phase 1 study of weekly everolimus (RAD001) in combination with docetaxel in patients with metastatic breast cancer. Cancer. 2012;118:2378-84.

209. Morita S, Kojima T, Kitamura T. Plat-E: an efficient and stable system for transient packaging of retroviruses. Gene Therapy. 2000;7:1063-6.

210. Fontana F, Hickman-Brecks CL, Salazar VS, Revollo L, Abou-Ezzi G, Grimston SK et al. N-cadherin regulation of bone growth and homeostasis is osteolineage stage-specific. J Bone Miner Res. 2017;32:1332-42.

211. Andrews S. (2010). FastQC: a quality control tool for high throughput sequence data. Available online at: http://www.bioinformatics.babraham.ac.uk/projects/fastqc.

212. Kim D, Paggi JM, Park C, Bennett C, Salzberg SL. Graph-based genome alignment and genotyping with HISAT2 and HISAT-genotype. Nature Biotechnology. 2019;37:907-15.

213. Haeussler M, Zweig AS, Tyner C, Speir ML, Rosenbloom KR, Raney BJ et al. The UCSC genome browser database: 2019 update. Nucleic acids research. 2019;47:D853-8.

214. Liao Y, Smyth GK, Shi W. featureCounts: an efficient general purpose program for assigning sequence reads to genomic features. Bioinformatics. 2014;30:923-30.

215. Dobin A, Davis CA, Schlesinger F, Drenkow J, Zaleski C, Jha S et al. STAR: ultrafast universal RNA-seq aligner. Bioinformatics. 2013;29:15-21.

216. Patro R, Duggal G, Love MI, Irizarry RA, Kingsford C. Salmon provides fast and bias-aware quantification of transcript expression. Nature Methods. 2017;14:417-9.

217. Wang L, Wang S, Li W. RSeQC: quality control of RNA-seq experiments. Bioinformatics. 2012;28:2184-5.

218. Robinson MD, McCarthy DJ, Smyth GK. edgeR: a Bioconductor package for differential expression analysis of digital gene expression data. Bioinformatics. 2010;26:139-40.

219. Subramanian A, Tamayo P, Mootha VK, Mukherjee S, Ebert BL, Gillette MA et al. Gene set enrichment analysis: a knowledge-based approach for interpreting genome-wide expression profiles. Proceedings of the National Academy of Sciences. 2005;102:15545-50.

220. Mootha VK, Lindgren CM, Eriksson K-F, Subramanian A, Sihag S, Lehar J et al. PGC-1α-responsive genes involved in oxidative phosphorylation are coordinately downregulated in human diabetes. Nature Genetics. 2003;34:267-73.

221. Jakic B, Buszko M, Cappellano G, Wick G. Elevated sodium leads to the increased expression of HSP60 and induces apoptosis in HUVECs. PloS One. 2017;12:e0179383.

222. Sivapackiam J, Kabra S, Speidel S, Sharma M, Laforest R, Salter A et al. 68Ga-Galmydar: A PET imaging tracer for noninvasive detection of doxorubicin-induced cardiotoxicity. PloS one. 2019;14:e0215579.

223. Harris TD, Kalogeropoulos S, Nguyen T, Liu S, Bartis J, Ellars C et al. Design, synthesis, and evaluation of radiolabeled integrin α v β3 receptor antagonists for tumor imaging and radiotherapy. Cancer Biotherapy and radiopharmaceuticals. 2003;18:627-41.

224. Harris TD, Kalogeropoulos S, Nguyen T, Dwyer G, Edwards DS, Liu S et al. Structure− activity relationships of 111In-and 99mTc-labeled quinolin-4-one peptidomimetics as ligands for the vitronectin receptor: potential tumor imaging agents. Bioconjugate chemistry. 2006;17:1294-313.

225. Harris TD, Cheesman E, Harris AR, Sachleben R, Edwards DS, Liu S et al. Radiolabeled divalent peptidomimetic vitronectin receptor antagonists as potential tumor radiotherapeutic and imaging agents. Bioconjugate chemistry. 2007;18:1266-79.

226. Meoli DF, Sadeghi MM, Krassilnikova S, Bourke BN, Giordano FJ, Dione DP et al. Noninvasive imaging of myocardial angiogenesis following experimental myocardial infarction. J Clin Invest. 2004;113:1684-91.

227. Sadeghi MM, Krassilnikova S, Zhang J, Gharaei AA, Fassaei HR, Esmailzadeh L et al. Detection of injury-induced vascular remodeling by targeting activated αvβ3 integrin in vivo. Circulation. 2004;110:84-90.

228. Pan D, Pramanik M, Senpan A, Allen JS, Zhang H, Wickline SA et al. Molecular photoacoustic imaging of angiogenesis with integrin-targeted gold nanobeacons. The FASEB Journal. 2011;25:875-82.

229. Schneider JG, Amend SR, Weilbaecher KN. Integrins and bone metastasis: integrating tumor cell and stromal cell interactions. Bone. 2011;48:54-65.

230. Massagué J. TGFbeta in cancer. Cell. 2008;134:215-30.

231. Parvani JG, Gujrati MD, Mack MA, Schiemann WP, Lu ZR. Silencing β3 integrin by targeted ECO/siRNA nanoparticles inhibits EMT and metastasis of triple-negative breast cancer. Cancer Res. 2015;75:2316-25.

232. Maschler S, Wirl G, Spring H, Bredow DV, Sordat I, Beug H et al. Tumor cell invasiveness correlates with changes in integrin expression and localization. Oncogene. 2005;24:2032-41.

233. Wendt MK, Taylor MA, Schiemann BJ, Schiemann WP. Down-regulation of epithelial cadherin is required to initiate metastatic outgrowth of breast cancer. Molecular Biology of the Cell. 2011;22:2423-35.

234. Park J, Schwarzbauer JE. Mammary epithelial cell interactions with fibronectin stimulate epithelial-mesenchymal transition. Oncogene. 2014;33:1649-57.

235. Tran DD, Corsa CA, Biswas H, Aft RL, Longmore GD. Temporal and spatial cooperation of Snail1 and Twist1 during epithelial-mesenchymal transition predicts for human breast cancer recurrence. Mol Cancer Res. 2011;9:1644-57.

236. Akhurst RJ, Hata A. Targeting the TGFβ signalling pathway in disease. Nat Rev Drug Discov. 2012;11:790-811.

237. Abe M, Harpel JG, Metz CN, Nunes I, Loskutoff DJ, Rifkin DB. An assay for transforming growth factor-beta using cells transfected with a plasminogen activator inhibitor-1 promoter-luciferase construct. Anal Biochem. 1994;216:276-84.

238. Ng CM, Cheng A, Myers LA, Martinez-Murillo F, Jie C, Bedja D et al. TGF-beta-dependent pathogenesis of mitral valve prolapse in a mouse model of Marfan syndrome. J Clin Invest. 2004;114:1586-92.

239. Neptune ER, Frischmeyer PA, Arking DE, Myers L, Bunton TE, Gayraud B et al. Dysregulation of TGF-beta activation contributes to pathogenesis in Marfan syndrome. Nat Genet. 2003;33:407-11.

240. Habashi JP, Judge DP, Holm TM, Cohn RD, Loeys BL, Cooper TK et al. Losartan, an AT1 antagonist, prevents aortic aneurysm in a mouse model of Marfan syndrome. Science. 2006;312:117-21.

241. Chiechi A, Waning DL, Stayrook KR, Buijs JT, Guise TA, Mohammad KS. Role of TGF-β in breast cancer bone metastases. Adv Biosci Biotechnol. 2013;4:15-30.

242. Nieto MA, Huang RY, Jackson RA, Thiery JP. EMT: 2016. Cell. 2016;166:21-45.

243. Bhola NE, Balko JM, Dugger TC, Kuba MG, Sánchez V, Sanders M et al. TGF-β inhibition enhances chemotherapy action against triple-negative breast cancer. J Clin Invest. 2013;123:1348-58.

244. Ohmori T, Yang JL, Price JO, Arteaga CL. Blockade of tumor cell transforming growth factor-betas enhances cell cycle progression and sensitizes human breast carcinoma cells to cytotoxic chemotherapy. Exp Cell Res. 1998;245:350-9.

245. Zhang K, Rodriguez-Aznar E, Yabuta N, Owen RJ, Mingot JM, Nojima H et al. Lats2 kinase potentiates Snail1 activity by promoting nuclear retention upon phosphorylation. EMBO J. 2012;31:29-43.

246. Parekh A, Das S, Parida S, Das CK, Dutta D, Mallick SK et al. Multi-nucleated cells use ROS to induce breast cancer chemo-resistance in vitro and in vivo. Oncogene. 2018;37:4546-61.

247. Salaroglio IC, Panada E, Moiso E, Buondonno I, Provero P, Rubinstein M et al. PERK induces resistance to cell death elicited by endoplasmic reticulum stress and chemotherapy. Mol Cancer. 2017;16:91.

248. Appenzeller-Herzog C, Hall MN. Bidirectional crosstalk between endoplasmic reticulum stress and mTOR signaling. Trends Cell Biol. 2012;22:274-82.

249. Hossain F, Sorrentino C, Ucar DA, Peng Y, Matossian M, Wyczechowska D et al. Notch signaling regulates mitochondrial metabolism and NF-κB activity in triple-negative breast cancer cells via IKKα-dependent non-canonical pathways. Front Oncol. 2018;8:575.

250. Kim JH, Chu SC, Gramlich JL, Pride YB, Babendreier E, Chauhan D et al. Activation of the PI3K/mTOR pathway by BCR-ABL contributes to increased production of reactive oxygen species. Blood. 2005;105:1717-23.

251. Zhang L, Yao Y, Zhang S, Liu Y, Guo H, Ahmed M et al. Metabolic reprogramming toward oxidative phosphorylation identifies a therapeutic target for mantle cell lymphoma. Sci Transl Med. 2019;11

252. Ling YH, Liebes L, Zou Y, Perez-Soler R. Reactive oxygen species generation and mitochondrial dysfunction in the apoptotic response to bortezomib, a novel proteasome inhibitor, in human H460 non-small cell lung cancer cells. J Biol Chem. 2003;278:33714-23.

253. Kracht MJL, de Koning EJP, Hoeben RC, Roep BO, Zaldumbide A. Bioluminescent reporter assay for monitoring ER stress in human beta cells. Sci Rep. 2018;8:17738.